

**MINERAL MAPPING IN OYMAAĞAÇ (BEYPAZARI – ANKARA)
GRANITOID BY REMOTE SENSING TECHNIQUES**

**A THESIS SUBMITTED TO
THE GRADUATE SCHOOL OF NATURAL AND APPLIED SCIENCES
OF
MIDDLE EAST TECHNICAL UNIVERSITY**

BY

BURCU FATMA PEKESİN

**IN PARTIAL FULFILLMENT OF THE REQUIREMENTS
FOR
THE DEGREE OF MASTER OF SCIENCE
IN
GEOLOGICAL ENGINEERING**

APRIL 2005

Approval of the Graduate School of Natural and Applied Sciences

Prof. Dr. Canan ÖZGEN
Director

I certify that this thesis satisfies all the requirements as a thesis for the degree of Master of Science.

Prof. Dr. Asuman G. TÜRKMENOĞLU
Head of Department

This is to certify that we have read this thesis and that in our opinion it is fully adequate, in scope and quality, as a thesis for the degree of Master of Science.

Prof. Dr. Vedat TOPRAK
Supervisor

Examining Committee Members

Assoc. Prof. Dr. Bora ROJAY	(METU, GEOE)_____
Prof. Dr. Vedat TOPRAK	(METU, GEOE)_____
Assoc. Prof Dr. Yusuf Kaan KADIOĞLU	(Ankara Univ., GEOE)_____
Assist. Prof. Dr. M. Lütfi SÜZEN	(METU, GEOE)_____
Assist. Prof. Dr. Nuretdin KAYMAKÇI	(METU, GEOE)_____

I hereby declare that all information in this document has been obtained and presented in accordance with academic rules and ethical conduct. I also declare that, as required by these rules and conduct, I have fully cited and referenced all material and results that are not original to this work.

Name, Last name : Burcu F. PEKESİN

Signature :

ABSTRACT

MINERAL MAPPING IN OYMAAĞAÇ (BEYPAZARI – ANKARA) GRANITOID BY REMOTE SENSING TECHNIQUES

Pekesin, Burcu F.

M.Sc., Department of Geological Engineering

Supervisor : Prof. Dr. Vedat Toprak

April 2005, 116 pages

The aim of this study is to extract information about mineral distribution and percentages of Oymaağaç granitoid (Beypazarı-Ankara) by using remote sensing techniques. Two methods are applied during the studies which are spectral analysis and Crosta techniques.

Spectral measurements are done for fresh and weathered samples collected at 32 locations. Mineral percentages are calculated using spectral mixture analysis for each sample by considering main, accessory and secondary mineral content of granodiorite. A total of 10 endmembers for fresh samples and 15 for weathered samples are used. USGS spectral library data is utilized through the analyses.

For Crosta technique (image analysis) the multispectral ASTER satellite image is used. Five alteration minerals are discriminated and their maps are generated during this analysis.

Interpretation and comparison of the results of both methods and testing these results with the existing petrographical and geochemical data indicate that: 1) according to the results of both spectral analyses and Crosta technique a zonation is not observed in the granitoid, 2) comparison of the results for alteration minerals of these two analyses are partly compatible but not exactly similar, 3) Results of spectral analysis do not fit geochemical nor modal analyses because of inconsistency of the data sets.

Keywords: Spectral unmixing, Crosta Technique, Oymağaç Granitoid.

ÖZ

UZAKTAN ALGILAMA TEKNİKLERİ İLE OYMAAĞAÇ GRANİTOYİDİ’NİN (BEYPAZARI – ANKARA) MİNERAL HARİTALAMASI

Pekesin, Burcu F.

Yüksek lisans, Jeoloji Mühendisliği Bölümü

Tez Yöneticisi : Prof. Dr. Vedat Toprak

Nisan 2005, 116 sayfa

Bu çalışmanın amacı uzaktan algılama teknikleriyle, Oymaağaç Granitoyidi’nde (Beypazarı-Ankara) mineral dağılımı ve yüzdeleri hakkında bilgi üretmektir. Çalışma sırasında spektral analiz ve Crosta tekniği olmak üzere iki metod uygulanmıştır.

Spektral ölçümler 32 lokasyondan toplanan taze ve bozunmuş örnekler için yapılmıştır. Mineral yüzdeleri her örnek için granitoyidin ana, tali ve ikincil mineral bileşenleri gözönüne alınarak spektral karışım analizi ile hesaplanmıştır. Bu analizler sırasında USGS spektral kütüphane veritabanı kullanılmıştır.

Crosta tekniği (görüntü analizi) için multispektral ASTER uydu görüntüsü kullanılmıştır. Bu işlem için beş alterasyon minerali belirlenmiş ve bu minerallerin haritaları elde edilmiştir.

Her iki metodla elde edilen sonuçların karşılaştırması ve yorumu ve bu sonuçların mevcut petrografik ve jeokimyasal data ile test edilmesi göstermiştir ki: 1) Spektral analiz ve Crosta tekniği sonuçlarına göre granitoyid içinde bir zonlanma gözlenmemiştir, 2) Her iki analizin alterasyon mineralleri için üretilen sonuçları kısmen uyumlu olsa da tümüyle benzer değilllerdir, 3) Veri setlerindeki uyumsuzluklar nedeniyle spektral analiz sonuçları ile ne jeokimyasal ne de modal analiz sonuçları arasında bir uyumluluk gözlenmemiştir.

Anahtar Kelimeler: Spektral ayrımsallaşma, Crosta Tekniği, Oymaağaç Granitoyidi

To My Beloved Parents

ACKNOWLEDGMENTS

I would like to express my special thanks and appreciation to Prof. Dr. Vedat TOPRAK for his guidance and supervision throughout this study. I really learnt a lot from his suggestions and fruitful discussions.

I also wishes to acknowledge to Assoc. Prof. Dr. Yusuf Kaan KADIOĞLU for his valuable comments and suggestions.

I am very grateful to Assist. Prof. Dr. Lütfi SÜZEN for his assistances and continuous support.

Appreciation is also extended to Assist. Prof. Dr. Nuretdin KAYMAKÇI for his skilled technical support.

Also, I would like to thank to my friends Taner SAN and Ayşe DAĞLIYAR for their helps and encouragements.

Finally, my deepest and unlimited gratitude and respect to my parents for their unconditional support, love, and their persistent encouragement throughout my thesis.

TABLE OF CONTENTS

PLAGIARISM.....	iii
ABSTRACT	iv
ÖZ.....	vi
DEDICATION.....	viii
ACKNOWLEDGMENTS	ix
TABLE OF CONTENTS.....	x
LIST OF TABLES.....	xiv
LIST OF FIGURES.....	xvi
LIST OF ABBREVIATIONS.....	xviii

CHAPTER

1. INTRODUCTION.....	1
1.1. Purpose and Scope	1
1.2. Study Area.....	1
1.3. Previous Studies	2
1.3.1. Geological Studies	3
1.3.2. Remote Sensing Studies.....	6
1.3.2.1. Reflectance Spectroscopy Studies.....	6
1.3.2.2. Crosta Technique	11
1.4. Method of Study.....	12

1.5. Layout of the Thesis.....	13
2. GEOLOGY	14
2.1. Regional Geology	14
2.2. Geology of Study Area.....	16
2.2.1. Oymaağaç Granodiorite	20
2.2.2. İsmailkayası Granodiorite	21
2.2.3. Tavuktaş Granodiorite	22
2.2.4. Çayırpınar Alkali Feldspar Granite (Aplitic Dyke)	23
3. BACKGROUND.....	24
3.1. Principles of Reflectance Spectroscopy	24
3.1.1. Absorption Processes	24
3.1.2. Causes of Absorption	25
3.1.2.1. Electronic Processes.....	25
3.1.2.1.1. Crystal Field Effect	25
3.1.2.1.2. Charge Transfer Absorption.....	25
3.1.2.1.3. Conduction Bands	26
3.1.2.1.4. Color Centers	27
3.1.2.2. Vibrational Processes.....	28
3.1.3. Spectral Variability	29
3.1.3.1. Crystallinity.....	29
3.1.3.2. Chemical Composition.....	30
3.1.3.3. Orientation	30

3.1.3.4.	Grain Size.....	31
3.1.3.5.	Transparency	31
3.1.3.6.	Water	31
3.1.4.	Spectral Libraries	31
3.2.	Spectral Unmixing	32
3.3.	Mineral Associations in Granodiorite Rocks	32
3.3.1.	Endmember Determination of Oymağaç Granitoid	33
3.4.	ASTER Data	36
4.	DATA	38
4.1.	Samples	38
4.2.	ASTER Data	41
5.	ANALYSES	43
5.1.	Methodology	43
5.2.	Spectral Analyses	45
5.3.	ASTER Image Analyses (Crosta Technique)	53
5.3.1.	Calcite	53
5.3.2.	Chlorite.....	56
5.3.3.	Epidote	59
5.3.4.	Illite	61
5.4.	Comparison of Spectral Analyses and Crosta Technique	63
5.5.	Combination Map	66
6.	FIELD VERIFICATION.....	69

7. DISSCUSSION	77
7.1. Data	77
7.2. Spectral Analyses	78
7.3. Image Analyses (Crosta Technique)	79
7.4. Results obtained	80
7.5. Field verification	80
8. CONCLUSIONS AND RECOMMENDATIONS	82
REFERENCES.....	83
APPENDICES	
A. Spectral Measurements of Rock Samples	88
B. Measured and calculated spectra of fresh samples	96
C. Measured and calculated spectra of weathered samples	106

LIST OF TABLES

TABLES

Table 1.1. Softwares used in this study.....	13
Table 2.1. Petrographic features used in the classification of Oymağaç Granitoid .	20
Table 3.1. Spectral reflectance regions and absorption features.....	27
Table 3.2. Positions of major spectral features in SWIR region of common groups..	28
Table 3.3. Mineral components of granitoid used for analysis.....	33
Table 3.4. ASTER baseline performance requirements.....	37
Table 4.1. Sample list with coordinates and lithology.....	40
Table 4.2. Removed haze amounts for ASTER bands.....	42
Table 5.1. Endmembers used in analysis and some properties.....	45
Table 5.2. Quantitative percentages of minerals for fresh samples	48
Table 5.3. Quantitative percentages of minerals for weathered samples.....	49
Table 5.4. Eigenvector statistics for ASTER bands 1, 3, 8, and 9	54
Table 5.5. Eigenvector statistics for ASTER bands 1, 2, 5, and 8.....	57
Table 5.6. Eigenvector statistics for ASTER bands 2, 5, 8, and 9.....	59
Table 5.7. Eigenvector statistics for ASTER bands 1, 3, 5, and 6.....	61
Table 5.8. Mineral percentages of spectral analysis and DN values corresponding with sample locations.....	64
Table 5.9. Decimal codes representing each mineral.....	66
Table 5.10. Represented minerals and number of pixels for each numeric value	67

Table 6.1. Mineral percentages using CIPW norm from geochemical data	70
Table 6.2. Modal mineral compositions of thin sections belonging to Oymağaç Granitoid	70

LIST OF FIGURES

FIGURES

Figure 1.1. Location of the study area.....	2
Figure 2.1. Regional geological map	15
Figure 2.2. Geological map of the study area	17
Figure 2.3. Modal mineralogic compositions of the rocks on QAPF diagram	18
Figure 2.4. A field view of enclaves in İsmailkayası Granodiorite.	21
Figure 2.5. Macroscopic view of İsmailkayası Granodiorite.....	22
Figure 2.6. Field view of Çayırpınar Alkali Feldspar Granite	23
Figure 3.1. Spectral signature diagrams.....	26
Figure 4.1. Sample location map.....	39
Figure 4.2. Band correlation graph between band 1 and band 9.....	41
Figure 4.3. RGB (321) band combination of the area.....	42
Figure 5.1. Flowchart of the study.	44
Figure 5.2. USGS spectral reflectance curves of major and minor minerals of granodiorite.....	46
Figure 5.3. USGS spectral reflectance curves of secondary minerals of granodiorite	46
Figure 5.4. SPECMIN “feature search” window	47
Figure 5.5. An example of worksheet used for calculation of the mixture spectrum .	52
Figure 5.6. Comparison of measured and calculated spectra.....	52
Figure 5.7. USGS spectral reflectance curve of calcite	54

LIST OF ABBREVIATIONS

VNIR:	Visible Near Infra Red
NIR:	Near Infra Red
SWIR:	Short Wave Infra Red
TIR:	Thermal Infra Red
VIS:	Visible
UV:	Ultra Violet
XRD:	X- Ray Diffractometer
JPL:	Jet Propulsion Laboratory
USGS:	United States Geological Survey
GPS:	Global Positioning System
ASTER:	Advanced Spaceborne Thermal Emission and Reflection Radiometer
NASA:	National Aeronautics and Space Administration
Landsat TM:	Landsat Thematic Mapper
UTM:	Universal Transverse Mercator
CIPW:	Cross Iddings Pirsson Washington
WGS:	World Geodetic System
PC:	Principal Component
DN:	Digital Number
SD:	Standard Deviation

CHAPTER 1

INTRODUCTION

1.1. Purpose and Scope

Use of remote sensing technology has been increasing in the recent years for various purposes in geological applications. The main aim in these applications is to extract information about the area that will contribute to other studies (such as field and lab works) in terms of data collection.

The main purpose in this study is to use remote sensing for mapping purposes in igneous intrusive terrains. Two main reasons for the selection of intrusive bodies are: 1) there is still little work done in these rocks compared to other rock types (particularly sedimentary rocks); and 2) there are considerable large number of plutonic bodies in Turkey need to be mapped. Therefore, the study is believed to contribute to field studies carried out in intrusive terrains.

The scope of the thesis is limited to two applications of remote sensing, namely spectral analysis applied to samples collected in the field and Crosta technique applied to the ASTER image of the study area.

1.2. Study Area

The study area is included within the Beypazarı Granitoid (exposed around Oymağaç village located approximately 15 km south of Beypazarı and is bordered at north by the Kirmirçayı River (Figure 1.1). It covers an area of approximately 52

km² between the latitudes 40° 01' 21" and 40° 05' 51" N and the longitudes 31° 52' 24" and 32° 00' 02" E. This area is contained the 1:25.000 scale map section of BOLU - H27-c3.

The main reason in the selection of this area is that the granitoid is mapped in the field in detail and different granitic rocks are recognized by previous works. Therefore, the map prepared and geochemical analysis carried out can be used as ground truth studies.

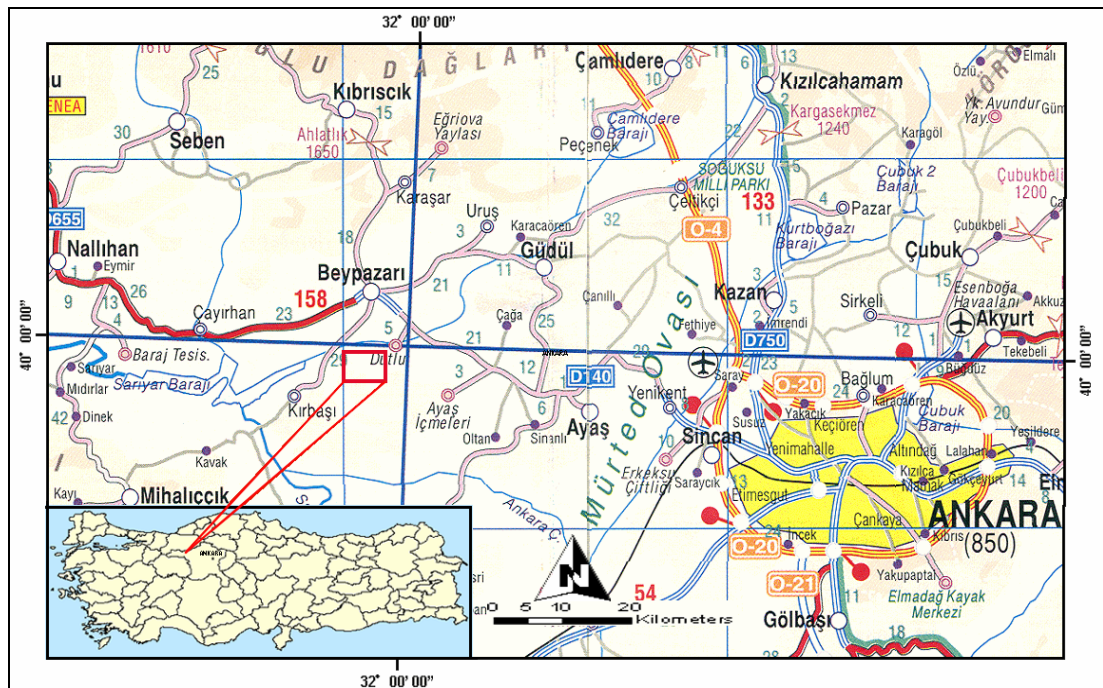


Figure 1.1. Location of the study area.

1.3. Previous Studies

Previous studies that will be mentioned there are categorized into two groups. The first group studies are about geology of the area and explain various local geological features. The second group studies are about the main theme of this study that deal with spectral characteristics of the minerals and tend to develop certain algorithms for remote sensing studies.

1.3.1. Geological Studies

The previous studies mentioned here will summarize general geological characteristics of the study area and surrounding regions. The studies are briefly explained below in chronological order.

Stchepinsky (1942) studied Beypazarı–Nallıhan–Bolu-Gerede region which is the first work involving the investigation area. He made a geological map of the area at 1/100.000 scale with major tectonic structures.

Rondot (1956) mapped Nallıhan-Beypazarı area with the compilation of the work by Stchepinsky (1942). He prepared a geological map of the area at 1/100.000 scale.

Van Der Meer Mohr (1956) mapped Beypazarı area at 1/25.000 scale and investigated potential of groundwater resources in the area. Formations are divided stratigraphically into five groups, e.g. older Paleozoic, Paleocene, Neogene, Pleistocene and recent deposits. He stated that most of the Neogene deposits are unconformably overlying crystalline bedrock. Two main rock types found in the crystalline rocks are granodiorite and porphyritic granite.

Gökmen (1965) studied lignite bearing Neogene basin. He estimated the reserve of lignite in the area as 70 million tones.

Brennich (1967) divided gypsum occurrences in Nallıhan-Beypazarı area into three groups according to their distribution as 1) Çayırhan gypsum, 2) Kırbaşı gypsum, and 3) Gypsum occurred at south and west of Beypazarı, and mapped these rocks at 1/100.000 scale. He stated that gypsum was located within a wide syncline with an axis in ENE – WSW direction.

Kayakıran and Çelik (1986) investigated Beypazarı trona deposits and determined quality of trona deposit by chemical analysis. They also attempted to calculate total amount of the trona in the region.

Helvacı *et al.* (1988) studied vertical and lateral distribution of clay and other authigenic minerals of Neogene sediments in Beypazarı.

Yağmurlu *et al.* (1988) investigated depositional setting and geometric structure of the Çayırhan and Koyunağılı lignite deposits of the Beypazarı Neogene basin. They recognized lower and upper lignite seams in the Çayırhan coal field and only an upper lignite seam in the Koyunağılı coal field.

Özpeker *et al.* (1991) studied mineralogical features of trona bearing Hırka Formation of Miocene age in the Beypazarı basin.

Tatar *et al.* (1993) explained the geology of the lower and upper lignite seams of Çayırhan coal basin. They suggested development strategies and mining method by investigating the geotechnical and geological features of coal seams.

Yohannes (1993) made geological and petrochemical investigations on Beypazarı granitoids for the purpose of petrogenesis. He indicated that the hornblende granitoids and the porphyry diorite dykes are the products of a volcanic arc whereas granite dyke is the result of pneumatolytic processes. A mantle derived magma and partial melting of lower crust is suggested for the source of hornblende granitoid.

Helvacı and Bozkurt (1994) studied geology, mineralogy and petrogenesis of Beypazarı granite. According to them, Beypazarı granite is homogeneous; it has a small variance within its body. Results of chemical analyses showed that Beypazarı Granites were formed by anatexis of older continental crusts, and are shallowly intruded to the region probably during the Late Cretaceous.

Yağmurlu and Helvacı (1994) studied sedimentological characteristics and facies of the evaporite bearing Kirmir Formation in the Beypazarı basin. They divided evaporite sequence into four lithofacies. These are in ascending order: 1) gypsiferous claystone facies, 2) thenardite-glauberite facies, 3) laminar gypsum facies, and 4) crystalline gypsum facies. The lithological and sedimentological features of the Kirmir Formation indicate fluvial, saline playa mudflat, hypersaline ephemeral playa lake and very shallow subaqueous playa lake depositional environments.

Karadenizli (1995) studied sedimentology of Upper Miocene-Pliocene gypsum series of Beypazarı basin. Based on sedimentary properties of gypsum, he defined three different facies; 1) Individual gypsum beds interbedded with green clays (open lake with short evaporitic phase), 2) Scattered gypsum crystals and bassanite within an organic rich mudstone (marginal swamps with evaporitic ground water), 3) Massive gypsum with thin clay laminations (closed lake with evaporitic lake water).

Demirci (2000) analyzed tectonic phases during Neogene-Quaternary period studying geological structures in the area between Beypazarı-Ayaş-Kazan-Çeltikçi. He recognized three phases with the following directions of maximum principal stresses, from the oldest to the youngest: 096/17, 189/17, and 308/88.

Gündoğan and Helvacı (2001) compared Upper Miocene evaporites of Beypazarı basin and Çankırı- Çorum basin on the basis of their sedimentologic and petrographic characteristics. They distinguished evaporites as a discrete lithofacies of the area. The Beypazarı basin evaporites consist mainly of a secondary gypsum lithofacies. However in the Çankırı-Çorum basin, the lower part of the sequence is mainly secondary gypsum and the upper part is mainly characterized by primary gypsum.

Zoroğlu and Kadioğlu (2003) studied Oymaağaç Granitoid which is included within Beypazarı Granitoids. Oymaağaç Granitoid is differentiated into Oymaağaç Granodiorite, İsmailkayası Granodiorite, Tavuktaş Granodiorite and Çayırpınar Alkali Feldspar Granite on the basis of field observations and petrographical features. Geological map (rock units and boundaries) prepared by them is used as reference map in this study.

Zoroğlu and Kadioğlu (2004) made geochemical analyses on Oymaağaç Granitoid. According to results, SiO₂, K₂O and Rb contents increase, whereas TiO₂, Fe₂O₃, MgO, CaO, Ba and Nb contents decrease from outer part to the inner part of the pluton.

İpekgil (2005) investigated the origin, source characteristics, evolution petrogenesis and emplacement mechanisms of Oymaağaç Granitoid. Field observations and

petrographic investigations indicate distinct differences in the abundances of quartz, amphibole minerals (e.g., hornblende) and of enclaves. But the chemical investigation does not show significant differences in the composition of the granitoid. The origin of Oymağaç Granitoid is concluded that it formed from upper continental crust material which mingled with the basic magma related to subduction process.

1.3.2. Remote Sensing Studies

Literature survey given here involves only two applications (methods) of remote sensing that are in the scope of this thesis. These are: 1) Reflectance Spectroscopy Studies, 2. Crosta Technique.

1.3.2.1. Reflectance Spectroscopy Studies

Hunt and Turner (1953) developed an infrared spectroscopic method for the determination of mineral constituents of rocks, both qualitatively and quantitatively. The method involves grinding rocks to a fine powder and examining the powder as a film on a conventional sodium chloride window.

Adams and Filice (1967) investigated spectral reflectance as a function of rock composition and mineralogy, particle size, particle shape, particle packing, and angle of illumination. They concluded that the most important variables are rock composition and mineralogy, and particle size. They first recognized that the reflectance is inversely related to the particle size. The absorption bands are deepest when the grain size is about one optical depth. They also noted the difficulties in reaching a unique interpretation of spectral data of mixtures of rocks with an admixture of opaque minerals.

Nash and Conel (1974) measured spectra of mixtures of powdered hyperstene, labradorite, and ilmenite. They noted that principle mixing effects are the proportionate darkening effect of opaque ilmenites; the persistence, the wavelength

stability, and the depth versus concentration proportionality of the 1 μm band of pyroxene.

Hunt (1977) summarized the processes responsible for the presence of a feature at a specific wavelength in the spectrum of a particulate mineral. He discussed bidirectional reflectance spectra of minerals caused by a variety of electronic and vibrational processes over visible and near infrared wavelengths (0.325 to 2.5 μm) with reference to specific minerals. Spectral data collected from a large selection of minerals were used to generate a spectral signature diagram that summarizes the optimum intrinsic information available from the spectra of particulate minerals.

Hunt (1979) studied near-infrared spectra of alteration minerals. He indicated many hydrothermal alteration mineral spectra display well defined and characteristic features in the regions near 1.4, 1.76, and 2.0 to 2.4 μm .

Hunt and Ashley (1979) showed that electronic transitions in the iron bearing constituent minerals produce diagnostic minima near 0.43, 0.65, 0.85, and 0.93 μm and vibrational transitions in clay and water bearing mineral constituents typically produce characteristic single or multiple features over limited spectral ranges near 1.4, 1.75, 1.9, 2.2, and 2.35 μm .

Blom *et al.* (1980) determined the spectral signatures of naturally occurring plutonic rock surfaces as a function of mineralogy and discriminated these rock types by evaluating different portions of the 0.45-2.45 μm region. They indicated that differences in albedo and absorption bands can be exploited to discriminate these rock types with high accuracy by using linear discriminant analysis.

Hunt and Evarts (1981) used the contrast of near infrared spectral features of primary magnesian silicate minerals and secondary hydrous-serpentine group minerals to indicate the degree of serpentinization of ultramafic rocks.

Hapke (1981a) presented a theory derived from radiative transfer equation for describing the scattering of light from particulate surfaces. He developed analytical

expressions for bidirectional reflectance, radiance factor, radiance coefficient, normal, hemispherical, bond, and physical albedos, integral phase function, phase integral, and limb-darkening profile.

Hapke (1981b) verified experimentally the theoretical bidirectional function and the predicted linear relation between the espat-function W , and absorption coefficient α . The predicted approximately linear dependence of the bidirectional espat-function W on the effective particle absorption optical thickness αD_e at least as high as 3.

Singer (1981) studied near infrared spectral reflectance data for systematic variations in weight percent of two component mixtures of ferromagnesian and iron oxide minerals. He produced two component mixtures of olivine-clinopyroxene, olivine-orthopyroxene, clinopyroxene-orthopyroxene, olivine-limonite, clinopyroxene-limonite, orthopyroxene-limonite, and olivine-magnetite. He concluded that spectral properties in an intimate mixture combine in a complex, nonadditive manner, with features demonstrating a regular but usually nonlinear variation as a function of endmember phase proportions.

Buckingham and Sommer (1983) investigated the ability of remote sensing devices to discriminate hydrothermally altered rock from surrounding unaltered rock. The penetration depth experiments defined that only the upper 50 μm of a rock surface contributes to the rock's reflectance spectrum.

Clark (1983) studied the spectral properties from 0.4 to 3.0 μm of mixtures of montmorillonite and opaque material (dark carbon grains) as a function of the weight fraction of opaques present and of the grain size of the opaques. He used Hapke theory to analyse spectral properties of mixtures of montmorillonite with charcoal and with carbon lamp black.

Gillette *et al.* (1983) used the factor analysis for separation of pure component spectra from a series of infrared mixture spectra. They stated this technique requires that each pure component spectrum have a nonoverlapped characteristic peak.

Gladwell *et al.* (1983) examined operating parameters of the Barringer hand-held reflectance radiometer and investigated the usage of this reflectance spectrometer as a backup instrument.

Johnson *et al.* (1983) found that a semiempirical method which uses a two-stream radiative transfer model to determine the relative proportions of mineral components in a mixture. This method has the advantage in that the fit is made to the entire reflectance spectrum using reasonable theoretical constraints.

Whitney *et al.* (1983) tested mineral discrimination ability of portable ratio-determining radiometer. They used ratio-determining device as opposed to a field spectrometer, because the ratio technique greatly reduces the effects of atmospheric and surficial variables.

Clark and Roush (1984) compared several methods including empirical methods and scattering theories. They indicated that bidirectional reflectance theories have the potential for use in deriving mineral abundance from a reflectance spectrum.

Cloutis *et al.* (1986) analyzed spectra of olivine and orthopyroxene mixtures to define the correlations between spectral and albedo parameters. They found that the ratio of areas for the 1 and 2 μm absorption bands is a sensitive indicator of the olivine-orthopyroxene abundance and is relatively insensitive to variations in mineral composition and particle size.

Ager and Milton (1987) investigated reflectance characteristics of lichens and their effects on the reflectance of rock substrates (granite, slate, and hornfels). Lichen cover masks as low as 30% the spectral features of spectrally flat rocks such as flat, hornfels and 60-80 % and the sharp spectral features of granite. The 2200 nm reflectance peak of lichens interferes with identification of the OH absorption band at 2200 nm in hydroxyl-bearing minerals.

Mustard and Pieters (1989) used Hapke's model for bidirectional reflectance to calculate the mass fractional abundance components of intimate mineral mixtures by

some assumptions. The simple model is accurate to within 7% for mixtures not containing low albedo components.

Clark *et al.* (1990) studied high resolution reflectance spectra of minerals. They studied in 0.2 to 3.0 μm region at resolving powers as high as 2240.

Johnson *et al.* (1992) presented a method for quantitatively modeling spectra as a function of endmember abundances in multicomponent mixtures, particle sizes, and illumination/viewing geometry.

Rollin *et al.* (1994) examined the effect of surface weathering and lichen cover on the spectral reflectance of granitic rocks in the region visible and infrared. The presence of lichen growth was found to affect both the overall shape of the reflectance spectrum and certain absorption features.

Younis *et al.* (1997) investigated weathering process effects on spectral reflectance of different rock types (limestone, calcarenite, lamproites, phyllite and quartzite) in a semi arid environment in Guadalentin basin, in SE Spain.

Taylor (2000) developed a new approach for determination of both the mineralogy and the lithology of drill core pulps using field spectrometry. He used material from a single drillhole through a mineralized sequence of rocks from central New South Wales. The comparison of spectrometry analyses with X-Ray Diffraction analyses indicated that for most major constituents, spectrometry provides an estimate of quantitative mineralogy that is as reliable as that provided by XRD.

Longhi *et al.* (2001) analyzed metamorphic rocks on the basis of absorption band position and shape, and classified on the basis of recurrent associations of absorption bands.

Ramsey *et al.* (2002) studied on the automated methods of mineral identification from reflectance spectra and give evidence that a simple algorithm, adapted from a well-known search procedure for Bayes nets, identifies the most frequently occurring classes of carbonates with a reliability equal to or greater than that of human experts.

They also compared the reliability of the procedure with several other automated methods adapted to the same purpose.

Saldanha *et al.* (2004) investigated the use of the Karhunen-Loeve (KL) transformation to contribute for the understanding of the relationship between the spectral data as obtained by a spectroradiometer and the chemical and mineralogical composition of soils originated from mafic/ultramafic rocks.

1.3.2.2. Crosta Technique

Crosta and Moore (1989) developed a methodology based on PCA which is called Feature Oriented Principle Components Selection (FPCS). This technique is based on the examination of PCA eigenvector to decide which of the principle component images contain spectral information about specific target materials. An important aspect of this technique is that it predicts whether the target surface is represented by dark or bright pixels in the relevant principle component image.

Loughlin (1991) tested FPCS on TM image subscene of Roberts Mountains area, Nevada. He used Landsat TM band sets to derive spectral information about hydroxides, iron oxides+hydroxides and iron oxides. He termed this technique as Crosta Technique.

Ruiz-Armenta and Prol-Ledesma (1998) compared several methods used for spectral enhancement of the images in order to detect hydrothermally altered rocks in an area in the western section of the Transmexican Volcanic Belt. They applied Selective Principle Component Analysis, Crosta Technique using six bands and four bands, Directed Principle Component Analysis, Decorrelation Stretch and HSI Transformation on Landsat TM image of the area. The method that proved to be the most efficient is found to be Crosta Technique using four TM bands combined with the HSI transformation.

Carranza and Hale (2002) tested a methodology which involves processing of Landsat TM image and integration of ground data in the Baguio district of the

Philippines to map hydrothermally altered zones in heavily vegetated terrains. The Crosta Technique and the software defoliant technique were applied to Landsat TM data to identify limonitic and clay alteration zones. However, these two techniques were inadequate and inappropriate for remote mapping of hydrothermal alteration in this area. They developed mineral imaging methodology using Landsat TM data.

Tangestani and Moore (2002) mapped the porphyry copper alteration in the Meiduk area, Iran by using Crosta technique and stretched-unstretched principal component transformations on Landsat TM bands.

Crosta *et al.* (2003) applied the Crosta technique to ASTER (Advanced Spaceborne Thermal Emission and Reflection Radiometer) bands covering the SWIR with the objective of mapping the occurrence of mineral end-members related to an epithermal gold prospect in Patagonia, Argentina.

1.4. Method of Study

This study is completed in four major steps.

The first step consists of literature review. This step contributed to the selection of remote sensing methods to be used in this study.

The second step involves sample collection by field studies and measurement of their reflectance spectra. The reflectance spectra of the samples are measured in the MTA (General Directorate of Mineral Research and Exploration) laboratories using field spectrometer.

The third step includes spectral mixture analyses and Crosta technique using ASTER images.

The last step is the compilation of the whole work and composing the text that interprets and discusses the results obtained. The softwares used in this study are tabulated in Table 1.1.

Table 1.1. Softwares used in this study.

Software	Purpose of use
SPECMIN	Spectral unmixing analyses
TNT Mips	Removal of path radiance Generating a subset of the study area from full ASTER image
Arc GIS	Digitization of geological map of the study area Mineral maps obtained by different analyses
MS Excel	Calculation of mixture spectrum Plotting of correlation diagrams of spectral and image analyses Calculation of CIPW Norm
PCI Geomatica	Registration of ASTER image

1.5. Layout of the Thesis

The thesis is divided into seven chapters. After this chapter, Chapter 2 presents information about geology of the study area. Chapter 3 gives a review of pertinent literature. The used data is described in Chapter 4. Chapter 5 explains the methods applied. Chapter 6 includes evaluation of results by some field data. Chapter 7 discusses the data, spectral and image analyses, obtained results and field verification. In Chapter 8, conclusions and recommendations are given. Appendix A contains detailed table of spectral measurements. Appendix B and Appendix C show the measured and calculated spectra of fresh and weathered samples, respectively.

CHAPTER 2

GEOLOGY

2.1. Regional Geology

Geological map of the study area and surrounding region is given in the map in Figure 2.1. This map is included within the Zonguldak and Ankara sheets of 1:500.000 scale map of Turkey prepared by MTA (General Directorate of Mineral Research and Exploration). The area contains 31 rock units of different age and lithology. In terms of regional geology the area lies in the “Sakarya Zone” and surrounded by the Pontides in the north and the Taurides in the south (Okay, 2001). An important rock association of the area is Beypazarı basin which is composed of two main rock sequences: 1) Neogene sedimentary and volcanic rocks, 2) Basement rocks.

Neogene units comprise carbonates, clastic, evaporates and volcanogenic units of Middle and Upper Miocene (Helvacı et al., 1988). This sequence is economically one of the most important units in Turkey due to its trona, lignite and bituminous shale and clay deposits (Yağmurlu and Helvacı, 1994).

Sedimentary sequence of Neogene of Beypazarı basin is divided into seven formations according to lithologic features. In ascending order, the sequence includes Çoraklar, Hırka, Akpınar, Çayırhan, Bozbelen, Kirmir formations, Sarıyar limestone (İnci et al., 1988). Volcanic rocks of the basin, on the other hand, belong to Galatean Volcanic Province (Erol, 1954; Rondot, 1956; Türkecan *et al.*, 1991) and cover large areas beyond the limits of the study area. İnci et al. (1988) named these units as Teke volcanics.

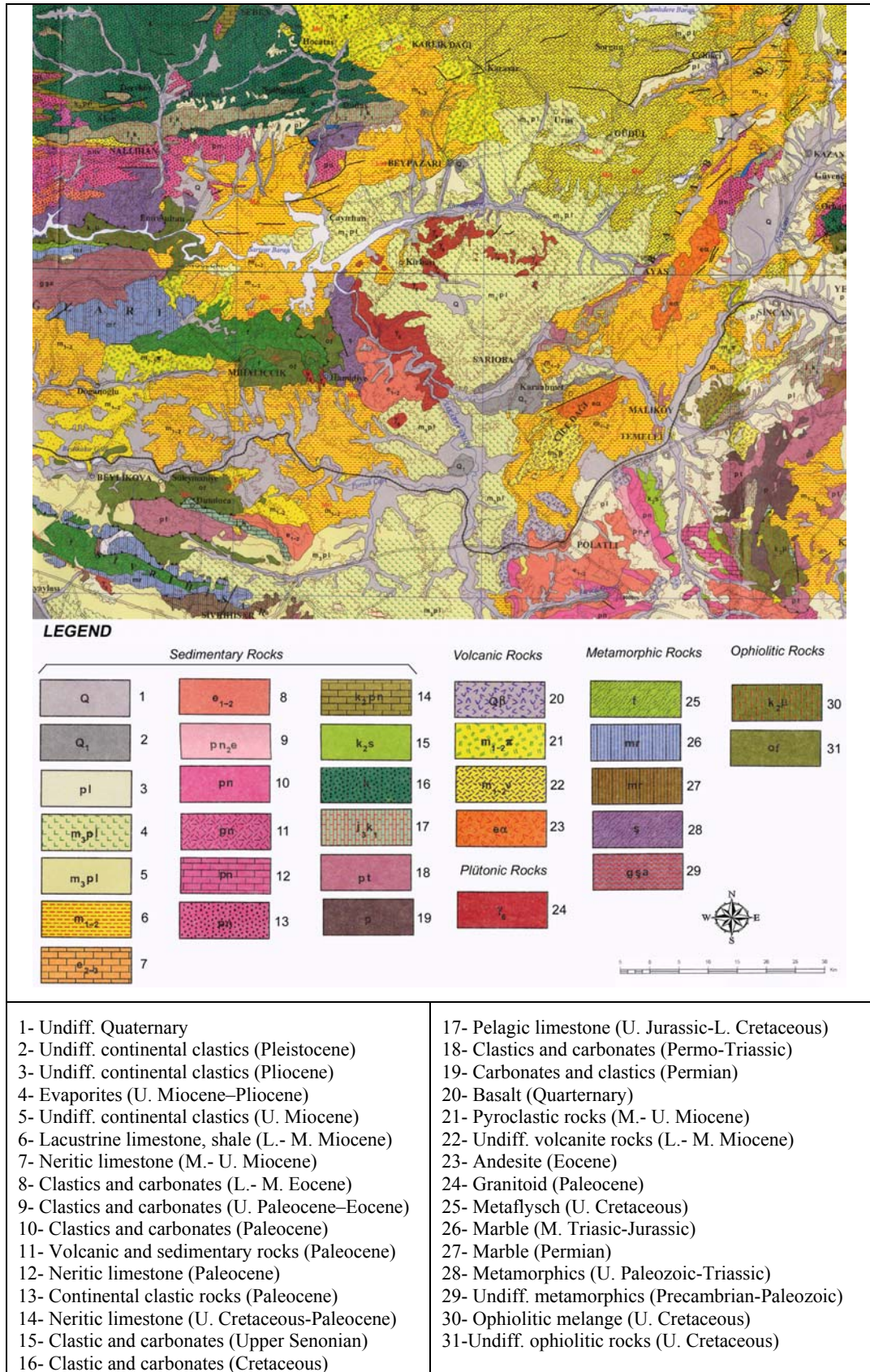


Figure 2.1. Regional geological map (from MTA 1/500.000 scaled map of Turkey)

Basement rocks are unconformably overlain by Neogene sequences and consist of metamorphic, ophiolitic, granitic, carbonaceous, and clastic rocks ranging in age from Paleozoic to Paleocene (Gündoğan and Helvacı, 2001). Beypazarı Granitoid is a part of basement rocks and is located south of Beypazarı (Figure 2.1).

2.2. Geology of Study Area

The rock unit which is the main focus of this study is “Oymaağaç granitoid” named due to its exposure in the close vicinity of Oymaağaç village (Zoroğlu and Kadioğlu, 2003). The granitoid is surrounded by light brown grayish, beige, considerably loose evaporates. They are exposed mainly at the southern and southwestern parts of the area (Zoroğlu and Kadioğlu, 2003). This dominant unit in the sequence is gypsiferous mudstone (Kayakıran and Çelik, 1986; Yohannes, 1993). Its thickness ranges from a few cm to tens of meter. These rocks, however, are beyond the scope of this study and will not be dealt here. Therefore, in this section geological features of only Oymaağaç granitoid will be explained.

Oymaağaç granitoid cuts Paleozoic metamorphic rocks that belong to Middle Sakarya Continent (Helvacı and Bozkurt, 1994). Time of intrusion of granitoid is determined as older than Paleocene and younger than Permian probably Upper Cretaceous by Helvacı and Bozkurt (1994). The granitoid is differentiated into four subunits by Zoroğlu and Kadioğlu (2003, 2004). These are from the youngest to the oldest: Oymaağaç granodiorite, İsmailkayası granodiorite, Tavuktaş granodiorite, and Çayırpınar Alkali Feldspar Granite (Figure 2.2). Each units display certain differences in color, texture, mineral proportions and grain size.

Detailed petrographic and microscopic examinations of the collected samples throughout the granitoid are carried out by Yohannes (1993), Zoroğlu and Kadioğlu (2003, 2004), İpekgil (2005). According to these studies, Oymaağaç granitoid is composed of major minerals of quartz, plagioclase, alkali-feldspar, hornblende, pyroxene and biotite, accessory minerals of sphene, zircon, pistacite, zeolite, apatite and opaque minerals; and secondary minerals of epidote, chlorite, sericite, calcite and clay minerals.

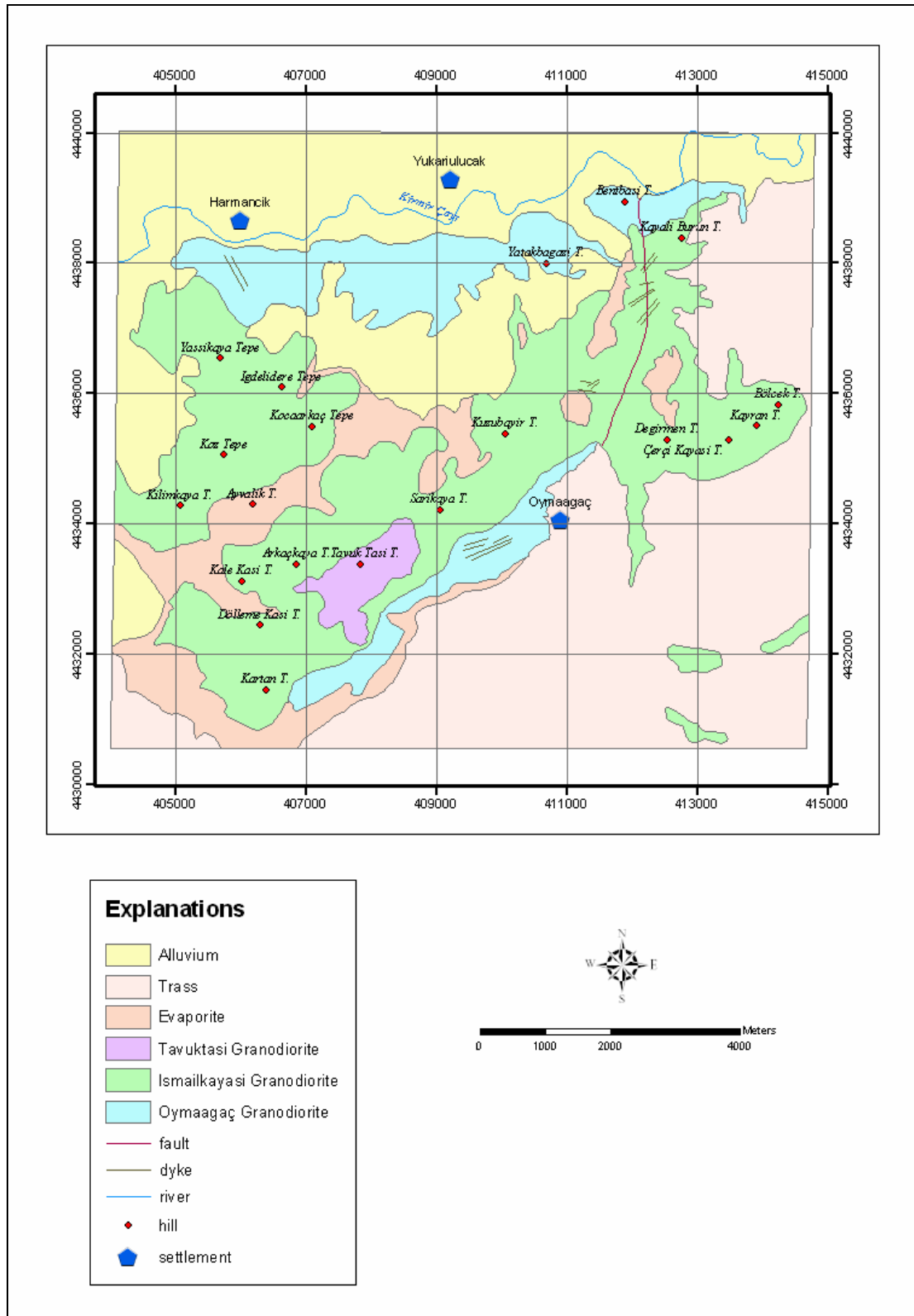


Figure 2.2. Geological map of the study area (modified after Zoroğlu and Kadioğlu, 2004).

Modal mineralogical compositions of the collected samples were determined by microscopic studies. According to Streckeisen (1976) diagram the granitoid rocks fall into granodiorite field (Zoroğlu and Kadioğlu, 2003; 2004; İpekçil, 2005) (Figure 2.3).

The granodiorite has gradational contact varying from outer zone to the inner part of the pluton. Alkali feldspar granite at NE direction cuts these three units in the form of aplitic dykes (Zoroğlu and Kadioğlu, 2003; 2004).

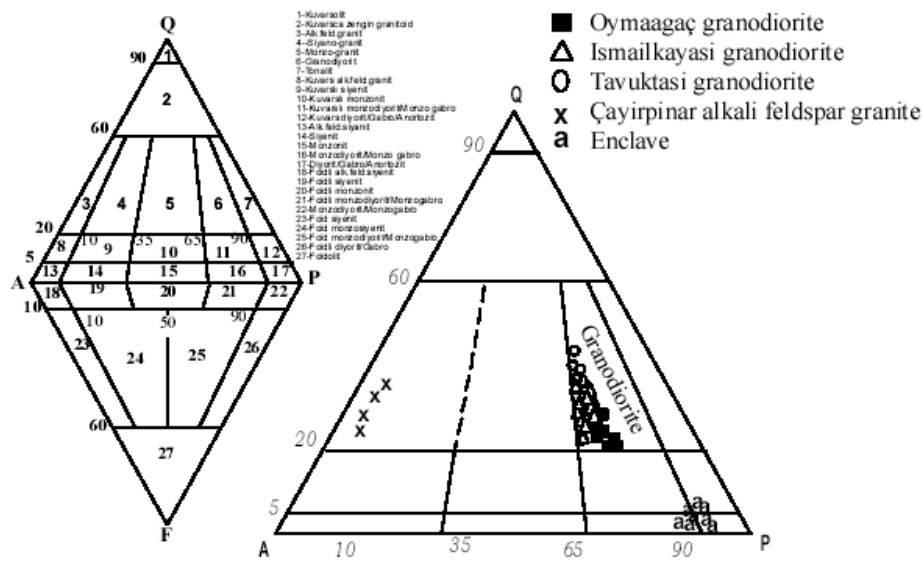


Figure 2.3. Modal mineralogic compositions of the rocks on QAPF diagram (Zoroğlu and Kadioğlu, 2004).

Quartz crystals have an anhedral crystal outline (Yohannes, 1993; İpekçil, 2005). They occur generally within the interstitial spaces among the early minerals. However, it is also observed as inclusions in the alkali-feldspars (İpekçil, 2005).

Plagioclase is represented by oligoclase and it shows polysynthetic and pericline twinning, prominently (Zoroğlu and Kadioğlu, 2003; 2004; İpekçil, 2005).

K-feldspar occurs dominantly as phenocrysts having a euhedral to subhedral crystals outline (İpekçil, 2005). They display Carlsbad twinning. String perthite is developed

due to albite – alkali feldspar exsolution in forming late stage solid solution (Yohannes, 1993).

Hornblende show simple twinning and characteristics of glomero-porphyric texture. In addition, inclusions of opaque minerals, titanite, plagioclase, and zircon can be observed within amphibole clusters (Zoroğlu and Kadioğlu, 2003; 2004).

Clinopyroxene is represented by diopside. It is found rarely in the central part of the granitoid (Yohannes, 1993).

Biotite has brown pleochroic color. They have euhedral to subhedral crystal outline (Yohannes, 1993; İpekgil, 2005).

Sphene crystals are euhedral and are probably early crystallizing phase. They are generally found with opaques (İpekgil, 2005).

Zircon occurs commonly as inclusion within plagioclase (Yohannes, 1993).

Pistacite occurs as a late stage crystallizing phase within interstitial space of early formed minerals (İpekgil, 2005).

Zeolite is found as stilbite in granitoid body. Stilbite is formed as a late crystallization product (Yohannes, 1993).

Apatite crystals can occur as isolated crystal or as inclusions mostly within feldspars. They show a well defined euhedral crystal shape (Yohannes, 1993; İpekgil, 2005).

Opaque minerals are mostly composed of titano-magnetite (Yohannes, 1993; İpekgil, 2005).

According to İpekgil (2005) the petrographical data is not sufficient to outline the zonation in the pluton and chemical data should also show the same trends. The petrographical studies of İpekgil (2005) support the study of Zoroğlu and Kadioğlu (2003, 2004). But the chemical investigation does not show significant differences in the composition of the Oymağaç Granitoid (İpekgil, 2005).

2.2.1. Oymaağaç Granodiorite

Oymaağaç Granodiorite is exposed on the north and southwest part of study area as the rim of the pluton (Figure 2.2). Within study area, any contact of Oymaağaç granodiorite with older units is not observed. It is covered by younger sedimentary units. Granodiorite is affected by N 45° E and N 30° W trending main joint systems (Zoroğlu and Kadioğlu, 2003; 2004).

Granodiorite contain mafic magmatic enclaves which range in size up to 30 cm and have a sharp contact with host rock. Enclaves are holocrystalline in terms of crystallinity (İpekgil, 2005).

Average grain size of rock is 0,3 mm. The granodiorite is composed of approximately 30 % of coarse feldspar minerals, 20-30 % of quartz mineral and 25 % of amphibole mineral (Table 2.1).

Dominant alteration types observed at the Oymaağaç Granodiorite chloritization, carbonatization, epidotization and clay alteration (Zoroğlu and Kadioğlu, 2003; 2004).

Table 2.1. Petrographic features used in the classification of Oymaağaç Granitoid (Zoroğlu and Kadioğlu, 2004).

	Feldspar phenocryst (%)	Quartz (%)	Amphibole (%)	Grain size of minerals (mm)	Mineralogical composition of enclaves
Oymaağaç Granodiorite	30	20 - 30	25	0.3	Diorite – Diorite Gabbro
İsmailkayası Granodiorite	20	30 - 40	15	0.5	Diorite – partially Quartzdiorite
Tavuktaş Granodiorite	5	40 - 50	5	1.5	Quartzdiorite – Monzodiorite

2.2.2. İsmailkayası Granodiorite

İsmailkayası granodiorite is the most widespread intrusive rock in the study area (Figure 2.2). It comprises two major joint systems which are oriented N40-50°E and N50-70°W. Alkali feldspar granite cuts it along the joint systems in the form of aplitic dykes (Zoroğlu and Kadioğlu, 2003; 2004).

It has a systematic change in mineralogical composition (amphibole content decreases and quartz content increases) and grain size from the outer zone to the inner part of the pluton. The mafic magmatic enclaves (diorite – quartz diorite composition) are finer grained, ovoid, rounded, with a sharp contact with host rock similar to Oymaağaç Granitoid (Figure 2.4). But the percentage of these enclaves is less than Oymaağaç granitoid.

The grains have an average size of 0.5 cm. Quartz constitutes about 30-40 % of rock and it is generally coarse (Figure 2.5). Amphibole minerals appear in their primary shapes and occupy 15 % of the rock. Sericitization, chloritization, clay alteration, and partially epidotization are main alteration types of the rock (Zoroğlu and Kadioğlu, 2003; 2004).



Figure 2.4. A field view of enclaves in İsmailkayası Granodiorite.



Figure 2.5. Macroscopic view of İsmailkayası Granodiorite.

2.2.3. Tavuktaş Granodiorite

Tavuktaş Granodiorite is exposed in the southeastern part of the study area and at the central part of pluton (Figure 2.2). It shows a gradual contact with İsmailkayası Granodiorite. Tavuktaş Granodiorite shows porphyric texture locally and contains approximately 5 % feldspar megacrysts. It has light beige to white color and granular texture. In field observations; it can be separated easily from Oymaağaç and İsmailkayası Granodiorites as being located at high altitudes, by its distinct light color, more quartz content and less amphibole content (Zoroğlu and Kadioğlu, 2003; 2004).

Tavuktaş Granodiorite consists of mainly 40-55 % quartz, 5 % amphibole (Table 2.1). Zircon, titanite, apatite and opaque minerals can be observed as accessory minerals in rock. Amphiboles appear mostly in primary mineral shape.

Epidotization and carbonatization are observed as secondary products along joints and fractures. Ovoid, rounded, ellipse enclaves can be observed similar to Oymaağaç and İsmailkayası Granodiorites, but these enclaves are light colored and mostly quartzdiorite and monzodiorite in composition (Zoroğlu and Kadioğlu, 2003; 2004).

2.2.4. Çayırpınar Alkali Feldspar Granite (Aplitic Dyke)

Aplitic dykes which vary a few cm to 100 m in thickness and change to a few km in length are observed almost all over the study area (Figure 2.6). The mafic magmatic enclaves are not included within these dykes. They have a light pink color and a sharp contact with host rock. These dykes are especially concentrated at Çayırpınar area and mentioned with this name. Alkali feldspar granite cuts granite and granodiorite along the main joints of the pluton at N 45° E direction (Zoroğlu and Kadioğlu, 2003; 2004).

The dykes are composed of quartz, alkali feldspar, plagioclase, and biotite. They are holocrystalline and hipidiomorphic and show graphic and myrmekitic textures (İpekgil, 2005).



Figure 2.6. Field view of Çayırpınar Alkali Feldspar Granite.

CHAPTER 3

BACKGROUND

This chapter introduces basic concepts used in this study. These are: 1) Reflectance Spectroscopy, 2) Spectral Unmixing, 3) Mineral Associations, 4) ASTER Image.

3.1. Principles of Reflectance Spectroscopy

Reflectance Spectroscopy is the study of light as a function of wavelength that has being reflected or scattered from a solid, liquid or gas. Photons of light incident on a mineral or rock, some are reflected from grain surfaces onto other grain surfaces, some passed through the grain onto other grains, and some are absorbed. They are reflected from the grain surfaces or refracted through a particle are said to be scattered. The scattered photons of light may encounter another grain or to be scattered away from the surface so they may be detected and measured. Photons are absorbed in minerals by several processes and the variety of absorption processes and their wavelength dependence allows us to derive information about the chemistry of a mineral or rock from its reflected light (Clark, 1999).

3.1.1. Absorption Processes

Photons entering an absorbing medium are absorbed according to Beer's Law:

$$I = I_0 \cdot e^{-kx}$$

where I is the observed intensity, I_0 is the initial intensity, k is an absorption coefficient, and x is the distance traveled by photon (Clark and Roush, 1984).

3.1.2. Causes of Absorption

The absorption features are caused by two general processes: electronic processes and vibrational processes.

3.1.2.1. Electronic Processes

Spectral reflectance characteristics of minerals are the result of different physical and chemical properties. Transitions between energy levels and compositional differences are manifested by absorption features at specific wavelengths. Absorption features can be caused by crystal field effects, charge transfer absorptions, conduction bands, and color centers.

3.1.2.1.1. Crystal Field Effects

The most common electronic process revealed in the spectral reflectance curves of minerals is due to unfilled electron shells of transition metal ions such as Fe, Ni, Cr, Co, etc. For all transition elements, d orbitals have identical energies in an isolated ion, but the energy levels split when the atom is located in a crystal field. This splitting of the orbital energy states enables an electron to be moved from a lower level into a higher one by absorption of a photon having an energy matching the energy difference between the states. This effect is called as the crystal field effect which varies with crystal structure from mineral to mineral, thus the amount of splitting varies and the same ion (Fe^{2+}) produces obviously different absorptions, making specific mineral identification possible from spectroscopy (Clark, 1999). Bidirectional reflection spectra of several minerals that contain ferrous iron are shown in Figure 3.1.

3.1.2.1.2. Charge Transfer Absorptions

Charge transfers, or inter-element electronic transitions, refer to the processes whereby absorbed energy causes an electron move between neighboring ions or between ions and ligands (Hunt, 1977). In Figure 3.1 spectral features of four

minerals (limonite, augite, carnotite, dumortierite) due to various types of charge transfer are illustrated. Limonite, augite, and carnotite illustrate various types of charge transfer spectral features. Dumortierite shows a strong feature in the visible due to π - π transitions.

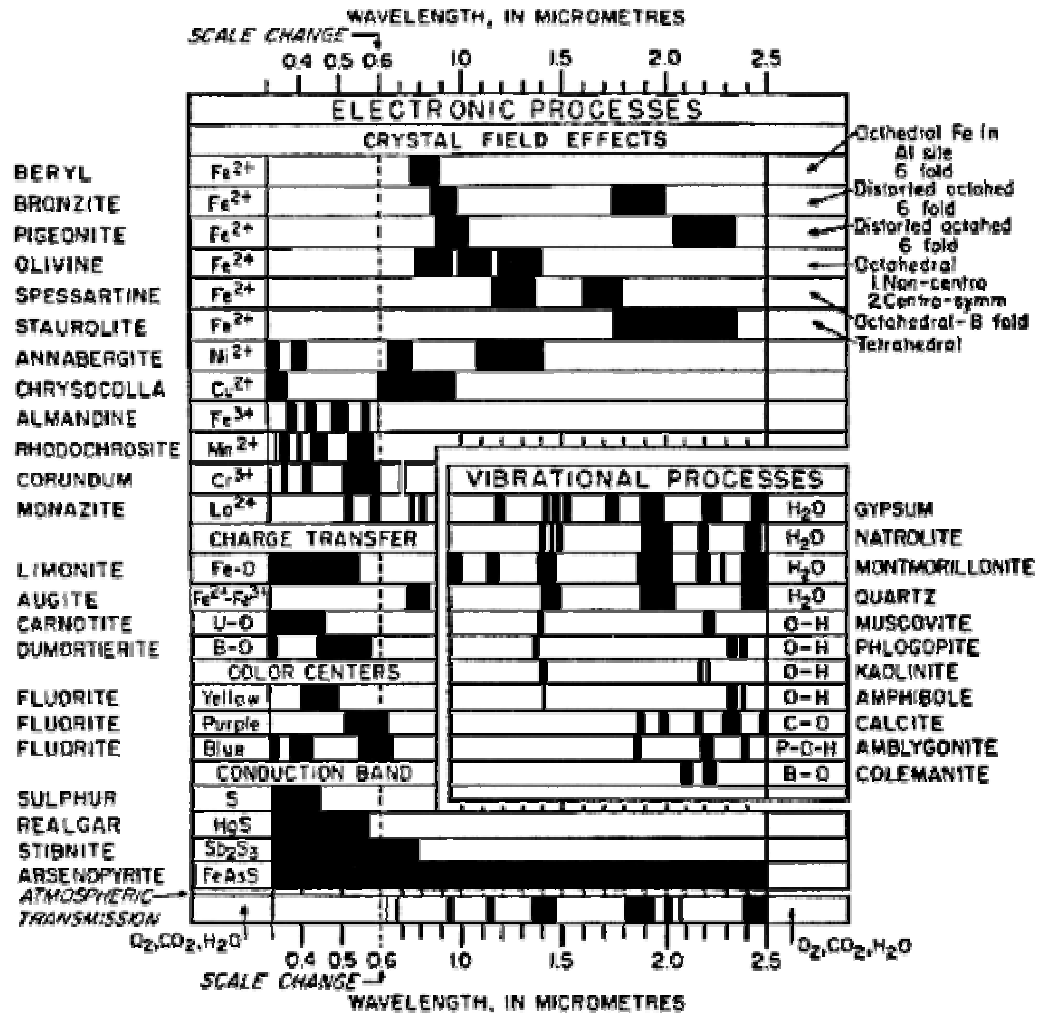


Figure 3.1. Spectral signature diagrams (from Hunt, 1977). The widths of the black bars indicate the relative widths of absorption bands.

3.1.2.1.3. Conduction Bands

In some periodic lattices the discrete energy levels of the outer shell electrons of the ions composing the lattice are broadened into energy bands by their proximity to each other. The electrons may exist in two energy levels; a higher level called the "conduction band" where electrons move freely throughout the crystal lattice,

and a lower energy region called the "Valence band" where electrons are attached to individual atoms. The difference between these two energy levels is called the *forbidden band* or *gap* (Hunt, 1977; Clark, 1999).

Figure 3.1 shows the spectra of four minerals, three of which, sulphur (S), cinnebar (HgS), and stibnite (Sb₂S₃) show well defined absorption edges marking the transition from intense absorption in the conduction band at shorter wavelengths to complete transmission in the forbidden gap at longer wavelengths. The fourth mineral spectrum, arsenopyrite (FeAsS), shows the conduction band extending completely across the VNIR range (Hunt, 1977).

3.1.2.1.4. Color Centers

Color Centers is the absorption phenomena by which a few minerals (for example yellow, purple and blue colors of fluorite) get their characteristic color. A color center is caused by irradiation (UV radiation) of an imperfect crystal lattice. Crystals in nature have lattice and these defects can produce discrete energy levels and electrons can become bound to them (Clark, 1999).

Spectral features are caused by color centers in natural crystals are illustrated in three fluorite spectra displayed in Figure 3.1.

As seen in Table 3.1, mechanisms such as Crystal Field Effects, Charge Transfer, Conduction Band Transitions and Color Centers are confined to the Visible and Near Infrared regions (Hauff, 2002).

Table 3.1. Spectral reflectance regions and absorption features (from Hauff, 2002).

REGION	DOMINANT MECHANISMS
VIS	Charge Transfer Ligand Identity
VIS / NIR	Crystal Field Effects Ligand Identity
SWIR	Vibrational Transitions
UV → SWIR	Conduction Bands

3.1.2.2. Vibrational Processes

The bonds in a molecule or crystal lattice behave like springs with weights attached that cause the system to vibrate. The frequency of vibration depends on the strength of each spring and their masses. The vibrational motions between atoms or molecules within a crystal lattice are called *normal modes* and *fundamentals*. The frequency of vibration depends on the strength of each spring and their masses. For a molecule with N atoms, there are 3N-6 normal modes of vibrations called *fundamentals*. Additional vibrations are called *overtones* when involving multiples of single fundamental, and *combinations* when involving different types of vibrations (Clark, 1999).

The absorption features observed in the SWIR, are the result of combinations and overtones of fundamental lattice vibrations which occur at longer wavelengths. The bonds giving rise to absorption features in the SWIR are found in molecules such as hydroxyl, water, carbonate and ammonia and between Al-OH, Mg-OH, and Fe-OH. Table 3.2 summarizes the common groups and the positions of their major spectral features in the SWIR region.

Table 3.2. Positions of major spectral features in SWIR region of common groups (from Hauff, 2002).

POSITION	MECHANISM	MINERAL GROUP
~1.4 μm	OH and WATER	CLAYS, SULFATES HYDROXIDES, ZEOLITES
~1.56 μm	NH ₄	NH ₄ SPECIES
~1.8 μm	OH	SULFATES
~1.9 μm	MOLECULAR WATER	SMECTITE
2.02, 2.12 μm	NH ₄	NH ₄ SPECIES
~2.2 μm	AL-OH	CLAYS, AMPHIBOLES SULFATES, MICAS
~2.35 μm	CO ₃ ⁻²	CARBONATES

All the identified spectral feature information is combined and displayed in spectra signature diagram in Figure 3.1. This figure serves to locate and identify the origin of

all electronic and vibrational features of particulate minerals. An atmospheric transmission spectrum is included at the bottom of Figure 3.1. This defines, to a large extent, those spectral ranges where data may be collected in terrestrial remote sensing applications (Hunt, 1977).

3.1.3. Spectral Variability

Spectral variability can be described as changes in the profiles and wavelengths of absorption features, diagnostic of specific mineral species, as a function of changes in physical parameters that define that species and its interaction with its environment. The chemical composition, crystallinity, associated phases, orientation, degree of weathering, paragenesis, habit, texture, grain size, reflectance (or albedo), presence of water, matrix, and transparency all influence the spectral curve and absorption features (Hauff, 2002). These variables all have to be considered during evaluation of the spectrum.

3.1.3.1. Crystallinity

Crystallinity can be described as the degree of ordering in a crystal lattice. This is controlled by the type, size, and arrangement of atoms and molecules within the unit cell, the charge on them and the bonds that hold them in a particular structural configuration (Hauff, 2002). Generally, variations in crystallinity are reflected by variations in the shapes of the diagnostic absorption features. The absorption features typically are well defined and sharp with increasing crystallinity.

Changes in crystal structure were observed by clay mineralogists and parameterized to the crystallinity indexes used in XRD. These indexes show a gradational change in spectral profile and water content which is a manifestation of changes in order.

Crystallinity can change with temperature, weathering processes which act upon a mineral structure to degrade it or create another phase, and mechanical processes.

3.1.3.2. Chemical Composition

The chemical composition one way of differentiating the species but since there is an overlap; it must be done within restricted environments. And except in generalities it is difficult to cross environments of paragenesis. In this case it is needed to understand the environments better from point of view of the spectral perspective and also to utilize the concept of site specific data bases.

One of the most useful applications of SWIR spectroscopy is the sensitivity to chemical substitution in mineral series. The vibrational energies of the structural bonds between atoms and molecules and within molecules change as a function of bond length. A major influence on the length of bonds is the ionic radius of the bonding elements and molecules. Ionic radius size is unique to specific atoms. Therefore as different sized atoms occupy different lattice sites, they will have different bond lengths to other lattice components. These bonds will vibrate at different energies and therefore have different wavelength values and subsequently can be uniquely identified by these wavelengths. Thus, any infrared active mineral group or solid solution series where chemical substitution is a defining factor in mineral speciation and sub-speciation can be defined within the infrared methodology (Hauff, 2002). This involves groups such as amphiboles, serpentines, chlorites, alunites, jarosites, carbonates, tourmalines, biotites, muscovites, smectites and illites.

Compositional variations are typically represented by shifts in the wavelength positions of diagnostic absorption features, with the overall characteristic spectral signature of the mineral remaining unchanged.

3.1.3.3. Orientation

Many minerals, notably phyllosilicates (clays, micas, serpentines, chlorites) show the effects of orientation of the crystallites along a preferred crystal axis. Because many of phyllosilicates have a platy or flake habit, will orient with the 001 basal plane or flat side of the crystallite up. These emphasize the water feature (Hauff, 2002).

3.1.3.4. Grain Size

The amount of light scattered and absorbed by a grain is dependent on grain size (Clark and Roush, 1984). A larger grain has a greater internal path where photons may be absorbed according to Beers Law. In a smaller grain there are proportionally more surface reflections compared to internal photon path lengths, or in other words, the surface area to volume ratio is a function of grain size (Clark, 1999).

3.1.3.5. Transparency

The effects of transparency are more an issue in field spectroscopy. In order to prevent this effect, a metal reflector can be put behind the crystal back reflecting the energy into the instrument detector (Hauff, 2002).

3.1.3.6. Water

Water is one of the substances for which infrared spectroscopy has the most sensitivity. Therefore, it apparently dominates most spectra for water bearing materials (Hauff, 2002).

3.1.4. Spectral Libraries

Extensive reference libraries of mineral spectra are a result of spectral variability. Several libraries of reflectance spectra of natural and man-made materials are available. United States Geological Survey (USGS) Spectral Library, The California Institute of Technology Jet Propulsion Laboratory (JPL), and Johns Hopkins University are offered free of charge.

However, these libraries offer only one or two spectra per mineral species and it is not sufficient to document the variability found in mineral species. The site-specific libraries are necessary because of spectral variability (Hauff, 2002).

3.2. Spectral Unmixing

Spectral unmixing method (Adams *et al.*, 1986) expresses that the spectrum measured depend linearly on the spectra of components.

Spectra of a material includes spectral features in the form of lines, bands, or slope changes whose positions, shapes, and intensity values are a consequence of a particular material's chemical constitution, atomic geometry, and, phase (Hunt, 1979). Diagnostic features of spectral data can be used to identify minerals even for mineral mixtures estimation of mineral abundance and grain size can be possible.

During this analysis, measured spectra of samples were assumed as a linear spectral mixture of individual mineral components within the rock. Spectral unmixing uses a summation of the pure endmember spectra multiplied by abundance of the endmember constituents. This mixture model can be expressed as:

$$R_{\text{mixture}} = \sum f_i \cdot R_{\text{min}} + \varepsilon \quad (0 \leq f_i \leq 1)$$

Where R_{mixture} mixture is the modeled mineral mixture reflectance, f_i is abundance of mineral, R_{min} library reflectance of mineral, and ε is random error (difference between modeled mineral mixture reflectance and measured reflectance spectra of mixture).

In order to estimate the relative proportions of minerals contained within representative samples, firstly endmembers have to be defined.

3.3. Mineral Associations in Granodiorite Rocks

Granodiorite is an intermediate colored, medium to coarse-grained rock that is one of the most abundant intrusive rocks. It falls between granite and quartz diorite, containing more dark minerals than granite but less than quartz diorite. Also, it contains more plagioclase than potassium feldspar. The light colored minerals are quartz and feldspar; the feldspar is a mixture of orthoclase and plagioclase. The dark colored crystals are hornblende and/or biotite.

Granodiorite, like diorite, is the result of fractional melting of a mafic parent rock above a subduction zone. It is commonly produced in volcanic arcs, and in cordilleran mountain building (subduction along the edge of a continent)

(<http://csmres.jmu.edu/geollab/Fichter/IgnRx/disthtml.html>).

3.3.1. Endmember Determination of Oymağaç Granitoid

Mineral association of Oymağaç Granitoid is based on the literature survey (Zoroğlu and Kadioğlu, 2003; 2004; Yohannes, 1993; İpekgil, 2005). In these studies mineralogic composition of granodiorite was determined via petrographic and geochemical methods.

Oymağaç Granitoid was composed of plagioclase (oligoclase), alkali feldspar (orthoclase, perthite), quartz and hornblende including minor amount of biotite with accessory minerals such as; sphene, zircon. Also diopside and stilbite were found as late crystallization products. Illite, chlorite, epidote, calcite, and zoisite were observed as alteration product. These mineral were tabulated in Table 3.3.

Table 3.3. Mineral components of granitoid used for analysis.

Major Minerals	Minor Minerals	Secondary Minerals
Quartz	Diopside	Illite
Oligoclase	Stilbite	Chlorite
Alkali feldspar	Sphene	Epidote
Hornblende	Zircon	Calcite
Biotite		Zoisite

The short descriptions of these minerals are given below.

Quartz: Quartz (SiO₂) is major constituent of all granitoid body. *Quartz4* is used as reference spectrum for quartz mineral during analyze. Water bearing quartz has diagnostic features at 1400 and 1900 nm, but not all quartz carries water. This can be confused with many minerals and mixtures. Quartz without water does not have any distinctive absorption features in VNIR and SWIR.

Oligoclase: Plagioclase is found to be of oligoclase $((\text{Na,Ca})\text{Al}(\text{Al,Si})\text{Si}_2\text{O}_8)$. As endmember *oligoclase2* is selected for analysis. Oligoclase spectrum shows a major absorption feature in 1935 nm.

Alkali feldspar: Alkali feldspars mainly are observed as orthoclase $(\text{KAlSi}_3\text{O}_8)$. In addition to this, perthite $(\text{KAlSi}_3\text{O}_8 + \text{NaAlSi}_3\text{O}_8)$ minerals are developed. During spectral mixture analyse *orthoclase2* is used among orthoclase spectra of USGS spectral library. Besides, perthite spectrum is only one of its kinds in USGS spectral library. Alkali feldspars do not exhibit strong absorption features VNIR and SWIR.

Hornblende: Hornblende $((\text{Ca,Na})_{2-3}(\text{Mg,Fe,Al})_5\text{Si}_6(\text{Si,Al})_2\text{O}_{22}(\text{OH})_2)$ is represented by *hornblende3* spectrum of USGS spectral library. Hornblende spectrum has a doublet feature in the 2300 nm to 2400 nm range.

Biotite: Biotite $(\text{K}(\text{Mg,Fe})_3(\text{AlSi}_3\text{O}_{10}(\text{OH})_2)$ is found in very small amounts. Only one biotite spectrum exists in USGS spectral library. Diagnostic features for biotite are found at $2250\pm 2340 - 2370$ and 2400 nm. The biotite spectrum can also be affected by the orientation of the mineral. Highly oriented biotites give very weak reflections and very low spectral response (Hauff, 2002).

Diopside: Clinopyroxenes are represented by diopside $(\text{CaMg}(\text{Si}_2\text{O}_6))$. *Diopside2* is selected as endmember. According to library description it has an absorption band at 1050 nm indicates the presence of ferrous iron in the crystal structure. Also diopside spectrum exhibits a large broad feature in 1914 and a major deep feature in 2314 nm.

Stilbite: Stilbite $(\text{NaCa}_2\text{Al}_5\text{Si}_{13}\text{O}_{36}\cdot 14\text{H}_2\text{O})$ is a zeolite group mineral. *Stilbite1* is found most representative for analysis. It is described in sample description as spectrally pure. The major absorption features of stilbite are in 964, 1158, 1419, and 1912 nm.

Sphene: Sphene (CaTiSiO_5) occurs commonly as large well developed crystals. This suggests that it is an early phase crystal. USGS spectral library has only one sample spectrum for sphene. Sphene spectrum does not exhibit very distinctive absorption features nevertheless it shows some small features in 2325 and 2255 nm.

Zircon: Zircon (ZrSiO_4) has unique spectrum in USGS spectral library. Zircon has some major absorption features in 1114, 1502, and 2074 nm.

Illite: Illite ($\text{K}_{1-1.5}\text{Al}_4(\text{Si}_{6.5-7}\text{Al}_{1-1.5})\text{O}_{20}(\text{OH})_4$) is produced by the alteration of alkali feldspar minerals. *Illite5* spectrum of USGS spectral library is preferred as reference spectra of illite. Distinctive absorption features are in 1400, 1900, and 2200 nm and between 2300-2500 nm differentiate interlayer water, structural water (OH^-), and some octahedral layer characteristics (Kruse and Hauff, 1991).

Chlorite: Chlorite ($(\text{Mg,Fe})_3(\text{Si,Al})_4\text{O}_{10}(\text{Mg,Fe})_3(\text{OH})_6$) is developed mostly at the expense of hornblende and biotite. *Chlorite5* spectrum of USGS spectral library is used in this study. The major absorption features produced by hydroxyl groups at approximately at 2250 and 2330 nm, as well as three absorption features produced by Fe^{2+} at 715, 890, and 1110 nm in VNIR. Magnesium bearing samples have three features in the lower wavelength regions around 1400 nm, a very sharp feature at 1395 nm, and features towards the lower wavelengths at the 2300 nm region.

Epidote: Epidote ($\text{Ca}_2(\text{Al,Fe})\text{Al}_2\text{O}(\text{SiO}_4)(\text{Si}_2\text{O}_7)(\text{OH})$) is known as alteration mineral. *Epidote1* is selected as endmember spectrum from USGS spectral library. The visible portion of the epidote spectrum is dominated by Fe^{3+} ligand field transitions with bands at 366, 457, 616, and 560 nm. It shows three bands at 1357, 1409, and 1548 nm which are probably OH overtones (Clark et al., 1990). The feature at 1500-1570 nm is one of the most diagnostic features for epidote. When epidote dominates the sample, the feature in the 2338-2346 nm regions is large and deep with well developed smaller minima at 2248-2258 nm. When present in small amounts, epidote can be confused with some chlorites, carbonates and possibly serpentine. Also it is possible to confuse with clinozoisite as the major absorption features share similar wavelengths (Hauff, 2002).

Calcite: Calcite (CaCO_3) is observed as alteration product. *Calcite3* is chosen as reference spectra amongst calcite spectrum of USGS spectral library. Calcite exhibits major absorption features at approximately 2350 and 2530 nm. Calcite can be missed if it is mixed with illite and/or chlorites in small amounts.

Zoisite: Zoisite ($\text{Ca}_2\text{Al}_3(\text{SiO}_4)_3(\text{OH})$) occurrence is related with alteration of plagioclase. During analyse single spectrum of USGS spectral library for zoisite is used. Zoisite spectrum has a long OH stretch position. The long position of first overtone near 1650 nm reflects the long position of the fundamental in zoisite (Clark et al., 1990).

3.4. ASTER Data

The Advanced Spaceborne Thermal Emission and Reflection Radiometer (ASTER) is a high spatial resolution, multispectral imaging radiometer that was launched on the first National Aeronautics and Space Administration (NASA) spacecraft of the Earth Observing System (Terra) in December 1999.

ASTER spectrally covers the visible and near-infrared, shortwave infrared, and thermal infrared regions with 14 spectral bands, and creates high spatial resolution (15-90 m) multispectral images of the Earth's surface. The primary science objective of the ASTER mission is to improve understanding of the local and regional scale processes occurring on or near the earth's surface and lower atmosphere, including surface-atmosphere interactions. Specific areas of the science investigation are: (a) land surface climatology, (b) vegetation and ecosystem dynamics, (c) volcano monitoring, (d) hazard monitoring, (e) aerosols and clouds, (f) carbon cycling in the marine ecosystem, (g) hydrology, (h) geology and soil, and (i) land surface and land cover change (Yamaguchi *et al.*, 1998).

ASTER consists of three different subsystems (Table 3.4): the visible and near-infrared (VNIR) system has three bands covering 0.52-0.86 μm with a spatial resolution of 15 m, the shortwave infrared (SWIR) subsystem has six bands covering 1.60-2.45 μm with a spatial resolution of 30 m; and the thermal infrared (TIR) subsystem has five bands covering 8.125-11.65 μm with a spatial resolution of 90 m. The VNIR system includes a separate, single spectral band radiometer inclined backward at an angle of 27.6° to provide an along-track stereo capability. Each ASTER scene covers 60x60 km^2 area on Earth surface. Cross-track pointing will

allow viewing of any spot on Earth a minimum of once every 16 days (Abrams, 2000). Table 3.4 shows the baseline performance requirements for the ASTER instrument.

Table 3.4. ASTER baseline performance requirements (Yamaguchi *et al.*, 1998).

Subsystem	Band No.	Spectral Range (μm)	Radiometric Resolution	Absolute Accuracy (σ)	Spatial Resolution	Signal Quantization Levels
VNIR	1	0.52 - 0.60	NEΔρ ≤ 0.5 %	≤ ± 4 %	15 m	8 bits
	2	0.63 - 0.69				
	3N	0.78 - 0.86				
	3B	0.78 - 0.86				
SWIR	4	1.600 - 1.700	NEΔρ ≤ 0.5 %	≤ ± 4 %	30 m	8 bits
	5	2.145 - 2.185	NEΔρ ≤ 1.3 %			
	6	2.185 - 2.225	NEΔρ ≤ 1.3 %			
	7	2.235 - 2.285	NEΔρ ≤ 1.3 %			
	8	2.295 - 2.365	NEΔρ ≤ 1.0 %			
	9	2.360 - 2.430	NEΔρ ≤ 1.3 %			
TIR	10	8.125 - 8.475	NEΔT ≤ 0.3 K	≤ 3K(200-240K)	90 m	12 bits
	11	8.475 - 8.825		≤ 2K(240-270K)		
	12	8.925 - 9.275		≤ 1K(270-340K)		
	13	10.25 - 10.95		≤ 2K(340-370K)		
	14	10.95 - 11.65				

Stereo Base-to-Height Ratio	0.6 (along-track)
Swath Width	60 km
Total Coverage in Cross-Track Direction by Pointing	232 km
MTF at Nyquist Frequency	0.25 (cross-track) 0.20 (along-track)
Band-to-Band Registration	0.2 pixels (intra-telescope) 0.3 pixels (inter-telescope)
Peak Data Rate	89.2 Mbps
Mass	406 kg
Peak Power	726 W

CHAPTER 4

DATA

Two sets of data are used in this study. These are the samples collected in the field and the ASTER satellite image. Basic characteristics of these data and pre-processes about these data are explained below.

4.1. Samples

Rock samples are collected in the field for spectral analysis at thirty two locations. At each location, both weathered and fresh samples are collected. During the selection of sample location, it is considered to collect enough samples from each granodiorite considering the extent on the area for each granitoid type. The coordinates of each sampling location is recorded using a Global Positioning System (GPS). The map of sample locations is shown in Figure 4.1

Spectra of collected rock samples are measured with ASD spectrometer used a directional light source and fiber optic probe to collect light. ASD FieldSpec® Pro is a portable spectrometer designed for field use with a sampling interval 2 nm and a spectral resolution of 10 nm. It covers a spectral range from 350 to 2500 nm (VIS-SWIR region). Raw radiance data are corrected to reflectance by reference to a Spectralon® (barium sulfate – BaSO₄) reflectance standard.

The fresh samples are measured three times from different points on sample. An average spectrum of these three measurements is used for analysis. All measurements are given in Table 4.1. A detailed table of all measurements with sample spectra is tabulated in Appendix A.

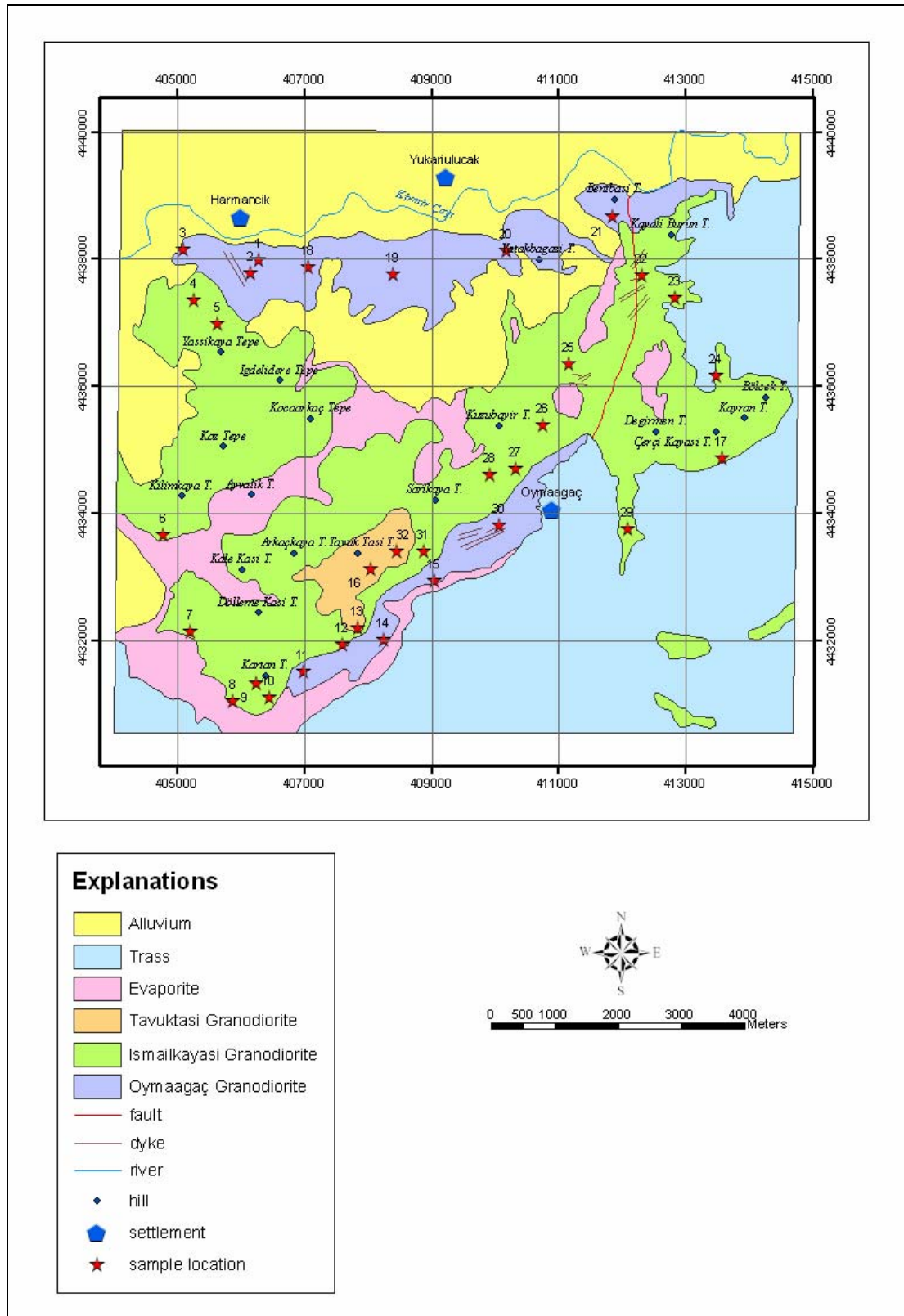


Figure 4.1. Sample location map.

Table 4.1. Sample list with coordinates and lithology (number of measurement is shown in bracket).

Location No	Coordinates		Samples		Lithology
	X	Y			
1	406284	4437986	fresh (3)	weathered (1)	Oymaağaç
2	406155	4437779	fresh (3)	weathered (1)	Oymaağaç
3	405088	4438155	fresh (3)	weathered (1)	Oymaağaç
4	405268	4437352	fresh (3)	weathered (1)	İsmailkayası
5	405639	4436979	fresh (3)	weathered (1)	İsmailkayası
6	404784	4433672	fresh (3)	weathered (1)	İsmailkayası
7	405205	4432143	fresh (3)	weathered (1)	İsmailkayası
8	405879	4431059	fresh (3)	weathered (1)	İsmailkayası
9	406234	4431328	fresh (3)	weathered (1)	İsmailkayası
10	406438	4431107	fresh (3)	weathered (1)	İsmailkayası
11	406976	4431513	fresh (3)	weathered (1)	Oymaağaç
12	407590	4431994	fresh (3)	weathered (1)	İsmailkayası
13	407830	4432207	fresh (3)	weathered (1)	Tavuktaş
14	408246	4432014	fresh (3)	weathered (1)	Oymaağaç
15	409037	4432951	fresh (3)	weathered (1)	Oymaağaç
16	408035	4433132	fresh (3)	weathered (1)	Tavuktaş
17	413565	4434873	fresh (3)	weathered (1)	İsmailkayası
18	407053	4437882	fresh (3)	weathered (1)	Oymaağaç
19	408392	4437763	fresh (3)	weathered (1)	Oymaağaç
20	410175	4438140	fresh (3)	weathered (1)	Oymaağaç
21	411852	4438667	fresh (3)	weathered (1)	Oymaağaç
22	412306	4437749	fresh (3)	weathered (1)	İsmailkayası
23	412828	4437388	fresh (3)	weathered (1)	İsmailkayası
24	413477	4436178	fresh (3)	weathered (1)	İsmailkayası
25	411155	4436355	fresh (3)	weathered (1)	İsmailkayası
26	410750	4435394	fresh (3)	weathered (1)	İsmailkayası
27	410330	4434700	fresh (3)	weathered (1)	İsmailkayası
28	409909	4434613	fresh (3)	weathered (1)	İsmailkayası
29	412092	4433767	fresh (3)	weathered (1)	İsmailkayası
30	408882	4433414	fresh (3)	weathered (1)	Oymaağaç
31	410070	4433808	fresh (3)	weathered (1)	İsmailkayası
32	408444	4433404	fresh (3)	weathered (1)	Tavuktaş

4.2. ASTER Data

A scene of study area taken from ASTER L1B 0007130900020309050937 image acquired on 13 July 2000 is used in this analysis. Preprocessing of image includes registering, removing haze effects and generating a subset of study area.

ASTER level-1B data have been registered to UTM Zone 36 WGS 84 using a first-order rotation by PCI Geomatica software.

Path radiance is the result the light scattering back to the satellite sensor by haze in the earth's atmosphere. Since the amount of scattering varies with wavelength, the path radiance effect is greatest for the shortest wavelengths, falling off rapidly with increasing wavelength (TNT Mips User Guide). In this study, linear regression method is used to calculate the path radiance. ASTER bands are correlated with band 1 and the haze amounts are determined (Figure 4.2). For band 1 haze amount is decided as 49. To remove path radiance this amount is subtracted from band 1. The haze amounts which are removed were listed in Table 4.2.

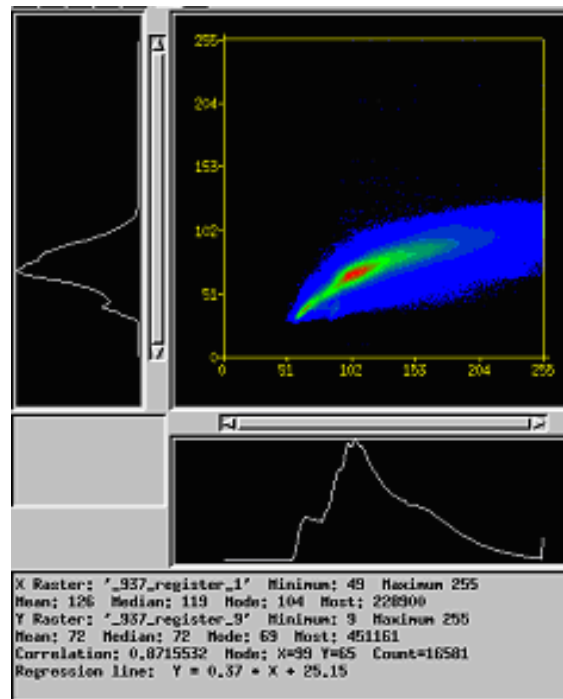


Figure 4.2. Band correlation graph between band 1 and band 9.

Table 4.2. Removed haze amounts for ASTER bands

ASTER Band No.	Removed value
Band 1	49
Band 2	30
Band 3	27
Band 4	15
Band 5	9
Band 6	7
Band 7	9
Band 8	9
Band 9	9

Before the processes the image is masked to the boundary of the study area. A subset from full ASTER scene is prepared from the granitoid boundary proposed by Zoroğlu and Kadioğlu (2003, 2004) (Figure 4.3).

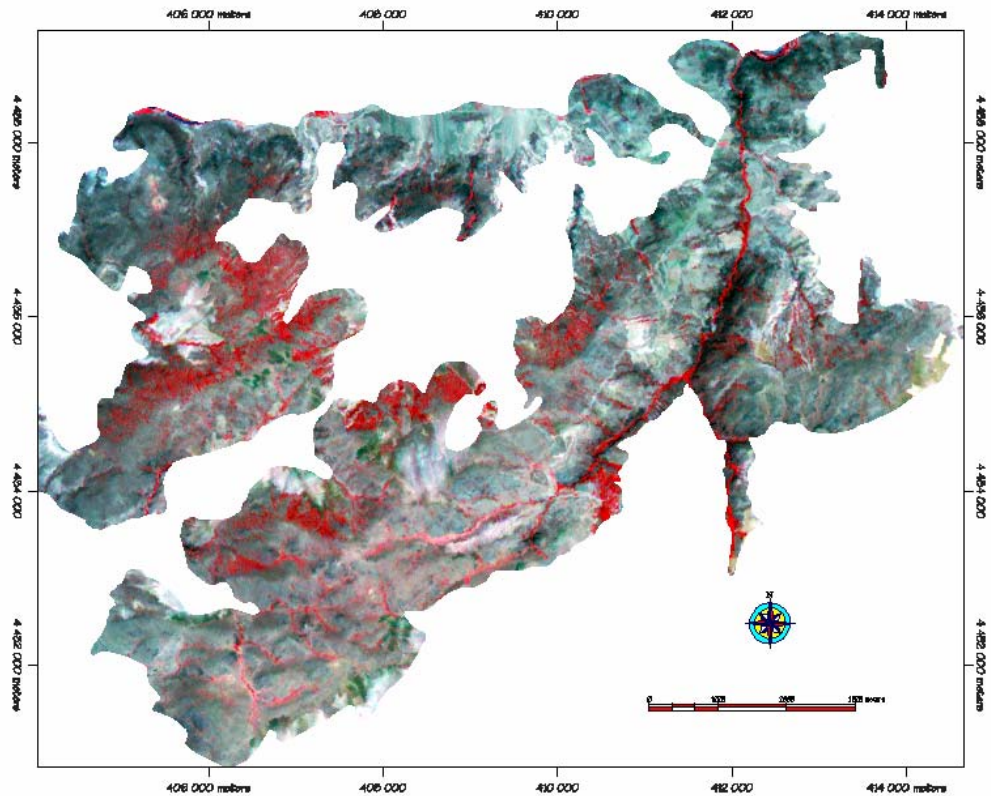


Figure 4.3. Boundary of the study area masked according to the granitoid boundary suggested by Zoroğlu and Kadioğlu (2003, 2004). The image is RGB (321) band combination of the area.

CHAPTER 5

ANALYSES

5.1. Methodology

A flowchart illustrating the methodology applied in this study is given in Figure 5.1. Two main methods are used to achieve the aim of the study. The first method involves the determination of mineral content percentages through the spectral analysis obtained by field spectrometry from representative samples of the study area. Collection and measurement of rock samples were explained in Chapter 4.

The second method is the analysis of ASTER satellite image using Crosta Technique. This technique is commonly applied for the detection of alteration minerals. After application of this technique, some threshold values are used for the preparation of the final maps.

The next step in the methodology is the comparison of the results of two techniques which is carried out by plotting the results of both techniques on the diagrams. Using the anomalies obtained by Crosta Technique, a combination map was created for alteration minerals.

The last step is the accuracy assessment by comparing the results of spectral analysis with geochemical and microscopic analysis obtained from the literature.

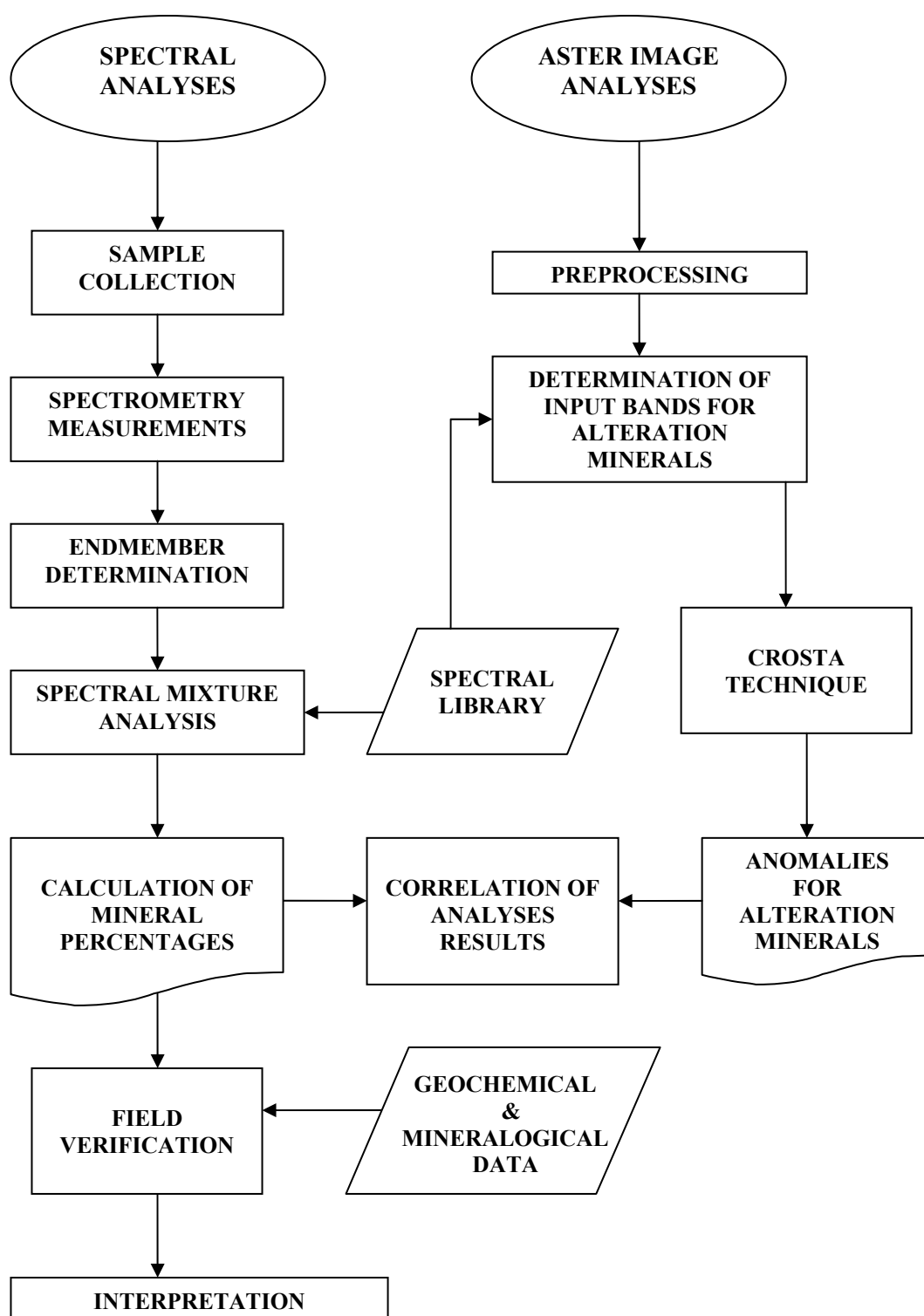


Figure 5.1. Flowchart of the study.

5.2. Spectral Analyses

In order to estimate the relative proportions of minerals contained within representative samples, firstly endmembers have to be defined. Although the endmembers in granodioritic rocks are reported in most textbooks, the selection of the endmembers is based on the analyses carried out by Yohannes (1993), Zoroğlu and Kadioğlu (2003, 2004), and İpekçil (2005). In these studies mineralogic composition of granodiorite was determined via petrographic and geochemical methods. Accordingly the granitoid is composed of plagioclase (oligoclase), alkali feldspar (orthoclase, perthite), quartz and hornblende including minor amount of biotite with accessory minerals such as; sphene, zircon. Also diopside and stilbite are found as late crystallization products. Illite, chlorite, epidote, calcite, and zoisite are observed as alteration product. Therefore these 15 minerals are selected to be analyzed in this study. Some properties of these minerals are tabulated in Table 5.1.

Table 5.1. Endmembers used in analysis and some properties.

Mineral	Formula	Occurrence	Position of major absorptions (nm)	Used USGS spectrum
Quartz	SiO ₂	Major	in TIR region	quartz4
Oligoclase	(Na,Ca)Al(Al,Si)Si ₂ O ₈	Major	1935	oligoclase2
Orthoclase	KAlSi ₃ O ₈	Major	in TIR region	orthoclase2
Perthite	KAlSi ₃ O ₈ + NaAlSi ₃ O ₈	Major	in TIR region	perthite
Hornblende	(Ca,Na) ₂ -3(Mg,Fe,Al) ₅ Si ₆ (Si,Al) ₂ O ₂₂ (OH) ₂	Major	doublet feature between 2300-2400	hornblende3
Biotite	K(Mg,Fe) ₃ (AlSi ₃ O ₁₀ (OH) ₂	Major	2250±2340, 2370, 2400	biotite
Diopside	CaMg(Si ₂ O ₆)	Minor	1050, 1914, 2314	diopside2
Stilbite	NaCa ₂ Al ₅ Si ₁₃ O ₃₆ .14H ₂ O	Minor	964, 1158, 1419, 1912	stilbite1
Sphene	CaTiSiO ₅	Minor	2325, 2255	sphene
Zircon	ZrSiO ₄	Minor	1114, 1502, 2074	zircon
Illite	K1-1.5Al ₄ (Si _{6.5} -7Al ₁ -1.5)O ₂₀ (OH) ₄	Secondary	1400, 1900, 2200 and between 2300-2500	illite5
Chlorite	(Mg,Fe) ₃ (Si,Al) ₄ O ₁₀ .(Mg,Fe) ₃ (OH) ₆	Secondary	715, 890, 1110, 1395, 1400, 2250, 2330, 2300	chlorite5
Epidote	Ca ₂ (Al,Fe)Al ₂ O(SiO ₄)(Si ₂ O ₇)(OH)	Secondary	366, 457, 616, 560, 1357, 1409, 1548, 1500-1570, 2338-2346, 2248-2258	epidote1
Calcite	CaCO ₃	Secondary	2350, 2530	calcite3
Zoisite	Ca ₂ Al ₃ (SiO ₄) ₃ (OH)	Secondary	1650	zoisite

The laboratory spectra of the determined minerals are gathered from USGS spectral library. In this library, some minerals have more than one spectrum including a series of grain sizes and/or solid solution series. In such cases, most representative library spectra were selected. The endmember spectra from USGS library used in this study for major, minor, and secondary components of granodiorite are illustrated in Figures 5.2 and 5.3.

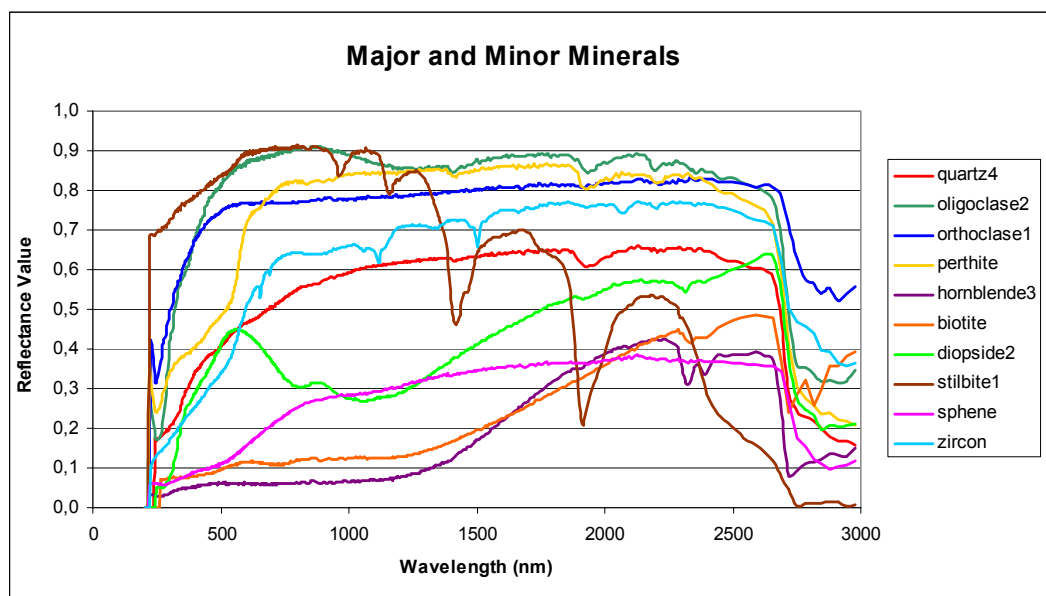


Figure 5.2. USGS spectral reflectance curves of major and minor minerals of granodiorite

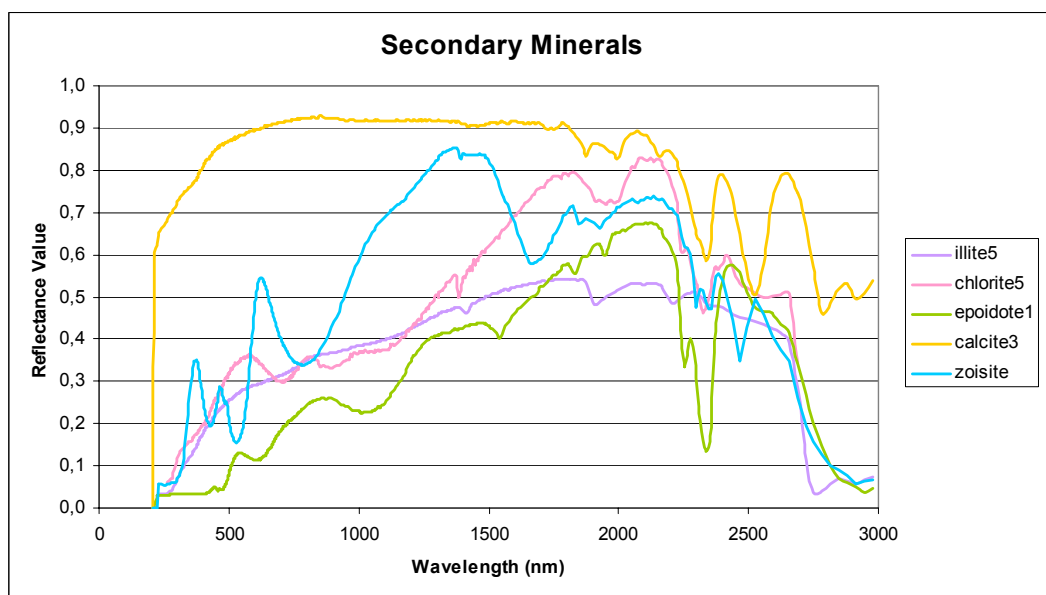


Figure 5.3. USGS spectral reflectance curves of secondary minerals of granodiorite.

Calculation of mineral percentage of the each sample is done with SPECMIN software using “search” function. SPECMIN software helps to search a sample according to the absorption characteristics of the sample spectrum. The user interface of feature search function of SPECMIN software is shown in Figure 5.4. Sample spectra are displayed in the sample spectra window. The sample spectrum is displayed in red and the significant spectral features for the spectrum are given in the “Features” list. By changing threshold value, number of absorption features may increase or decrease. During this study, the threshold value is determined as 0.50. When the selected sample spectrum is “searched”, the active spectral library (USGS) investigates the spectra that contain listed feature(s). Some minerals are listed according to coinciding absorption features with sample spectra. The defined end-members are selected from this list and attached to another part. Finally, the selected end-members are mixed and end-member proportions are calculated automatically by the software. The above mentioned process is applied all fresh and weathered samples collected in the area. The percentages of the minerals are listed in Table 5.2 and Table 5.3 for fresh and weathered samples, respectively.

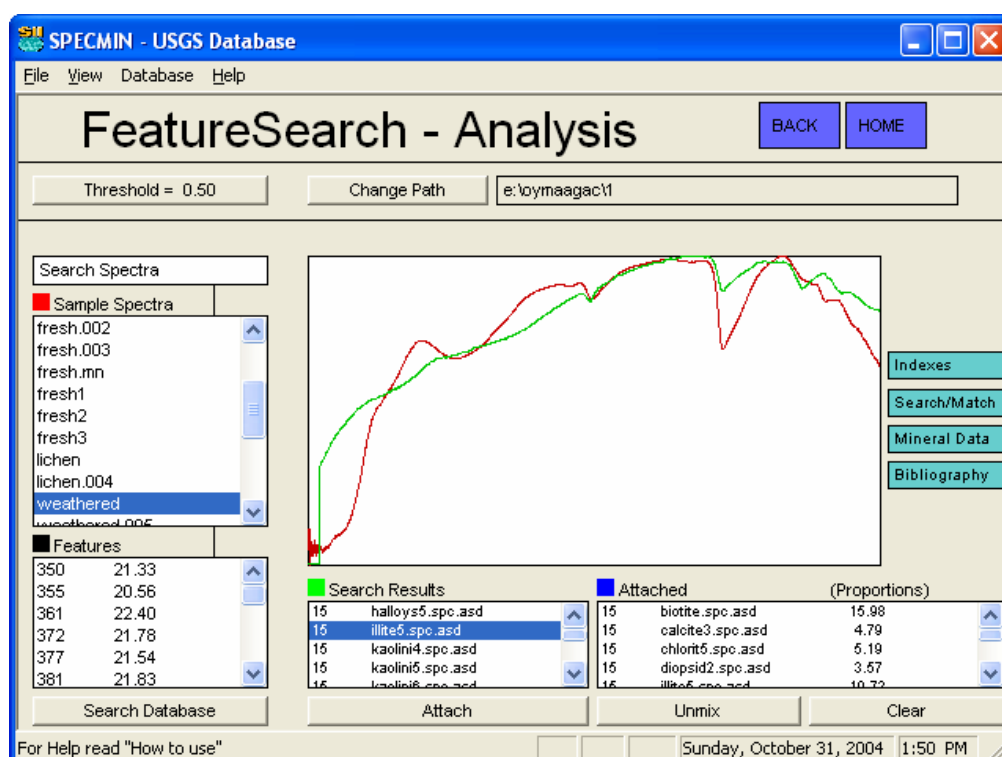


Figure 5.4. SPECMIN “feature search” window.

Table 5.2. Quantitative percentages of minerals for fresh samples (O: Oymaağaç; I: İsmailkayası; T: Tavuktaş granodiorite). Values are given in percentages.

Sample No	quartz4	oligoclase2	orthoclase2	perthite	hornblende3	biotite	diopside2	stilbite1	sphene	zircon	Lithology
1	25.1	16.2	-	14.8	17.8	-	8.5	3.7	13.9	-	O
2	-	55.4	-	11.3	2.4	6.4	-	10.3	14.2	-	O
3	-	54.9	-	25.3	-	11.8	1.2	6.8	-	-	O
4	15.3	22.3	-	5.4	13.7	-	10.2	6.9	26.2	-	I
5	-	57.2	-	12.9	9.8	7.0	0.7	4.5	7.9	-	I
6	-	52.0	-	8.4	9.5	-	5.3	7.7	17.1	-	I
7	-	63.0	-	16.8	1.7	13.9	-	4.6	-	-	I
8	3.4	51.2	-	18.3	12.7	-	5.4	6.1	2.9	-	I
9	-	68.1	-	15.7	8.7	0.1	-	7.4	-	-	I
10	4.8	60.9	-	14.0	10.9	4.2	-	5.2	-	-	I
11	4.6	62.1	-	18.3	11.1	0.7	-	3.2	-	-	O
12	6.8	47.9	-	9.8	17.3	-	3.3	4.4	10.5	-	I
13	19.4	32.3	-	10.7	14.1	3.9	-	8.8	10.8	-	T
14	-	56.3	-	11.6	9.7	7.8	-	4.1	10.5	-	O
15	0.2	46.3	-	5.8	12.9	0.8	1.1	8.6	24.3	-	O
16	1.6	48.1	-	9.3	11.8	-	-	6.3	22.9	-	T
17	-	52.0	-	10.8	5.5	6.6	-	7.6	17.5	-	I
18	18.2	28.0	-	11.6	20.8	-	13.6	5.6	2.2	-	O
19	19.6	38.6	-	12.2	12.9	3.7	6.2	5.6	1.2	-	O
20	0.3	54.5	-	13.1	14.1	-	12.1	5.9	-	-	O
21	12.0	24.8	-	6.6	13.5	-	14.3	7.2	21.6	-	O
22	-	44.5	-	13.2	7.1	5.0	-	5.7	24.5	-	I
23	7.8	53.9	-	22.6	7.4	5.6	-	2.7	-	-	I
24	8.5	55.1	-	16.4	7.1	4.5	-	8.4	-	-	I
25	21.6	41.9	-	9.7	10.9	-	1.0	7.3	7.6	-	I
26	-	57.8	-	13.9	7.5	8.4	-	6.6	5.8	-	I
27	3.0	53.8	-	21.9	2.9	12.1	-	6.3	-	-	I
28	-	58.8	-	12.8	6.6	3.4	-	8.6	9.8	-	I
29	7.0	57.5	-	6.8	12.1	-	-	7.3	9.3	-	I
30	-	59.1	-	19.9	5.3	5.3	6.4	3.7	0.3	-	O
31	1.1	61.3	-	16.0	6.8	9.5	-	5.3	-	-	I
32	5.8	60.4	-	16.3	-	5.5	-	6.1	5.9	-	T

Table 5.3. Quantitative percentages of minerals for weathered samples (O: Oymaağaç granodiorite; I: İsmailkayaı granodiorite; T: Tavuktaşı granodiorite). Values are given in percentages.

Sample No	quartz4	oligoclase2	orthoclase2	perthite	hornblende3	biotite	diopside2	stilbite1	sphene	zircon	illite5	chlorite5	epidote1	calcite3	zoisite	Lithology
1	9.4	-	-	23.6	-	15.9	3.6	7.3	-	9.6	19.7	5.2	-	4.8	0.9	O
2	5.6	30	-	29.2	-	20.0	1.2	3.6	-	0.8	-	6.8	-	2.8	-	O
3	15.3	9.6	-	27.7	-	17.3	1.3	6.8	-	11.0	-	6.8	1.7	2.5	-	O
4	19.4	27.4	-	14.1	4.8	12.3	-	2.6	11.6	-	-	5.9	-	1.9	-	I
5	22.3	18.1	-	21.1	3.4	1.5	-	4.8	13.1	-	9.7	4.8	-	1.2	-	I
6	46.6	14.0	-	12.0	13.5	-	4.9	0.7	-	3.9	2.1	-	0.2	1.4	0.7	I
7	20.1	17.1	-	16.1	-	3.2	5.6	4.9	23.2	-	-	7.1	-	2.7	-	I
8	3.8	-	-	24.1	-	7.3	6.6	7.9	-	13.6	29.1	0.3	3.8	0.6	2.9	I
9	6.3	27.3	-	33.3	9.2	-	-	2.2	16.1	-	-	4.4	-	1.2	-	I
10	18.9	25.6	-	17.0	10.6	-	-	2.1	21.3	-	1.0	2.7	-	0.8	-	I
11	16.7	13.1	-	7.9	9.4	0.9	-	3.7	25.8	-	19.5	0.1	-	2.0	0.9	O
12	4.2	36.2	-	26.1	1.5	9.4	-	2.4	15.2	-	0.3	3.4	-	1.3	-	I
13	9.7	27.8	-	20.1	6.4	8.6	-	4.0	14.7	-	5.0	1.0	0.5	1.5	0.7	T
14	14.0	31.6	-	19.5	6.6	8.5	-	1.3	13.4	-	-	3.3	-	1.4	0.4	O
15	7.1	42.6	-	14.2	7.1	1.7	-	2.6	18.0	-	-	5.2	-	1.5	-	O
16	12.3	20.8	-	16.0	12.6	-	-	2.3	23.0	-	11.0	0.3	0.1	1.5	0.1	T
17	30.2	3.1	-	6.2	6.8	3.3	-	4.5	16.5	-	25.8	0.2	0.3	1.6	1.5	I
18	6.4	33.2	-	25.1	-	23.5	-	3.6	-	0.2	-	5.3	-	2.7	-	O
19	9.1	27.9	-	28.3	-	16.5	1.8	5.1	-	-	1.0	7.8	-	2.5	-	O
20	13.1	37.0	-	28.5	-	2.1	8.8	0.9	-	3.2	-	4.3	1.8	0.3	-	O
21	13.3	29.4	-	24.9	-	11.6	-	2.8	11.3	-	-	5.3	-	1.4	-	O
22	33.5	21.9	-	14.8	-	15.5	-	4.0	-	0.7	1.1	4.5	-	3.8	0.2	I
23	-	29.5	-	36.5	-	12.2	4.1	3.7	1.2	-	2.6	7.8	-	2.4	-	I
24	11.0	34.9	-	22.5	-	13.7	3.8	5.2	-	-	-	6.8	-	2.1	-	I
25	-	-	-	4.7	-	5.5	5.9	8.5	4.6	16.6	46.1	-	1.7	3.6	2.8	I
26	20.7	35.5	-	15.9	6.5	7.4	-	2.0	7.0	-	-	4.0	-	1.0	-	I
27	31.6	18.4	-	13.7	11.2	0.1	-	2.2	9.6	-	10.7	1.8	-	0.7	-	I
28	30.5	20.8	-	18.0	-	12.6	-	4.3	-	3.4	4.2	2.7	0.8	1.1	1.6	I
29	25.8	46.4	-	20.8	4.3	0.4	-	0.7	-	-	-	0.6	1.0	-	-	I
30	13.1	-	-	26.8	-	-	5.7	6.1	-	1.4	24.4	1.6	3.4	3.0	1.9	O
31	24.2	31.5	-	23.6	0.5	9.4	-	1.7	2.1	-	-	5.0	-	2.0	-	I
32	31.5	-	-	7.2	8.6	-	-	5.7	6.5	-	37.3	1.0	-	1.6	0.6	T

Following observations can be made from Table 5.2 for fresh samples:

- For 12 samples quartz percentage could not be obtained. In addition to this, calculated percentages are lower than the expected values excluding sample 1 (25.1 %) and sample 25 (21.6 %).
- For 21 samples oligoclase percentages are higher than 50 % which is rather high than expected results.
- No orthoclase is identified in any of the samples.
- For all of the samples abundant presence of perthite is detected which is assumed to be added by perthitization of some orthoclase minerals.
- Hornblende percentage could not be calculated for only 2 samples.
- According to previous studies, it is known that biotite content is very small. This is, more or less, confirmed by the analysis. In 11 samples biotite is absent. The maximum calculated percentage of biotite is 13.9 %. For 18 samples, biotite percentage is calculated as less than 10 %.
- Diopside is identified in 14 samples ranging from 0.7 % to 14.3 %.
- Stilbite is detected in all samples ranging in percentages from 2.7 to 10.3.
- Spheue is an accessory component of granodiorite. It is expected to occur in very small amounts. In the analysis sphene is not identified for 10 samples. In 10 samples the percentages are less than 10. In the rest 12 samples, on the other hand, the percentage is higher than 10 with a maximum of 26.2 % in sample no: 4.
- Zircon percentage could not be detected for any sample.

Following observations can be made from Table 5.3 for weathered samples:

- Quartz percentages range between minimum of 3.8 % and maximum of 46.6 %. In two samples (No: 23 and 25) quartz is not detected.
- For 5 samples oligoclase could not be detected. Calculated percentages are usually more than 20 %.
- Orthoclase is not detected in any sample.
- For more than half of the samples, perthite percentage is more than 20 %.
- Hornblende could not be identified in 15 samples. In Oymağaç granodiorite samples, hornblend is detected in 8 samples out of 11.

- Biotite content of 6 samples could not be calculated.
- Diopside percentage could be identified for 12 samples. Among calculated values the maximum percentage is 8.8 %.
- Stilbite percentages were obtained for all samples. These percentages change between 0.7 % and 7.9 %.
- Spheue could be could be detected in 19 samples. 13 of the calculated percentages range between 1.2 % and 25.8 %.
- Number of samples for which zircon percentage could be calculated are 11. Only 3 of them are over 10 %.
- Illite percentage could be acquired of 18 samples. The calculated values for 5 of them are more than 20 %.
- Chlorite presence could not be defined for just 2 samples. Maximum chlorite content is 7.8 %.
- For 11 samples, epidote percentage was obtained which is maximum 3.8 %.
- Except only one sample for all samples calcite content was calculated. The upper limit of calculated percentages is 4.8 %.
- Zoisite percentage could be found out for 13 samples.

In order to evaluate the results of spectral analysis, mineral percentages were computed using Microsoft Excel. A modeled spectrum was obtained for each sample by multiplication of the calculated percentages of each mineral with library spectra of these minerals and summation of all values. An example of this process can be seen in Figure 5.5 for fresh sample no 1. This calculation is repeated for all 32 fresh and weathered samples. The result of these calculations is shown in Figure 5.6. The red and blue lines correspond to calculated spectra (mixture) and measured values, respectively. Details of these data are given in Appendix B and Appendix C. By the comparison of measured and modeled spectra, an assessment of goodness of fit can be made. The reason of the vertical shift between two spectra is the intensity difference. When measuring sample surfaces, if rock surface is not flat, there is a reduction in the intensity of the signal detected by the sensor.

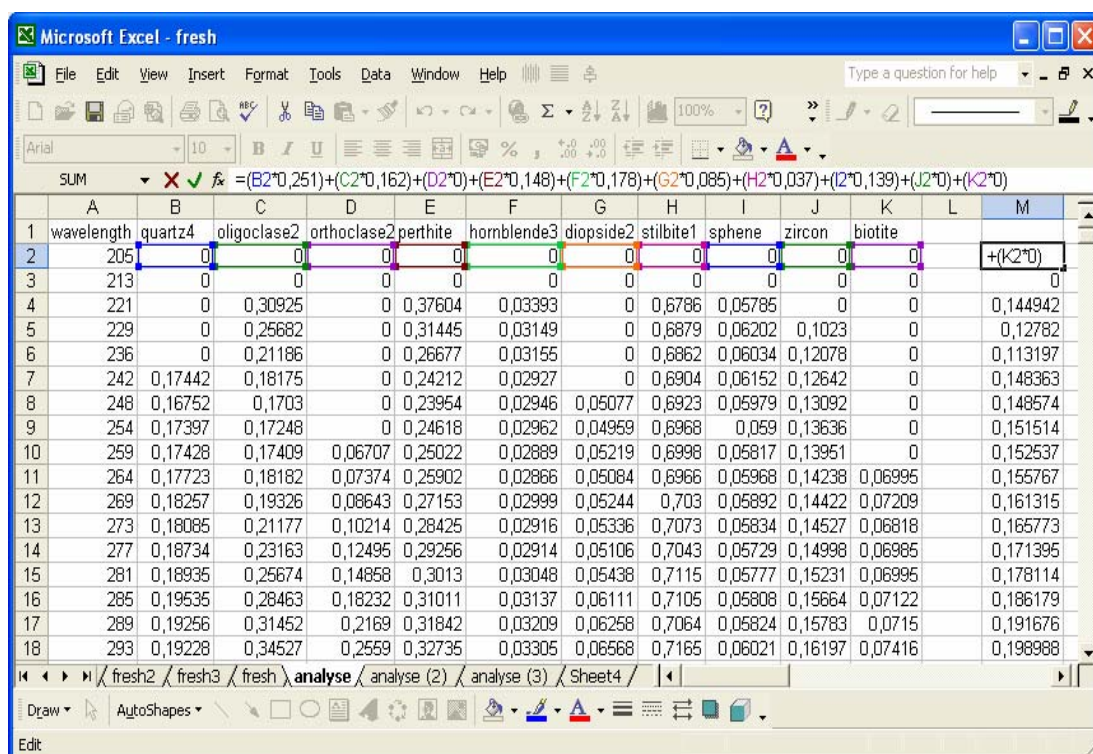


Figure 5.5. An example of Excel worksheet used for calculation of the mixture spectrum.

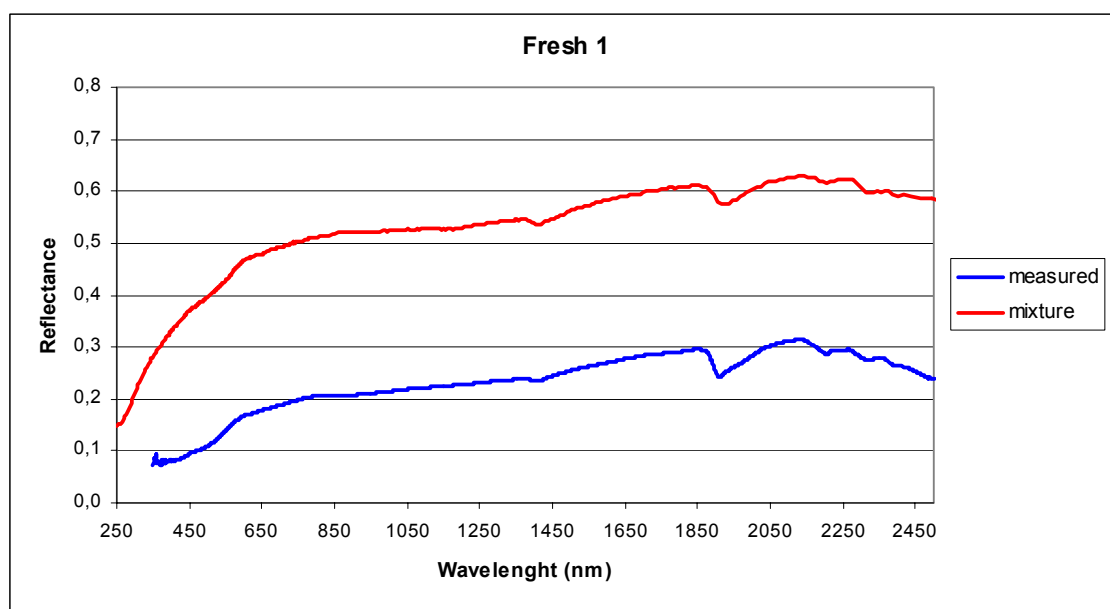


Figure 5.6. Comparison of measured and calculated spectra.

5.3. ASTER Image Analyses (Crosta Technique)

In this section the Crosta Technique (also referred to as Feature Oriented Principle Components Selection-FPCS) developed by Crosta and Moore (1989) will be applied to the ASTER image of the study area. This technique is based on the examination of eigenvector values to determine the principle components that concentrate spectral information about specific target materials. An important aspect of this technique is that it predicts whether the target materials are represented by bright or dark pixels in the principle component images according with the magnitude and sign of the eigenvectors. This technique was used for mineral exploration on four and six selected bands of Landsat TM data (Crosta and Moore, 1989; Loughlin, 1991; Ruiz-Armenta and Prol-Ledesma, 1998; Tangestani and Moore 2001; Carranza and Hale, 2002) and on ASTER data (Crosta et al, 2003).

During this analysis ASTER image is used. Preprocessing of the used ASTER data was explained in Chapter 4.

The analyses are carried out for five minerals. These are calcite, chlorite, epidote, and illite. The reason for the selection of these minerals is that these minerals are alteration products in the study area. They can be utilized in this technique because the Crosta Technique is widely used for alteration mapping. This technique is very successful to enhance some target minerals which has a smaller variance.

5.3.1. Calcite

In order to determine input bands for Crosta, the USGS library spectrum of calcite is superimposed on ASTER data band intervals (Figure 5.7). The selection of four bands as input for the Crosta Analysis is based on the spectral characteristics of calcite. Mapping of calcite is carried out using ASTER bands 3, 9, 1, and 8. As it is seen on the spectrum, calcite minerals give high reflectance values in ASTER band 3 and band 9 and low reflectance values in ASTER band 1 and band 8.

Principle Component transformation for calcite is shown in Table 5.4. Eigenvector statistics of input bands shows that PC4 shows a high negative loading from band 8 (-0.6177) and high positive loading from band 9 (0.7853). The positive sign of band 8 and negative sign of band 9 indicate that calcite minerals will be mapped as bright pixels (Figure 5.8a).

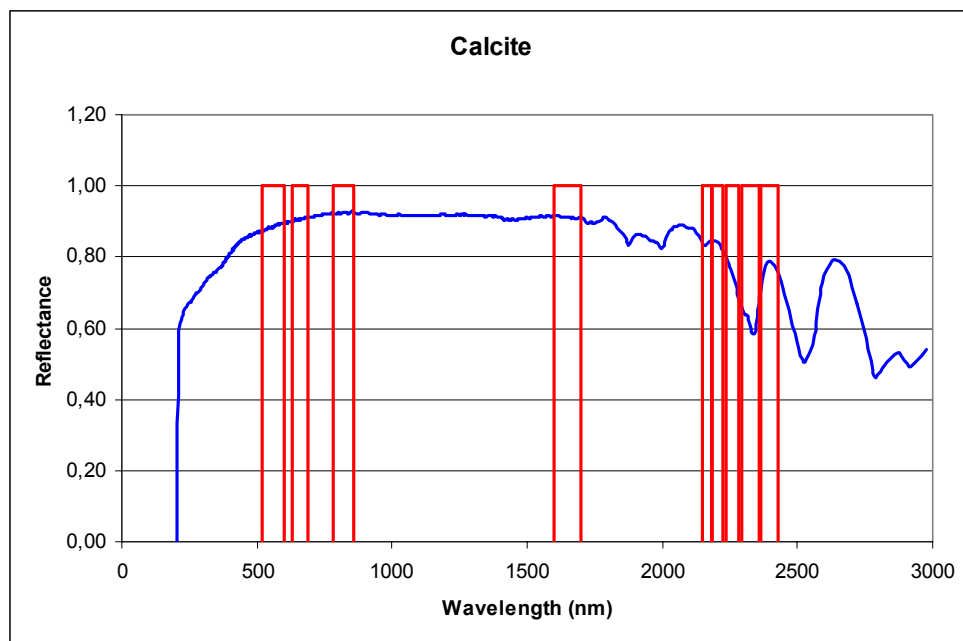


Figure 5.7. USGS spectral reflectance curve of calcite.

Table 5.4. Eigenvector statistics for ASTER bands 1, 3, 8, and 9.

	Band 1	Band 3	Band 8	Band 9
PC1	0.7647	0.3004	0.4674	0.3264
PC2	0.1188	0.8031	-0.4550	-0.3659
PC3	-0.6320	0.5146	0.4393	0.3779
PC4	0.0416	0.0017	-0.6177	0.7853

Threshold value for calcite is calculated by Mean + 2 (Standard Deviation). Mean and standard deviation values are acquired from histogram of PC4 (Figure 5.9). According to these values, threshold for calcite is determined as 187,2528 (152,87 + 2x(17,1914)). Some calcite anomalies are acquired by putting this threshold value into operation for PC4. After threshold, some lower concentrations of calcite are excluded and calcite minerals were mapped in red color as shown in Figure 5.8b.

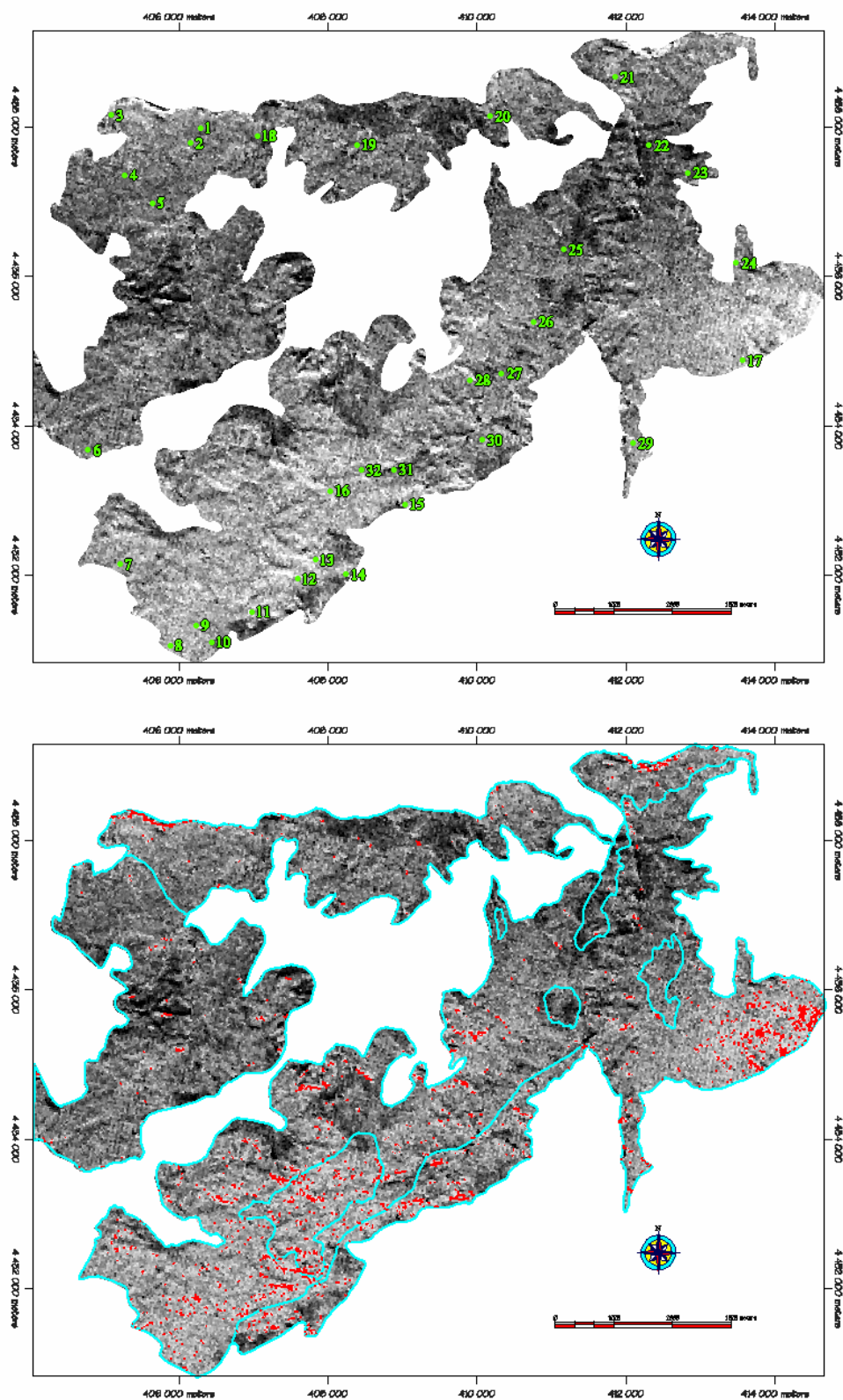


Figure 5.8. Resultant image for calcite produced by Crosta technique. a) PC4 (bright pixels represents calcite rich parts), b) Red indicates calcite anomalies after threshold is applied.

Calcite anomalies are mostly concentrated in the southern and eastern parts of the study area. A direct relationship can not be observed between the distribution of calcite anomalies and determined granodiorite zones.

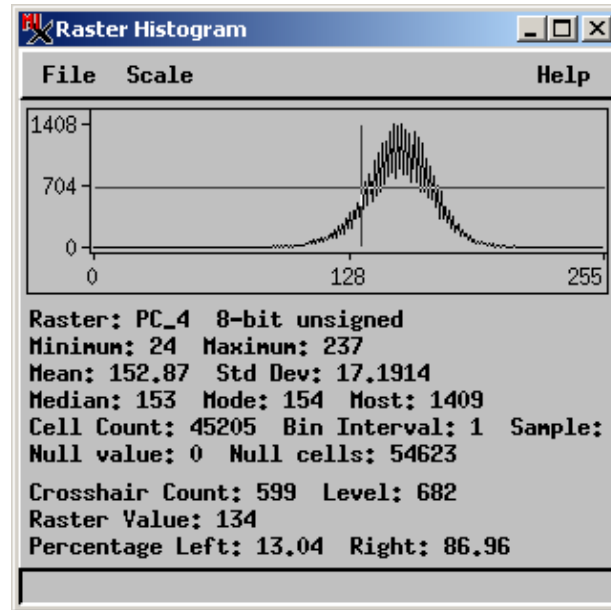


Figure 5.9. Histogram of PC4 for calcite used to determine the threshold values.

5.3.2. Chlorite

Identification of chlorite is possible due to its major absorption features. The ASTER bands 1, 2, 5, and 8 are chosen taking into account the spectral characteristics of chlorite (Figure 5.10). Chlorite has high reflectance values in ASTER bands 1 and 5 and strong absorption values in bands 2 and 8. The principle components which have high eigenvalues with opposite signs are determined (Table 5.5).

PC4 has high loadings with opposite signs for ASTER bands 5 and 8. In PC4, band 5 has negative value and band 2 has positive value. This indicates that chlorite will be indicated by dark pixels in the resultant map. By multiplying the values by -1 in PC4, chlorite bearing pixels would be mapped as bright pixels (Figure 5.11a).

To calculate threshold for invert of PC4, $\text{Mean} + 2(\text{SD})$ is computed and the threshold value is defined as - 97.3016.

By applying threshold, the lower concentrations of chlorite are masked. In the resultant map the chlorite anomalies are shown as yellow (Figure 5.11b).



Figure 5.10. USGS spectral reflectance curve of chlorite.

Table 5.5. Eigenvector statistics for ASTER bands 1, 2, 5, and 8.

	Band 1	Band 2	Band 5	Band 8
PC1	0.5877	0.6634	0.2993	0.3535
PC2	-0.4232	-0.2355	0.5379	0.6900
PC3	0.6894	-0.7102	0.0950	0.1063
PC4	0.0176	0.0057	-0.7823	0.6226

Distribution of chlorite does not show a specific relationship between the boundaries of the rock units mapped in the area. Elongated pattern of anomalies in most places indicate that chlorite is related to some structural elements in the area. These elements might be fractures (faults) or the dykes existing in the area.

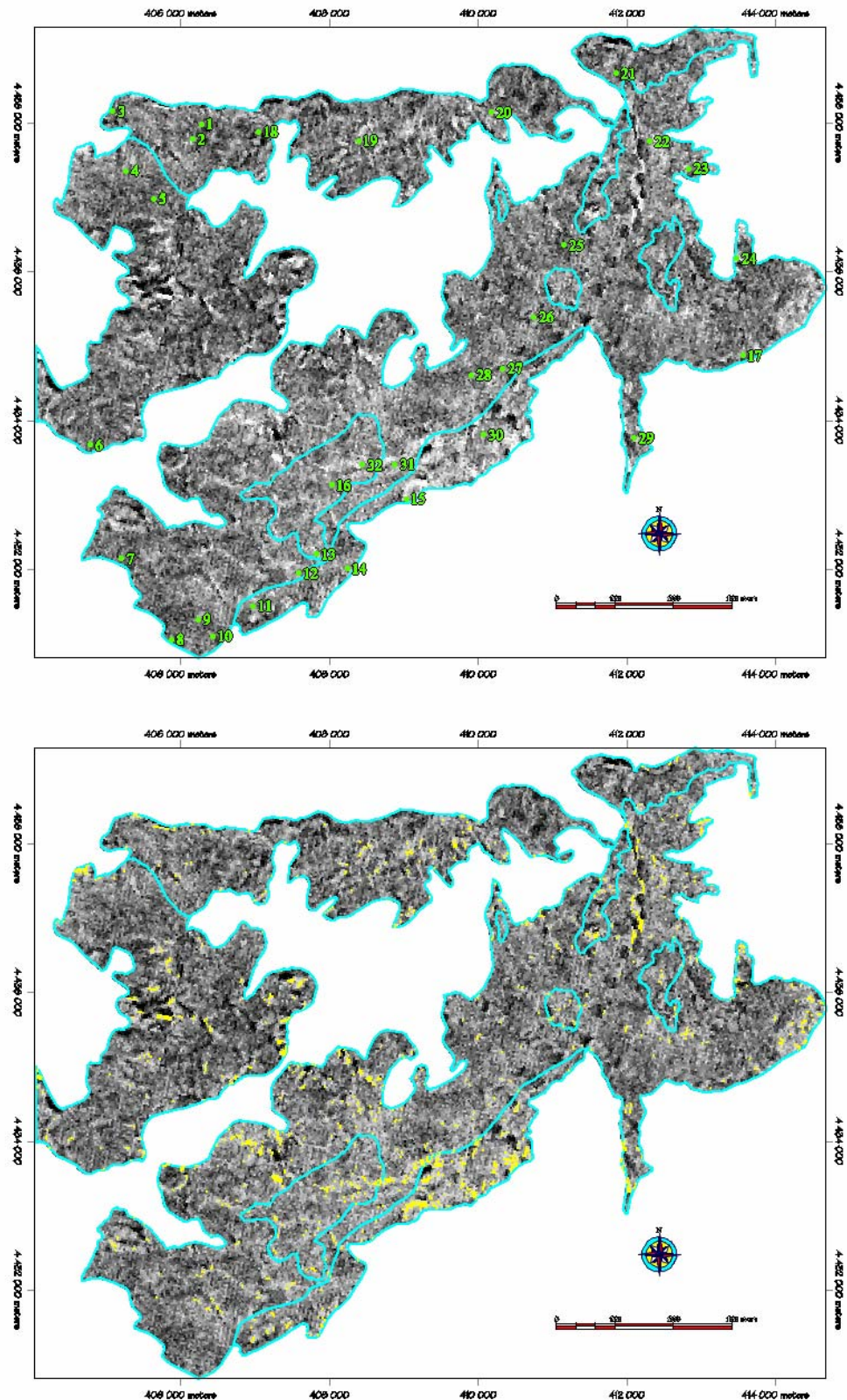


Figure 5.11. Resultant image for chlorite produced by Crosta technique. a) PC4 inverted (bright pixels represents chlorite rich parts), b) Yellow indicates chlorite anomalies after threshold is applied.

5.3.3. Epidote

Epidote has absorption features in the spectral regions of band 2 and 8 and reflectance features in the spectral regions of bands 5 and 9 (Figure 5.12). The results of principal components analysis of bands 2, 5, 8 and 9 (Table 5.6) show that the epidote is mapped by PC4. Epidote can be mapped as dark pixels in PC4 due to the fact that the contribution was positive loading from band 8 and negative loading from band 5. By negating PC4, epidote is mapped as bright pixels (Figure 5.13a).

By application of $\text{Mean} + 2(\text{SD})$, the threshold value is computed as -97.3944. In order to map bright pixels of invert PC4, this threshold value is used as a lower limit for DN values of PC4. Epidote minerals are represented in pink color in Figure 5.13b after the threshold is applied. Spatial distribution of epidote anomalies looks similar to that of chlorite. The linear form of the anomalies can be associated with certain lineaments e.g. dykes or faults existing in the area.

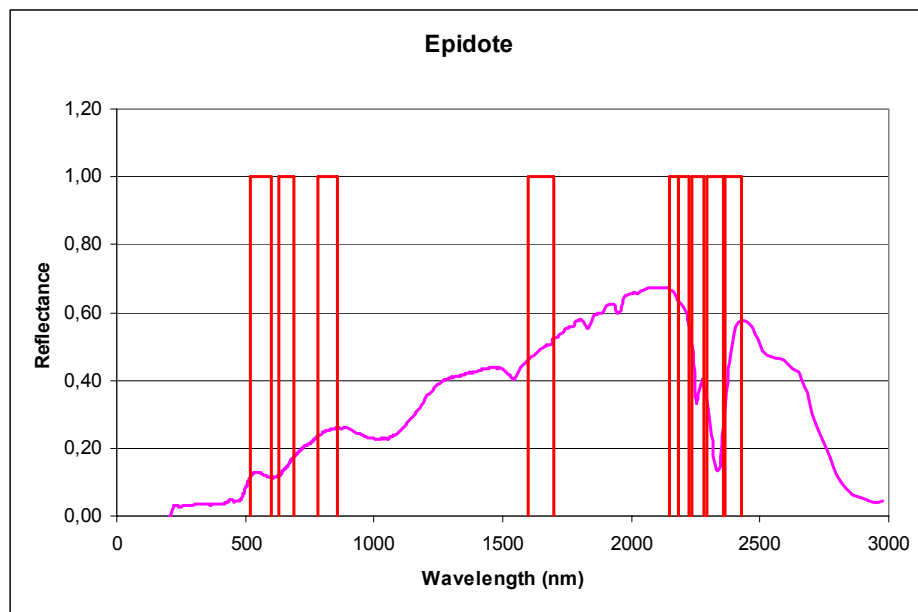


Figure 5.12. USGS spectral reflectance curve of epidote.

Table 5.6. Eigenvector statistics for ASTER bands 2, 5, 8, and 9.

	Band 2	Band 5	Band 8	Band 9
PC1	0.7552	0.3711	0.4411	0.3121
PC2	-0.6535	0.3800	0.5003	0.4223
PC3	-0.0468	0.3083	0.4228	-0.8508
PC4	0.0222	-0.7892	0.6135	0.0177

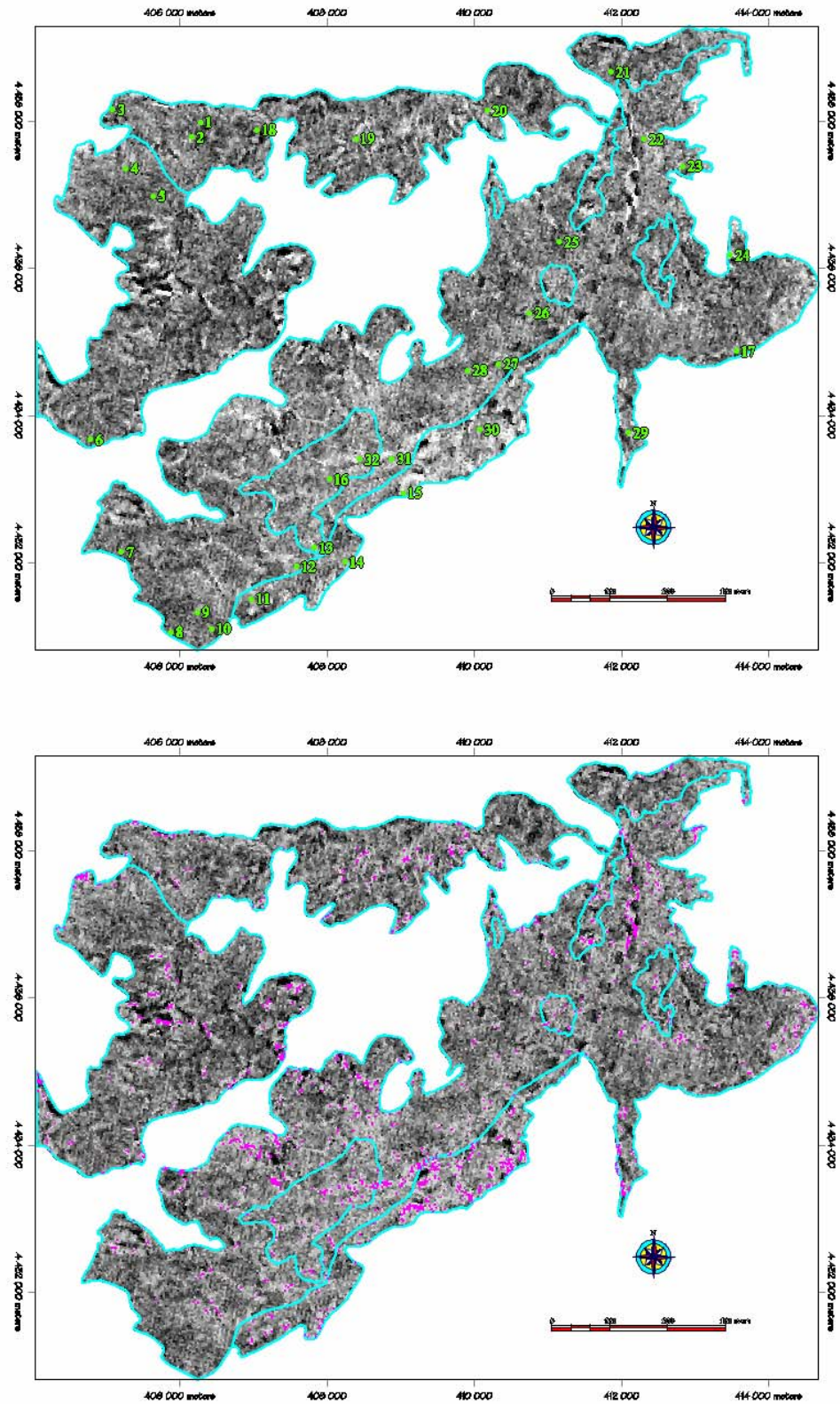


Figure 5.13. Resultant image for epidote produced by Crosta technique. a) PC4 inverted (bright pixels represents epidote rich parts), b) Pink indicates epidote anomalies after threshold is applied.

5.3.4. Illite

Mapping of illite is carried out using ASTER band 1, 3, 5, and 6. Illite has high reflectance feature in band 1 and 5 and strong absorption feature in band 3 and 6 (Figure 5.14). The PCA eigenvector statistics of these bands (Table 5.7) show that PC4 have high and opposite loadings.

PC4 image is needed to be negated, so that illite is illustrated by bright pixels in the image (Figure 5.15a). Via calculation of Mean + 2(SD) formulation for PC4, the threshold is computed as $-114.785 + 2(16.5395) = -81.706$. In the resultant image, after the threshold is applied, illite minerals are represented by blue color (Figure 5.15b). It is mapped mainly at the margin of Oymaağaç granodiorite (or rim of pluton). In addition, some illite anomalies are clustered at northeast boundary of Tavuktaş granodiorite.

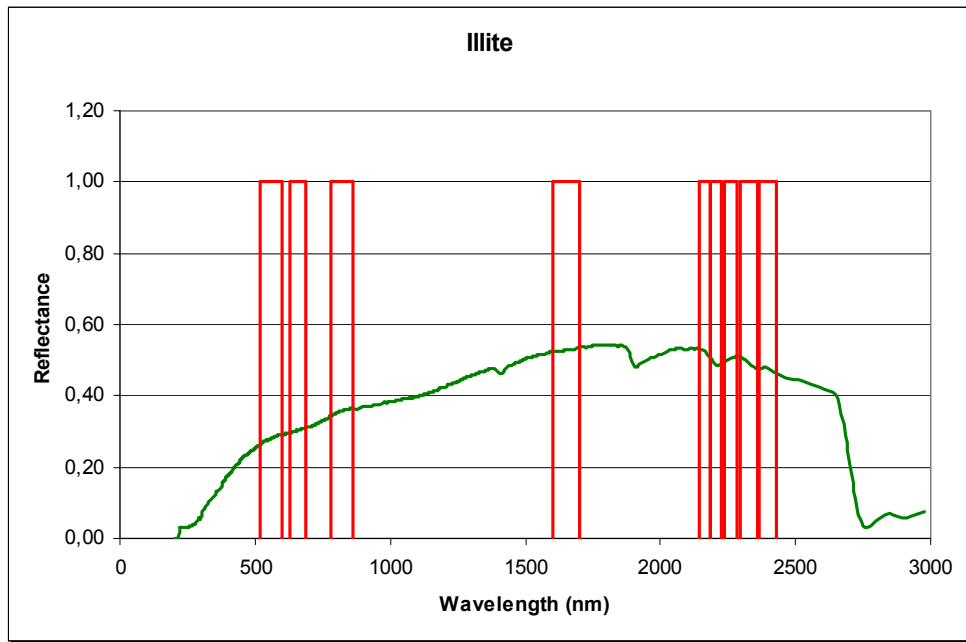


Figure 5.14. USGS spectral reflectance curve of illite

Table 5.7. Eigenvector statistics for ASTER bands 1, 3, 5, and 6.

	Band 1	Band 3	Band 5	Band 6
PC1	0.7555	0.3021	0.3917	0.4296
PC2	0.0736	0.8421	-0.3361	-0.4153
PC3	-0.6503	0.4467	0.3797	0.4832
PC4	0.0317	0.0064	-0.7678	0.6399

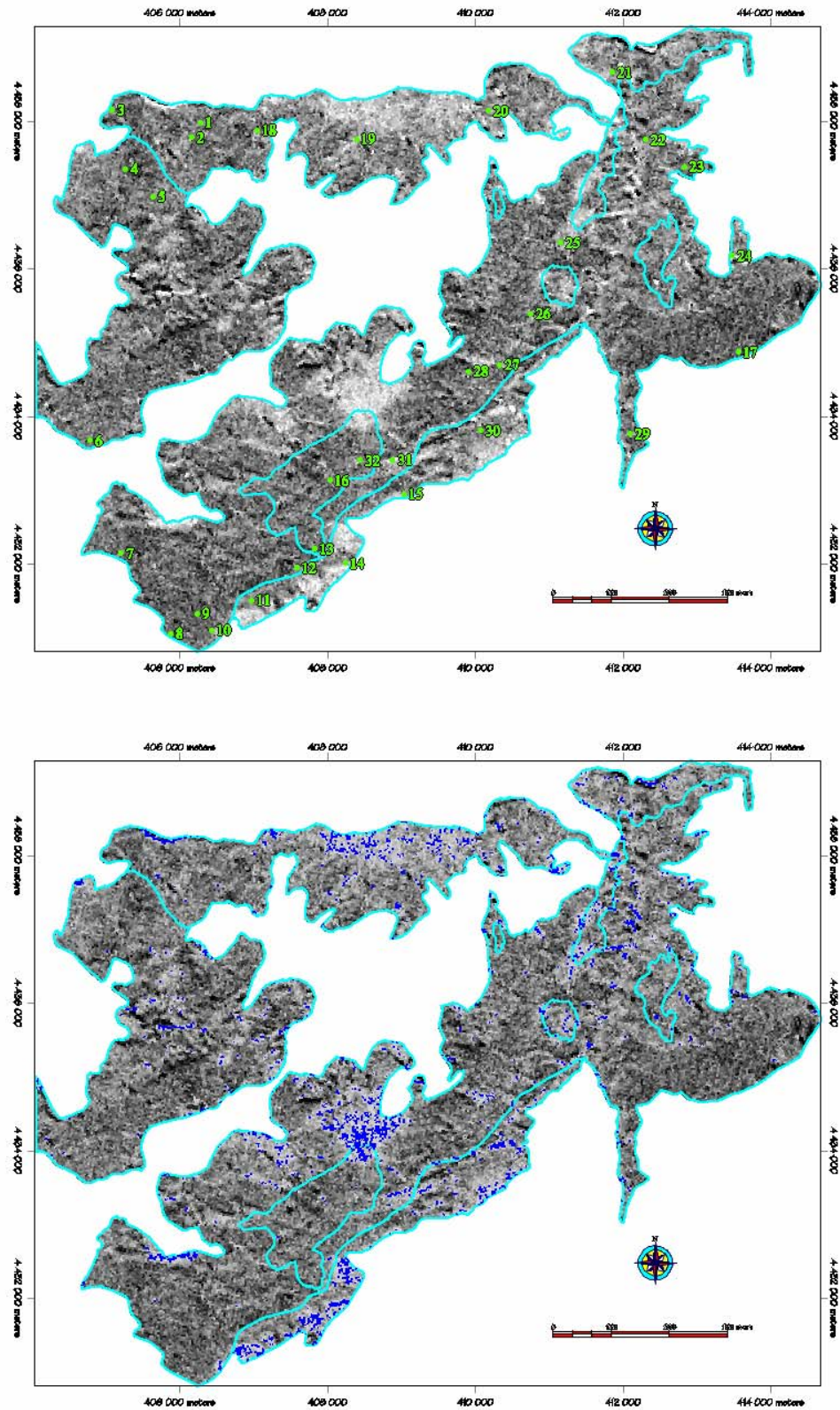


Figure 5.15. Resultant image for illite produced by Crosta technique, a) PC4 inverted (bright pixels represents illite rich parts). b) Blue color shows illite anomalies after threshold is applied.

5.4. Comparison of the Spectral Analyses and Crosta Technique

The relationship between results of spectral analysis and Crosta technique is examined in this section for a better understanding on the correlation of both results. To achieve this, the results obtained by two methods are plotted on a scatter diagram as shown in Figure 5.16. The vertical axis of the plot corresponds to the percentage of that mineral obtained by the spectral analysis carried out in the second section of this chapter. Horizontal axis, on the other hand, shows the DN value of the location of this sample read from the resultant map obtained by Crosta technique explained in the previous section. To eliminate uncertainties in the exact location of the sample, a 3*3 window around the sample location is assigned and the average value of this window is calculated.

Two values obtained by each method are plotted against each other. The procedure is applied only for four alteration minerals, namely, calcite, chlorite, epidote, and illite. Mineral percentages and calculated DN values obtained after the process are shown in Table 5.8.

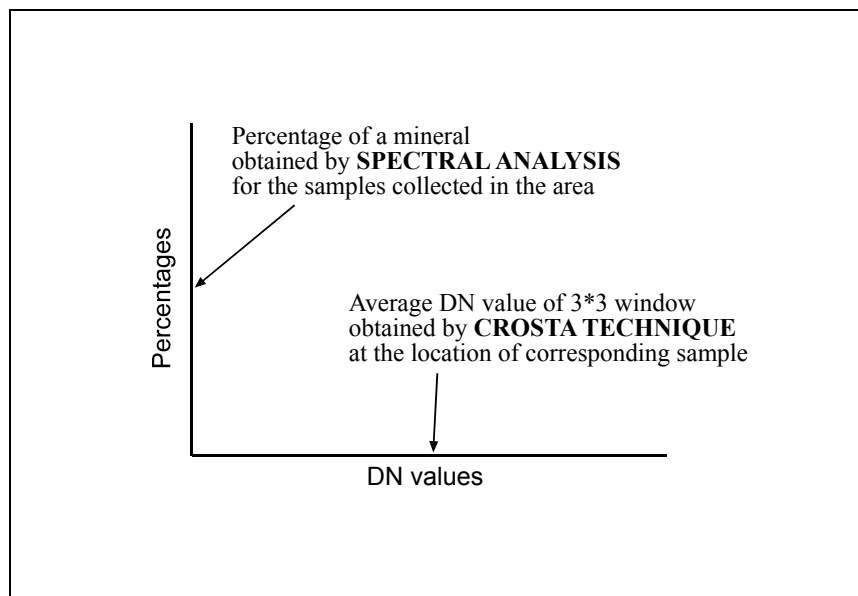


Figure 5.16. Scatterplot used to compare values of minerals obtained by two methods.

Table 5.8. Mineral percentages of spectral analysis and DN values corresponding with sample locations (O: Oymaağaç granodiorite; I: Ismailkayası granodiorite; T: Tavuktaş granodiorite).

Location No	calcite3 (%)	DN values 3x3	chlorite5 (%)	DN values 3x3	epidote1 (%)	DN values 3x3	illite5 (%)	DN values 3x3	Lithology
1	4,8	155,89	5,2	139,22	-	139,22	19,7	121,44	O
2	2,8	146,56	6,8	138,33	-	138,33	-	122,67	O
3	2,5	147,22	6,8	147,89	1,7	148,22	-	118,56	O
4	1,9	145,67	5,9	142,22	-	142,78	-	124,89	I
5	1,2	152,44	4,8	138,22	-	138,11	9,7	114,11	I
6	1,4	145,56	-	128,78	0,2	128,89	2,1	102,33	I
7	2,7	171,56	7,1	141,78	-	142,44	-	127,33	I
8	0,6	167,22	0,3	151,00	3,8	151,33	29,1	130,78	I
9	1,2	174,22	4,4	138,00	-	139,67	-	126,00	I
10	0,8	169,89	2,7	131,78	-	132,44	1	119,56	I
11	2	170,11	0,1	119,33	-	120,44	19,5	107,89	O
12	1,3	172,89	3,4	124,56	-	125,67	0,3	117,11	I
13	1,5	166,44	1	114,78	0,5	115,67	5	110,78	T
14	1,4	162,22	3,3	128,22	-	130,00	-	103,56	O
15	1,5	156,00	5,2	111,00	-	111,67	-	116,78	O
16	1,5	168,67	0,3	131,22	0,1	131,78	11	118,44	T
17	1,6	167,78	0,2	132,56	0,3	133,56	25,8	122,00	I
18	2,7	148,56	5,3	143,11	-	143,33	-	110,78	O
19	2,5	160,33	7,8	113,67	-	112,67	1	84,44	O
20	0,3	142,56	4,3	117,44	1,8	117,22	-	106,78	O
21	1,4	134,00	5,3	158,44	-	158,56	-	113,11	O
22	3,8	123,56	4,5	119,22	-	119,00	1,1	122,33	I
23	2,4	134,11	7,8	142,00	-	141,22	2,6	118,22	I
24	2,1	179,00	6,8	85,33	-	83,44	-	60,89	I
25	3,6	158,89	-	164,33	1,7	165,22	46,1	107,44	I
26	1	121,22	4	147,00	-	148,67	-	131,00	I
27	0,7	143,44	1,8	142,00	-	142,44	10,7	118,44	I
28	1,1	156,00	2,7	139,56	0,8	140,11	4,2	120,89	I
29	-	160,44	0,6	131,00	1	132,44	-	110,67	I
30	3	160,89	1,6	118,44	3,4	118,67	24,4	112,78	O
31	2	121,44	5	131,67	-	130,56	-	71,78	I
32	1,6	155,44	1	120,56	-	121,33	37,3	110,78	T

These minerals are plotted in the same diagram separately for different rock type to see if there is any relationship between the rock types and the mineral associations. The results of these analyses are shown in Figure 5.17.

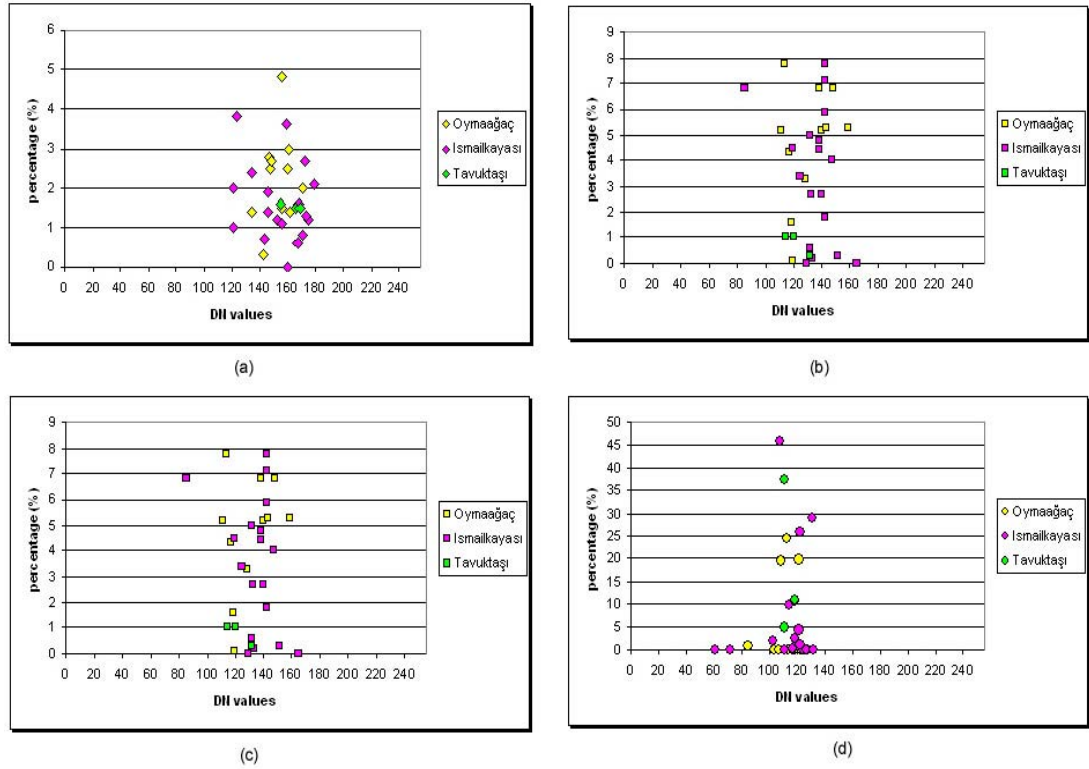


Figure 5.17. Scatterplots of the percentage and DN values for each alteration minerals (a) calcite, (b) chlorite, (c) epidote, (d) illite.

The patterns of the diagrams in Figure 5.17 indicate that none of the minerals form a distinct cluster in relation to the lithological units mapped in the area. Most of the minerals are observed in a narrow DN interval with varying percentage values. The distribution of the mineral for three rock types, on the other hand, seems to be random. Two main reasons for this can be:

- 1) The alteration mineral in different rock types are the products of the same parent mineral, and therefore there is no difference in the end product,
- 2) The boundaries of the lithological units are not consistent with the analysis.

5.5. Combination Map

After generation of potential areas for each alteration mineral, a combination map is produced using all information available. The main aim of this process is to display some areas that may include more than one mineral type simultaneously.

To realize this, binary raster data of each mineral type was multiplied by different decimal code. These values are shown in Table 5.9. In each class the number indicates the presence of associated mineral indicated by this number. For example the code 110 indicates the presence of epidote and chlorite; the code 1101 indicates presence of illite, epidote and calcite; the code 1111 indicates presence of all minerals.

Table 5.9. Decimal codes representing each mineral.

Mineral	Decimal code
Calcite	1
Chlorite	10
Epidote	100
Illite	1000

Total theoretical number of classes formed by these four minerals is 15. These classes and their total counts are given in Table 5.10. Three classes in the table are distinguished by their percentages. These are class “1”: calcite with 31.75 %, class “110”: epidote+chlorite with 19.64 % and class “1000”: illite with 34.05 %. These three classes make up 85.44 % of the whole altered areas.

The resultant map of these classes is shown in Figure 5.18 for 15 classes. White pixels in the map are “non-classified” pixels where no alteration mineral is detected.

Table 5.10. Represented minerals and number of pixels for each numeric value.

Class No	Code	Count	%	Minerals
-	0	**		No mineral
1	1	4475	31,75	Calcite
2	10	125	0.89	Chlorite
3	11	42	0.30	Calcite-Chlorite
4	100	159	1.13	Epidote
5	101	10	0.07	Epidote-Calcite
6	110	2768	19.64	Epidote-Chlorite
7	111	672	4.77	Epidote-Chlorite-Calcite
8	1000	4799	34.05	Illite
9	1001	111	0.79	Illite-Calcite
10	1010	10	0.07	Illite-Chlorite
11	1011	3	0.02	Illite-Chlorite-Calcite
12	1100	63	0.45	Illite-Epidote
13	1101	2	0.01	Illite-Epidote-Calcite
14	1110	744	5.28	Illite-Epidote-Chlorite
15	1111	111	0.79	Illite-Epidote-Chlorite-Calcite
	TOTAL	14094	100.00	

Following observations are made from combined mineral map (Figure 5.18):

- Calcite (1) and illite (1000) are most widespread alterations detected in the area. Calcite has anomalies along a belt parallel to the orientation of the intrusive body in the southern and eastern parts. This part of the area is covered by a thin gypsum cover (Figure 2.2) (Zoroğlu and Kadioğlu, 2003). This might be the reason for the high concentration of calcite. Illite is although distributed throughout the area its common exposures are confined to Oymağaç Granodiorite.
- Chlorite (10) and epidote (100) have similar distribution and pattern. These minerals show high concentration scattered at different parts of the area.

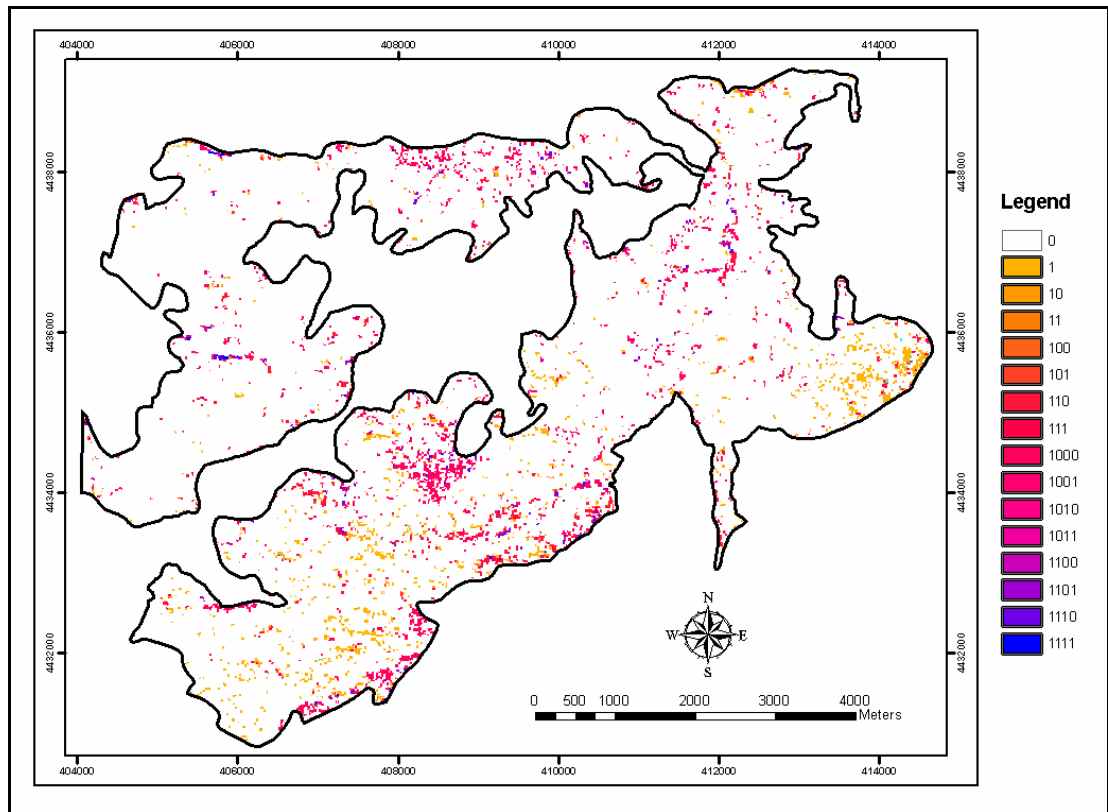


Figure 5.18. Combined map of alteration minerals.

- Combination of epidote-chlorite (110) minerals as seen in Table 5.10 is one of the most widespread alterations detected in the area.
- Illite-calcite (1001) is restricted only to some small areas randomly distributed in the region.
- Epidote-chlorite-calcite (111) combination (propylitic alteration minerals) covers large area particularly at southern part of the area. It has a very similar pattern to epidote-chlorite combination.
- Illite-epidote-chlorite (1110) is also commonly observed and has a similar pattern to epidote-chlorite distribution.

CHAPTER 6

FIELD VERIFICATION

The results of spectral analysis are checked with the field data to test the accuracy of method applied in the thesis. During assessment of results, geochemical analyses of Zoroğlu and Kadioğlu (2004) and microscopic analyses of Zoroğlu (2001) are used. CIPW Norm calculation using major oxide (% weight) and trace element (ppm) values are converted to mineral percentages. This calculation in fact is not reliable because all components of geochemical results could not be utilized as input and because the outputs do not match exactly with defined mineral constituents of the granodiorite. However, this is the only way to compare the field data with the analysis carried out in this study.

Calculated percentages of minerals reported by Zoroğlu and Kadioğlu (2004) matching endmembers of spectral analysis are listed in Table 6.1. There are four minerals in this list, namely, quartz, plagioclase, diopside and sphene.

Mineral percentages obtained with modal mineral analysis made by Zoroğlu (2001) are tabulated in Table 6.2. Four minerals that exist in this list are quartz, plagioclase, hornblende, sphene.

For each mineral the percentages are graduated using symbols for: 1) spectral analysis (this study), 2) modal analysis (Zoroğlu, 2001) and 3) geochemical analysis (Zoroğlu and Kadioğlu, 2003). Arc GIS software is used to generate the maps.

Table 6.1. Mineral percentages using CIPW norm from geochemical data

Sample	X	Y	Quartz	Plagioclase	Diopside	Sphene
2	409468	4433219	21,91	44,76	3,37	0,7
51	411811	4438780	22,23	44,4	3,59	0,7
54	408692	4437469	20,22	44,76	3,35	0,74
56	407655	4438018	42,02	0	0	12,26
89	406775	4435415	22,57	44,08	3,2	0,7
91	406617	4434976	22,5	43,84	3,83	0,74
14	410895	4435402	21,83	41,83	3,22	0,7
18	414233	4435907	20,49	47,21	4,03	0,72
31	411726	4435602	23,23	42,62	4,15	0,58
48	412278	4437800	20,31	45,05	3,93	0,7
50	412712	4437721	21,05	45,12	4,15	0,6
59	405939	4431230	22,35	41,94	3,68	0,66
62	406118	4432133	24,53	39,95	3,02	0,57
72	406726	4432974	24,7	40,14	2,81	0,54
83	405186	4432332	24,12	43,04	3,98	0,63
84	405074	4432493	21,36	43,28	4,86	0,64
66	407504	4433375	20,14	44,26	3,66	0,7
69	407715	4433529	31,5	35	0,84	0,29
5	410157	4433835	36,72	31,59	0	0
49	412752	4438346	37,99	27,76	0,46	0,12

Table 6.2. Modal mineral compositions of thin sections belonging to Oymağaç Granitoid

Sample	X	Y	Quartz	Plagioclase	Hornblende	Sphene
1	409730	4433372	16,16	45,63	20	1
2	409468	4433219	21,22	54,44	18,5	0,3
3	409162	4433080	25,4	52,8	21	0
15	412167	4433224	18,85	55,88	22	0
16	413847	4435385	21,69	54,87	19,4	0
17	413876	4435973	19,11	58,41	22	3,9
7	409267	4434217	19,33	54,89	24	0,1
8	408917	4434031	18,07	51,73	21	0
9	409673	4434391	20,85	53,05	23	0,4
10	409966	4435182	23,34	57,4	22	0
27	412335	4436226	24,4	50,8	13	0,1
28	412221	4435453	22,47	51,96	14	1
29	412174	4435656	24,83	48,42	12	0,3
30	411784	4435830	25,88	56,64	14	0,1
31	411726	4435602	23,12	51,85	13	0,1
33	411441	4435992	24,31	52,29	12,4	0,1
40	411519	4436587	20,06	51,33	11	0
47	412286	4437566	21,65	48,8	14	0
48	412278	4437800	22,57	48,14	12	0,6
51	411811	4438780	36,09	43,11	7	1
65	407212	4433120	31,46	49,81	6	0
66	407504	4433375	26,47	45,57	5	0,4
67	407755	4433222	34,42	40,85	5,3	0,4
68	408029	4433549	25,75	49,3	5,8	0,3
69	407715	4433529	32,22	45,03	4,9	0,2
70	408029	4433721	26,91	42,18	6,2	0
71	407077	4432866	20,02	52,61	7,1	0,6
72	406726	4432974	24,97	41,47	6,2	0
73	406445	4433212	23,56	42,72	4,4	0,3
74	406265	4433373	30,86	41,01	3	0,3
75	405891	4432433	43,6	40,46	0,3	0

Frequency of the samples and distribution within the area are different for all analyses. The results of the analyses are illustrated in Figures 6.1 to 6.5 for quartz, oligoclase, hornblende, pyroxene and sphene, respectively.

Following observations are made from these maps:

- For quartz from Figure 6.1, relatively low concentrations of spectral, geochemical and modal analysis are observed around Sarıkaya Tepe on the map. According to results of modal analysis, Tavuktaş Tepe is the area where highest concentrations of quartz observed.
- At southern part of the study area, oligoclase shows relatively high concentrations for spectral and modal analyses (Figure 6.2).
- As seen in Figure 6.3, for hornblende high concentrations of spectral analysis commonly are observed in Oymaağaç Granodiorite and low concentrations of modal analysis are concentrated on Tavuktaş Granodiorite
- According to results of spectral and geochemical analyses, diopside is observed at low concentrations mostly at southern part of the study area (Figure 6.4).
- It is noted that there is no significant relation between the results of spectral, modal and geochemical analyses of sphene (Figure 6.5).

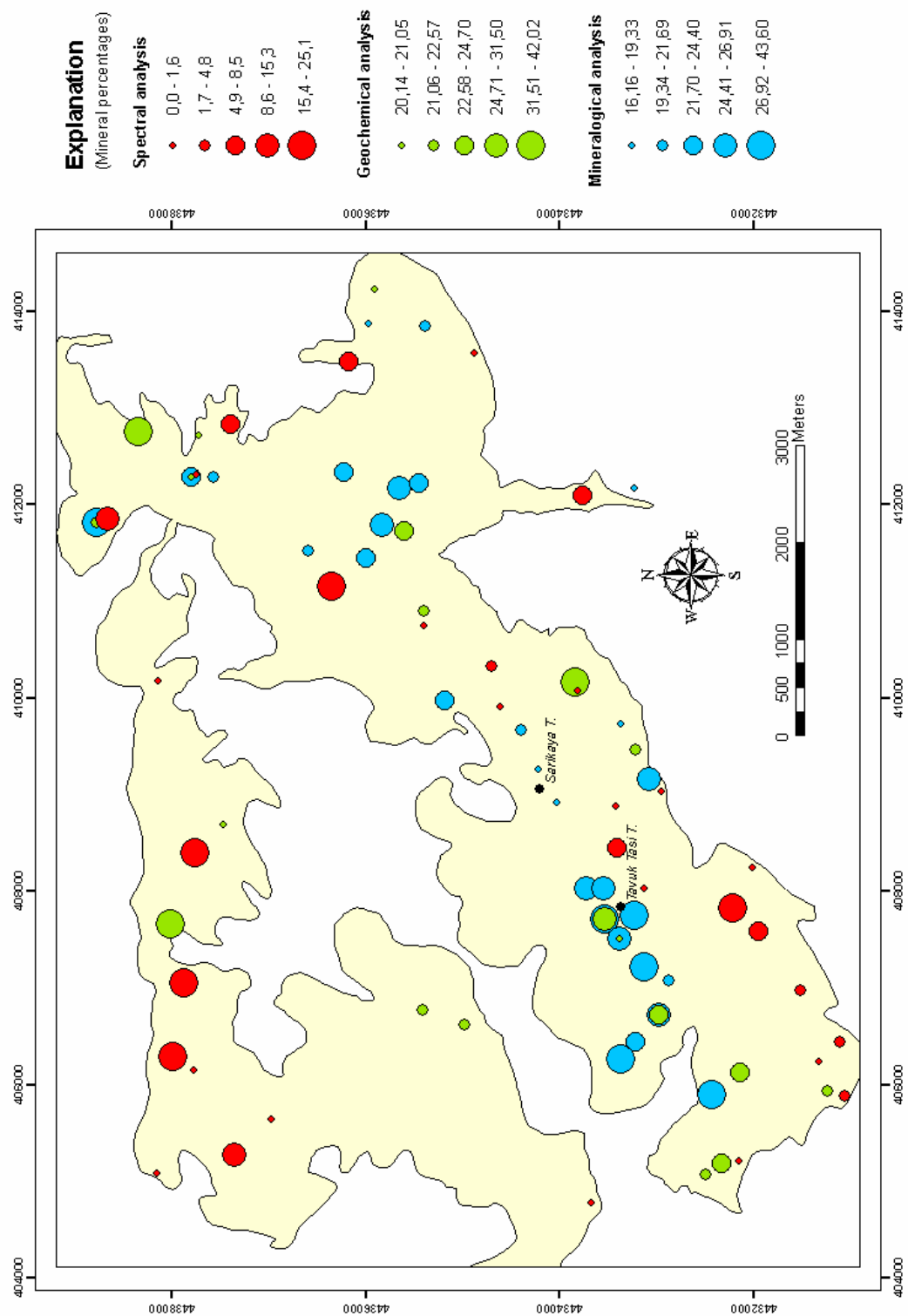


Figure 6.1. Comparison of spectral analysis with modal and geochemical analysis for quartz.

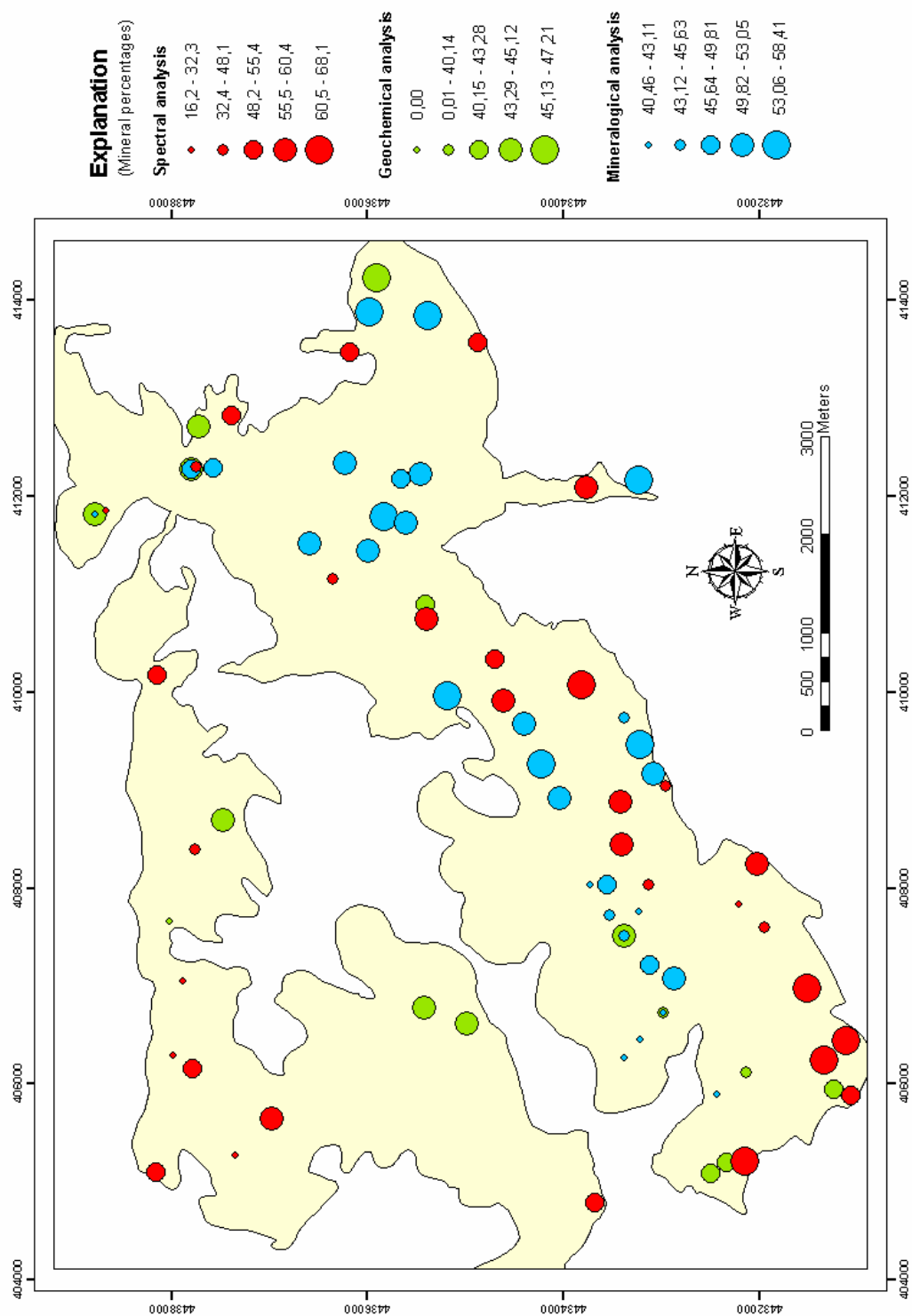


Figure 6.2. Comparison of spectral analysis with modal and geochemical analysis for oligoclase.

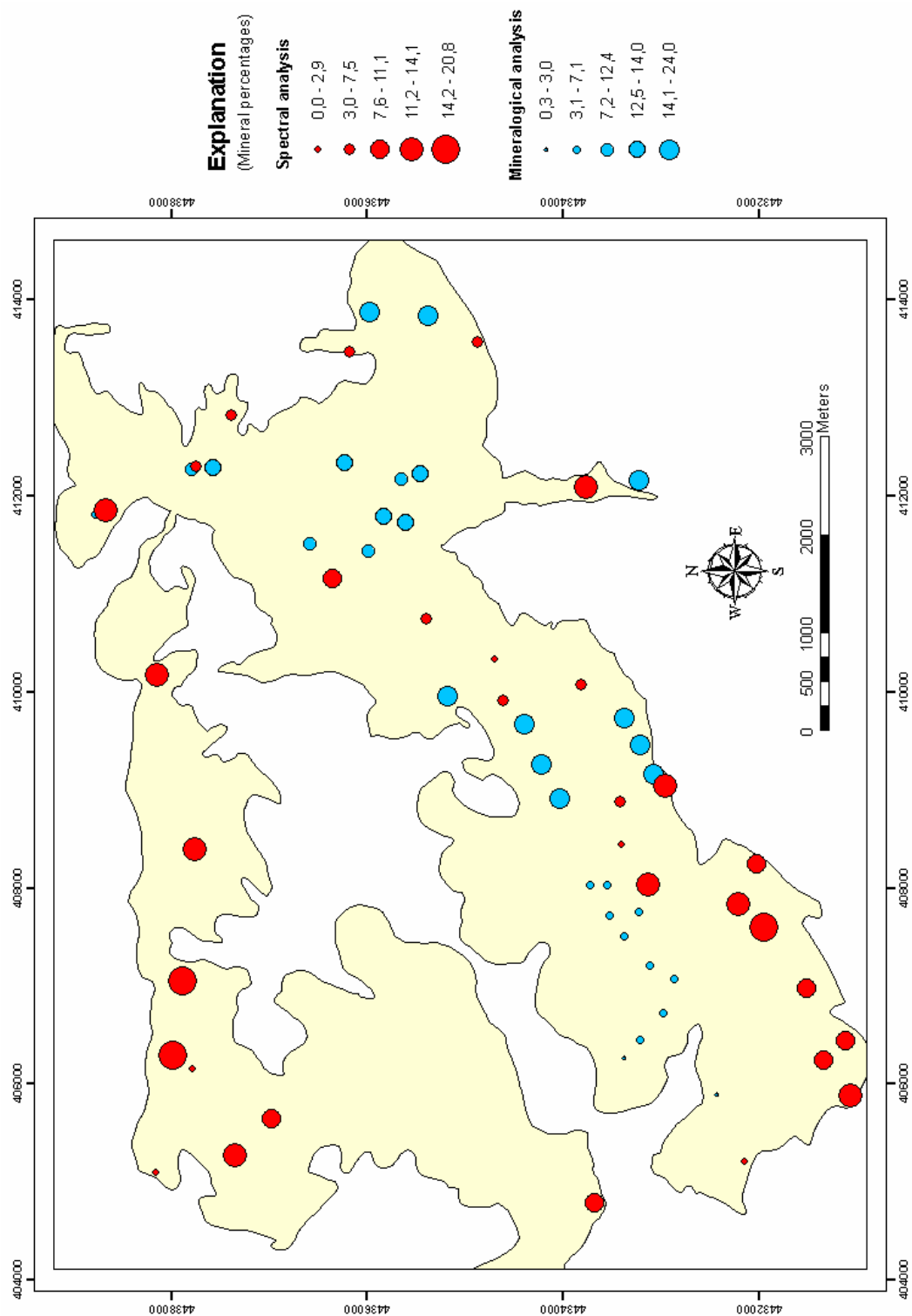


Figure 6.3. Comparison of spectral analysis with modal analysis for hornblende.

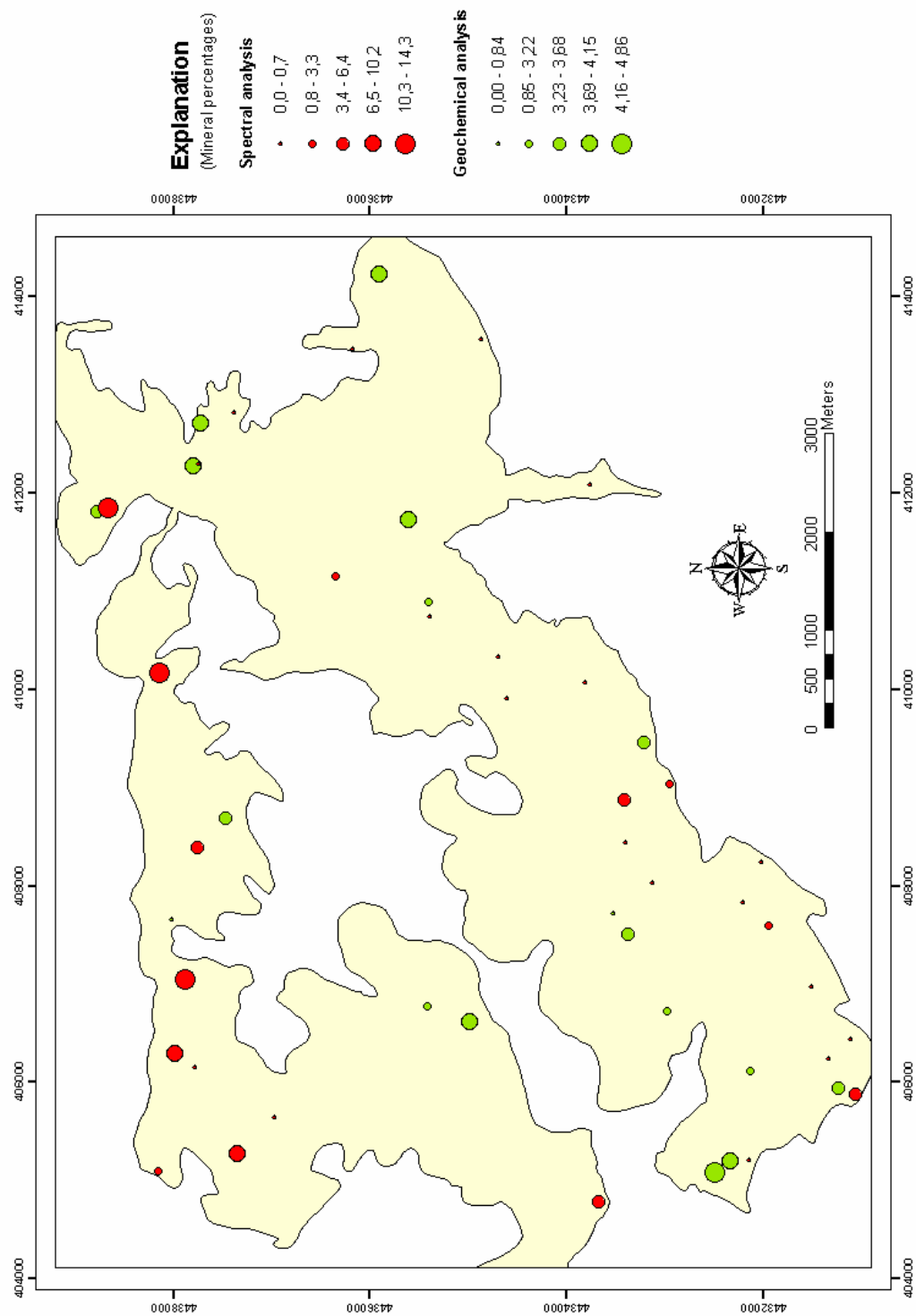


Figure 6.4. Comparison of spectral analysis with geochemical analysis for diopside.

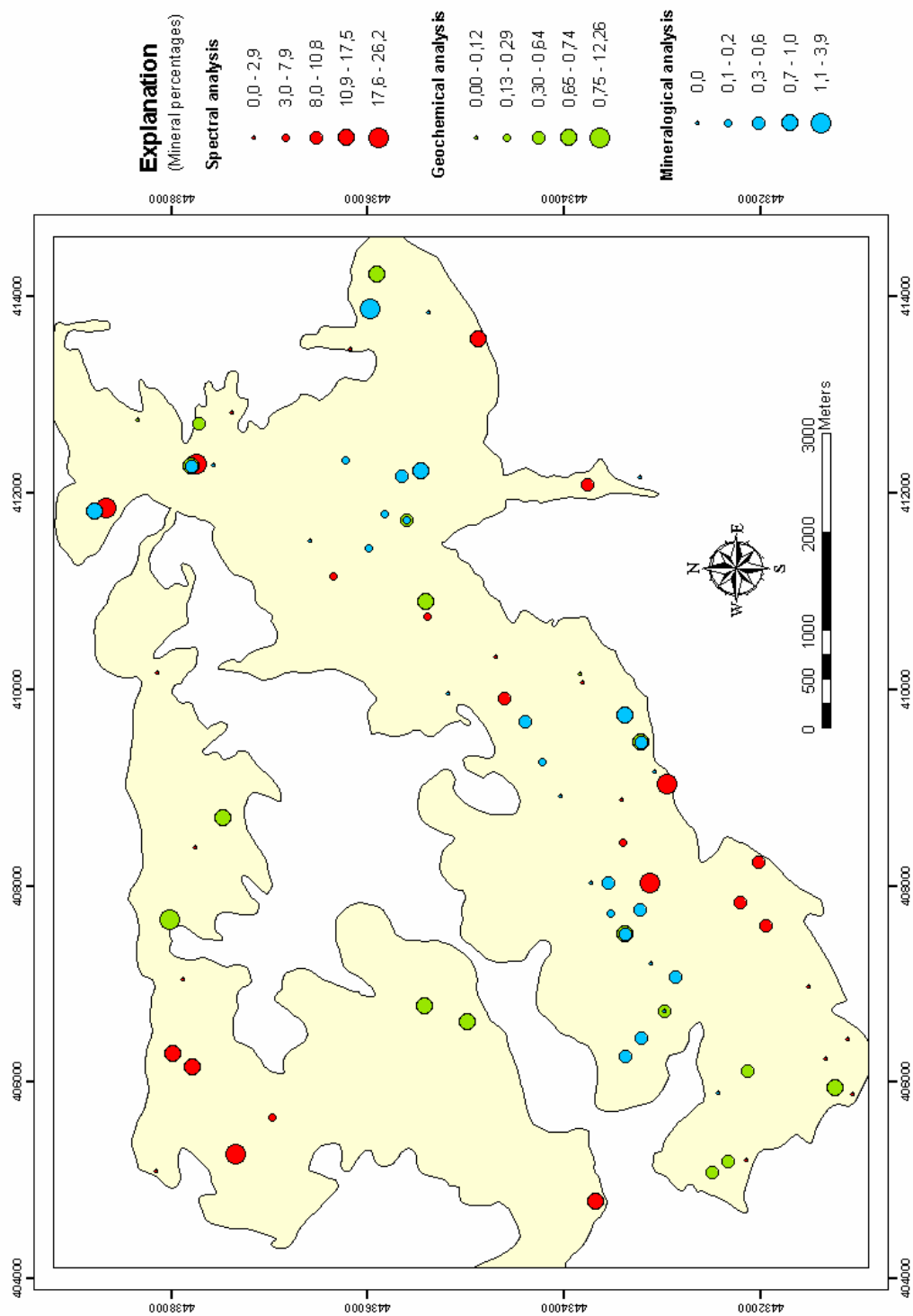


Figure 6.5. Comparison of spectral analysis with modal and geochemical analysis for sphene.

CHAPTER 7

DISCUSSION

Five aspects of the thesis will be discussed here. These are: 1) the data used in the study, 2) spectral analysis made in the first part of the methodology, 3) image analysis (Crosta technique) made in the second part, 4) results obtained in the study, and 5) field verification of remotely sensed data.

7.1. Data

The quality of the sample is very important in the accuracy of the results. Samples should express the variability of the area and exhibit a significant change in mixture proportions. In this study a total of samples are collected randomly. However, a larger number of samples based on a systematic (grid-based) sampling could be collected. This, in turn, would increase time and expenses, and therefore is avoided.

Three types of samples are collected at each locality. These are fresh samples, altered samples and lichen-covered samples. For each fresh sample, 3 measurements are made from different points of the sample surface and then the average is calculated. For the weathered samples, on the other hand, only one measurement is made. This is because of the homogeneous nature of the surface of weathered samples. The lichen-covered samples are not considered in this study because of the problem in the definition of “lichen” in spectral library.

Selection of endmembers is of great importance for mixture analyze, since choosing a different mineral can produce a great difference in the results. Grain size and

mineral compositions are considered during selection of representative spectra of mineral components. In addition to this, some spectral library data can belong to a specific site and it is not suitable for all rock types.

Image analysis is carried out using ASTER image. It has a spatial resolution 30x30 m for SWIR region and this resolution can be low to map some alteration types. Although its spatial resolution is not suitable for small-area applications. An advantage of ASTER data is the spectral resolution that allows mapping certain minerals.

7.2. Spectral Analyses

The use of spectral library as reference spectra of endmembers proves to be a feasible way in approaching mineral spectra measured from rock samples. But, to obtain information about mineralogical composition of granodiorite using spectral analysis is relatively difficult. Absorption bands for granodiorite are not so significant. The major minerals of granodiorite (quartz, alkali feldspar) have no diagnostic absorption signatures in VNIR and SWIR region. These minerals show distinctive emission minima in TIR region (8500-11500nm). This interval could not be used during analysis for the reason that spectral range of used field spectrometry does not include TIR region.

Some features and wavelength positions of the spectral profile can be influenced by some physical properties of mineral. As mentioned before, chemical composition, crystallinity, associated phases, orientation, degree of weathering, paragenesis, habit, texture, grain size, albedo, presence of water, matrix, and transparency are some of the factors affecting spectral signature of the minerals (Hauff, 2002). This spectral variability necessitates site specific spectral libraries. Existing spectral libraries can not be representative for all applications.

In Oymaağaç granitoid some opaque minerals are reported to be titanomagnetite (Yohannes, 1993; İpekgil, 2005). These opaque minerals are not considered as endmember during mixture analysis. Although a rock spectrum is combination of the

true spectra of its constituents (Hunt, 1979), the presence of very small amounts of opaque minerals has a much greater effect on the mixture spectra (Hunt and Evarts, 1981; Clark, 1983). These minerals when mixed with other minerals reduce the spectral reflectance and spectral contrast of the mixture and suppress the absorption features of the other minerals. Consequently, dominant spectral features can be originated by minor mineral components.

Similarly, for mixtures of some minerals it is impossible to make a percentage model accurately. These minerals might interact or mask some absorption features with each other. In this study, quartz – chlorite and illite – quartz are some mineral mixtures which causes influence on the reflectance.

In literature, spectral mixture analysis generally is used for binary and ternary mineral mixtures (Singer, 1981; Johnson *et al.*, 1983; Cloutis *et al.*, 1986) to determine relative proportion of components in a mixture. In this study, however, ten minerals for fresh samples and fifteen minerals for weathered samples are used as endmembers for the granodiorite. The excessiveness of the endmembers can have a negative effect on the accuracy of results.

7.3. Image Analyses (Crosta Technique)

The mineralogical information in this study is extracted using Crosta Technique from ASTER multispectral data. This technique is straightforward, easy and effective to map alteration minerals. Two prominent factors during this analysis are 1) selection of the bands to be processed, and 2) determination of threshold.

In this study, in general, there was not a major problem in the selection of bands considering the endmembers used and the spectral characteristics of ASTER image. The only problem encountered is in the discrimination of chlorite and epidote that have similar absorption and reflectance characteristics in corresponding ASTER bands. To solve the problem different bands are used for these minerals that area believed to differentiate them from each other.

Mineral maps created by Crosta Technique and mapping the density of these minerals are partly a function of user-defined threshold levels. These thresholds are defined to map only pixels with a high potential abundance of the target mineral.

7.4. Results obtained

The most significant result of the spectral analysis is the absence of orthoclase which is expected to occur in the granitoid in the area. In addition to this, the absence of zircon in all fresh samples, absence or low-percentage presence of quartz in some samples particularly for fresh ones are other striking results of the analyses.

Visual interpretation of some sample spectra which belong to different zones of Oymağaç Granitoid, suggest that there is no big difference between the samples. However, it is possible to get similar reflectance curves for two different rock samples. Also, it is observed that alteration processes did not significantly mask the dominant absorption features detected in the spectra of fresh samples for most of the altered spectra. The overall spectrum of fresh samples show certain absorption features approximately in 1419, 1910, 2205, and 2323 nm. For weathered samples, it is possible to observe some changes in the direction and magnitude of these absorption points. Also, most of the weathered samples have a large feature between 902-919 nm.

The mineral percentages calculated using spectral mixture analyses are not exactly consistent with mineralogical and petrographical results of previous studies (Zoroğlu and Kadioğlu, 2003; İpekgil, 2005). Nevertheless, obtained results are acceptable when the mineral percentages are considered for a granodiorite.

7.5. Field verification

Field verification of this study is made using modal analyses and geochemical analyses published in the literature (Zoroğlu, 2001; Zoroğlu and Kadioğlu, 2004). This test, however, is not successful mostly because of the inconsistencies existing in the nature and differences between results of spectral, petrographic, and geochemical

analyses. All major oxide and trace element values obtained by geochemical analysis can not be entered as input to the CIPW Norm calculation. This causes the calculation of some unrelated minerals with sample rock and incorrect calculation of the mineral percentages. This inconsistency is a general problem and a way should be suggested to fit the results of remotely sensed data and geochemical data.

CHAPTER 8

CONCLUSIONS AND RECOMMENDATIONS

8.1. Conclusions

The major conclusions of this study are:

According to the results of both spectral analyses and Crosta technique, a zonation is not verified in the granitoid.

The comparison of the results for alteration minerals of these two analyses is partly compatible but not exactly in accordance.

The results of spectral analysis do not fit geochemical nor modal analyses because of inconsistency of the data sets.

8.2. Recommendations

Some major minerals of granitoid (orthoclase, quartz) do not have distinctive spectral signatures in VNIR-SWIR region of spectrum. These minerals show emissivity features in TIR region. The field spectrometer used in this study does not include TIR region so this region of spectrum could not be used in this study. TIR bands of ASTER image are not analyzed, in order to interfix between two analyses. However, such a study can be more successful by involving TIR region.

REFERENCES

- Abrams, M., 2000, The Advanced Spaceborne Thermal Emission and Reflection Radiometer (ASTER): data products for the high spatial resolution imager on NASA's Terra platform. *International Journal of Remote Sensing*, v.21, no.5, pp.847-859.
- Adams, J. B., and Filice, A. L., 1967, Spectral reflectance 0.4 to 2.0 microns of silicate rock powders, *Journal of Geophysical Research*, v.72, pp.5705-5715.
- Adams, J.B., Smith, M.O., and Johnson, P.E, 1986, Spectral Mixture Modelling: A New Analysis of Rock and Soil Types at the Viking Lander Site, *Journal of Geophysical Research*, v.91, pp.8098-8112.
- Ager, C. M., and Milton, N. M., 1987, Spectral reflectance of lichens and their effects on the reflectance of rock substrates, *Geophysics*, v.52, no.7, pp.898-906.
- ASTER Users Handbook, Abrams, M., Hook, S., Version 2, Jet Propulsion Laboratory California Institute of Technology
- Blom, R. G., Abrams, M. J., and Adams, H. G., 1980, Spectral reflectance and discrimination of plutonic rocks in the 0.45- to 2.45- μm region, *Journal of Geophysical Research*, v.85, pp.2638-2648.
- Brennich, G., 1967, Nallıhan-Beypazarı jips zuhurları, M.T.A. Report No: 4821.
- Buckingham, W. F., and Sommer, S. E., 1983, Mineralogical characterization of rock surfaces formed by hydrothermal alteration and weathering – Application to remote sensing, *Economic geology*, v.78, pp.664-674.
- Carranza, E. J. M., and Hale, M., 2002, Mineral imaging with Landsat Thematic Mapper data for hydrothermal alteration mapping in heavily vegetated terrain. *International Journal of Remote Sensing*, v.23, pp.4827-4852.
- Clark, R. N., 1983, Spectral properties of mixtures of montmorillonite and dark carbon grains: Implications for remote sensing minerals containing chemically and physically adsorbed water, *Journal of Geophysical Research*, v.88, pp.10635- 10644
- Clark, R. N., 1999, Chapter 1: Spectroscopy of Rocks and Minerals, and Principles of Spectroscopy, in *Manual of Remote Sensing*, Volume 3, Remote Sensing for the Earth Sciences, (A.N. Rencz, ed.) John Wiley and Sons, New York, pp.3-58.
- Clark, R. N., and Roush, T. L., 1984, Reflectance spectroscopy: Quantitative analysis techniques for remote sensing applications, *Journal of Geophysical Research*, v.89, pp.6329-6340.
- Clark, R. N., King, T. V. V., Klejwa, M., and Swayze, G. A., 1990, High spectral resolution reflectance spectroscopy of minerals, *Journal of Geophysical Research*, v.95, pp.12653-12680.

- Cloutis, E. A., Gaffey, M. J., Jackowski, T. L., and Reed, K. L., 1986, Calibration of phase abundances , composition, and particle size distribution for olivine-orthopyroxene mixtures from reflectance spectra, *Journal of Geophysical Research*, v.91, pp.11641-11653.
- Crosta, A. P., and Moore, J. McM., 1989, Enhancement of Landsat Thematic Mapper imagery for residual soil mapping in SW Minas Gerais State Brazil: a prospecting case history in greenstone belt terrain. *Proceedings of the 9th Thematic Conference on Remote Sensing for Exploration Geology*, pp.1173-1187.
- Crosta, A. P., De Souza Filho, C. R., Azevedo, F., and Brodie, C., 2003, Targetting key alteration minerals in epithermal deposits in Patagonia, Argentina, using ASTER imagery and principle component analysis, *International Journal of Remote Sensing*, v.24, n.21, pp.4233-4240.
- Demirci, C. Y., 2000, Structural Analysis in Beypazarı – Ayaş – Kazan – Peçenek Area NW of Ankara (Turkey), Ph. D. Thesis, Middle East Technical University, Ankara.
- Erol, O., 1954, Köroğlu-Işık dağları volkanik kütesinin orta bölümleri ile Beypazarı-Ayaş arasındaki Neojen havzasının jeolojisi hakkında rapor, MTA Report No: 2279.
- Gillette, P. C., Lando, J. B., and Koenig, J. L., 1983, Factor analysis for seperation of pure component spectra from mixture spectra, *Analytical Chemistry*, v.55, pp.630-633.
- Gladwell, D. R., Lett, R. E., and Lawrence, P., 1983, Application of reflectance spectrometry to mineral exploration using portable radiometers, *Economic Geology*, v.78, pp.699-710.
- Gökmen, V., 1965, Nallıhan-Beypazarı (Ankara) civarındaki linyit ihtiva eden neojen sahasının jeolojisi hakkında rapor, M.T.A. Report No: 3802.
- Gündoğan, İ., and Helvacı, C., 2001, Sedimentological and petrographical aspects of Upper Miocene evaporites in the Beypazarı and Çankırı-Çorum Basins, Central Anatolia, Turkey, *International Geology Reviews*, v.43, pp.818-829.
- Hapke, B., 1981a, Bidirectional reflectance spectroscopy 1. Theory, *Journal of Geophysical Research*, v.86, pp.3039-3054.
- Hapke, B., 1981b, Bidirectional reflectance spectroscopy 2. Experiments and observations, *Journal of Geophysical Research*, v.86, pp.3055-3060.
- Hauff, P. L., 2002, *Applied Reflectance Spectroscopy*, Spectral International Inc.
- Helvacı, C., and Bozkurt, S., 1994, Beypazarı (Ankara) granitinin jeolojisi, mineralojisi ve petrojenezi, *Geological Bulletin of Turkey*, v.37, 2, pp.31-42.
- Helvacı, C., Yılmaz, H., and İnci, U., 1988, Clay minerals of neogene sediments in Beypazarı (Ankara) district and their vertical and lateral distribution, *Geological Engineering*, v.32-33, pp.33-42.

- Hunt, G. R., 1977, Spectral signatures of particulate minerals, in the visible and near-infrared, *Geophysics*, v.42, pp.501-513.
- Hunt, G. R., 1979, Near-infrared (1.3-2.4 μm) spectra of alteration minerals-Potential for use in remote sensing, *Geophysics*, v.44, pp.1974-1986.
- Hunt, G. R., and Evarts, R. C., 1981, The use of near-infrared spectroscopy to determine the degree of serpentinization of ultramafic rocks, *Geophysics*, v.46, pp.316-321.
- Hunt, J. M., and Turner, D. S., 1953, Determination of mineral constituents of rocks by infrared spectroscopy, *Analytical Chemistry*, v.25, pp.1169-1174.
- İnci, U., Helvacı, C., Yağmurlu, F., 1988. Stratigraphy of Beypazarı Neogene basin, Central Antolia, *Newsl. Stratigr.*, v.18 (3) pp.165-18.
- İpekgil, C., 2005, Geology and Petrology of Beypazarı-Oymağaç Granitoids, M. Sc. Thesis, Middle East Technical University, Ankara, 94 p.
- Johnson, P. E., Smith, M. O., and Adams, J. B., 1992, Simple algorithms for remote determination of mineral abundances and particle sizes from reflectance spectra, *Journal of Geophysical Research*, v.97, no.E2, pp.2649-2657.
- Johnson, P. E., Smith, M. O., Taylor-George, S., and Adams, J. B., 1983, A semi-empirical method for analysis of the reflectance spectra of binary mineral mixtures, *Journal of Geophysical Research*, v.88, pp.3557-3561.
- Karadenizli, L., 1995, Sedimentology of the Upper Miocene-Pliocene gypsum series of the Beypazarı Basin, West of Ankara, Central Anatolia, Turkey, *Geological Bulletin of Turkey*, v.38, no.1, pp.57-65.
- Kayakıran, S., and Çelik, E., 1986, Beypazarı trona (doğal soda) yatağı maden jeolojisi raporu, Cilt I, M.T.A. Report No: 8079.
- Kruse, F., A., and Hauff, P. L., 1991, Identification of illite polytype zoning in disseminated gold deposits using reflectance spectroscopy and x-ray diffraction – potential for mapping with imaging spectrometers, *IEEE Transactions on Geoscience and Remote Sensing*, v.29, no.1, pp.101-104.
- Longhi, I., Sgavetti, M., Chiari, R., Mazzoli, C., 2001, Spectral analysis and classification of metamorphic rocks from laboratory reflectance spectra in the 0.4–2.5 mm interval: a tool for hyperspectral data interpretation, *International Journal of Remote Sensing*, v.22, n.18, pp.3763-3782.
- Loughlin, W. P., 1991. Principal Component Analysis for alteration mapping, *Photogrammetric Engineering and Remote Sensing*, v.57, pp.1163-1169.
- Mustard, J. F., and Pieters C. M., 1989, Photometric phase functions of common geologic minerals and applications to quantitative analysis of mineral mixture reflectance spectra, *Journal of Geophysical Research*, v.94, pp.13619-13634.
- Nash, D. B., and Conel, J. E., 1974, Spectral reflectance systematics for mixtures of powdered hypersthene, labradorite, and ilmenite, *Journal of Geophysical Research*, v.79, pp.1615-1621.

- Okay, A., Tansel, İ., Tüysüz, O., 2001, Obduction, subduction and collision as reflected in the Upper Cretaceous-Lower Eocene sedimentary record of western Turkey, *Geol. Mag.* 138 (2), pp.117-142.
- Özpeker, I., Çoban, F., Esenli, F., and Eren, R. H., 1991, Mineralogical features of dolomite in the Hırka Formation (Beypazarı-Ankara), *Geological Bulletin of Turkey*, v.34, pp.23-26.
- Ramsey, J., Gazis, P., Roush, T., Spirtes, P., and Glymour, C., 2002, Automated Remote Sensing with Near Infrared Reflectance Spectra: Carbonate Recognition, Data Mining and Knowledge Discovery, v.6, pp.277-293.
- Rollin, E. M., Milton, E. J., and Roche, P., 1994, The influence of weathering and lichen cover on the reflectance spectra of granitic rocks, *Remote Sensing of Environment*, v.50, pp.194-199.
- Rondot, J., 1956, 1/100.000 lik 39/2 (güney kısmı) ve 39/4 nolu paftaların jeolojisi Seben-Nallıhan-Beypazarı ilçeleri, M.T.A. Report No: 2517.
- Ruiz-Armenta, J. R. and Prol-Ledesma, R. M., 1998, Techniques for enhancing the spectral response of hydrothermal alteration minerals in Thematic Mapper images of Central Mexico, *International Journal of Remote Sensing*, v.19, pp.1981-2000.
- Singer, R. B., 1981, Near-infrared spectral reflectance of mineral mixtures: Systematic combinations of pyroxenes, olivine, and iron oxides, *Journal of Geophysical Research*, v.86, pp.7967-7982.
- Stchepinsky, V., 1942, Rapport sur la geologie de la region de Beypazarı-Nallıhan-Bolu-Gerede, M.T.A. Report No: 1312, 19 p.
- Streckeisen, A., 1976. To each plutonic rock its proper name, *Earth Science Review*, **12**, pp.1-33.
- Tangestani, m. H. and Moore, F., 2002, Porphyry copper alteration mapping at the Meiduk area, Iran, *International Journal of Remote Sensing*, v.23, pp.4815-4826.
- Tatar, Ç., Helvacı, C., Köse, H., and Şimşir, F., 1993, Geology of the lower and upper coal seams and mining methods at Çayırhan coal basin, Beypazarı, Turkey, *Mining Engineering*, pp.1071-1076.
- Taylor, G. R., 2000, Mineral and Lithology Mapping of Drill Core Pulps Using Visible and Infrared Spectrometry, *Natural Resources Research*, v. 9, n. 4, pp.257-268.
- TNT Mips User Guide, Introduction to Remote Sensing of Environment.
- Türkecan, A., Hepşen, N., Papak, İ., Akbaş, B., Dinçel, A., Karataş, S., Özgür, İ., Akay, E., Bedi, Y., Sevin, M., Mutlu, G., Sevin, D., Ünay, E. and Saraç, G., 1991, Seben-Gerede (Bolu), Güdül-Beypazarı (Ankara) ve Çerkeş-Orta-Kurşunlu (Çankırı) yörelerinin (Köroğlu dağları) jeolojisi ve volkanik kayaçların petrolojisi, MTA Report No: 9193.
- Van Der Meer Mohr, H.E.C., 1956, Beypazarı bölgesinde jeolojik ve hidrojeolojik saha çalışmaları hakkında rapor, M.T.A. Report No: 2554, 28 p.

- Whitney, G., Abrams, M. J., and Goetz, F. H., 1983, Mineral discrimination using a portable ratio-determining radiometer, *Economic Geology*, v.78, pp.688-698.
- Yağmurlu, F., and Helvacı, C., 1994, Sedimentological characteristics and facies of the evaporite-bearing Kirmir Formation (Neogene), Beypazarı basin, central Anatolia, Turkey, *Sedimentology*, v.41, pp.847-860.
- Yağmurlu, F., Helvacı, C., and İnci, U., 1988, Depositional setting and geometric structure of Beypazarı lignite deposits, Central Anatolia, *International Journal of Coal Geology*, v.10, pp.337-360.
- Yamaguchi, Y., Kahle, A. B., Tsu, H., Kawakami, T., and Pniel, M., 1998, Overview of Advanced Spaceborne Thermal Emission and Reflection Radiometer (ASTER), *IEEE Transactions on Geoscience and Remote Sensing*, v.36, n0.4, pp.1062-1071.
- Yohannes, E. B., 1993, Geology and petrology of the Beypazarı granitoids, M. Sc. Thesis, Middle East Technical University, Ankara, 132 p.
- Younis, M. T., Gilabert, M. A., Melia, J., and Bastida, J., 1997, Weathering process effects on spectral reflectance of rocks in a semi-arid environment, *International Journal of Remote Sensing*, v.18, n.16, pp.3361-3377.
- Zoroğlu, O., 2001, Beypazarı Granitoidinin Petrolojisi ve Anklavlarının Kökeni, Yüksek Lisans Tezi, Ankara Üniversitesi, 115 p.
- Zoroğlu, O., and Kadioğlu, Y. K., 2003, Oymaağaç (Beypazarı – Ankara) Granitoidinin Jeolojisi ve Petroğrafisi, *Gazi University Journal of Science*, v.16(2), pp.299-308.
- Zoroğlu, O., and Kadioğlu, Y. K., 2004, Oymaağaç Granitoidinin Normal Zonlu Kristalleşme Özelliği, Beypazarı – Ankara, *Fırat Üniversitesi Fen ve Mühendislik Bilimleri Dergisi*, v.16(1), pp.81-95.

APPENDIX A

Table A1: Spectral Measurements of Rock Samples.

Location No	Coordinates		Samples	Spectra of samples
	X	Y		
1	406284	4437986	fresh	
			weathered	
2	406155	4437779	fresh	
			weathered	
3	405088	4438155	fresh	
			weathered	
4	405268	4437352	fresh	
			weathered	

Table A1 continued: Spectral Measurements of Rock Samples.

Location No	Coordinates		Samples	Spectra of samples
	X	Y		
5	405639	4436979	fresh	
			weathered	
6	404810	4433389	fresh	
			weathered	
7	405167	4431920	fresh	
			weathered	
8	405735	4430848	fresh	
			weathered	

Table A1 continued: Spectral Measurements of Rock Samples.

Location No	Coordinates		Samples	Spectra of samples
	X	Y		
9	406234	4431328	fresh	
			weathered	
10	406438	4431107	fresh	
			weathered	
11	406976	4431513	fresh	
			weathered	
12	407608	4431917	fresh	
			weathered	

Table A1 continued: Spectral Measurements of Rock Samples.

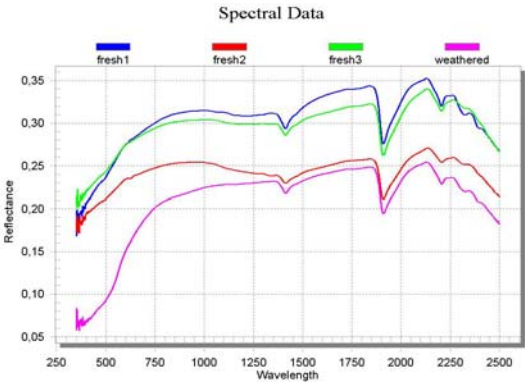
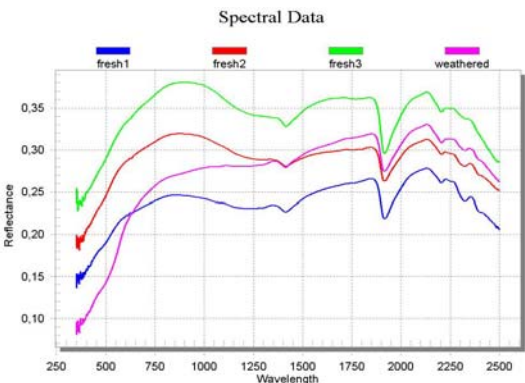
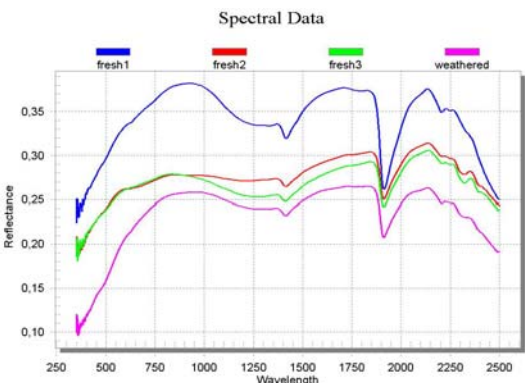
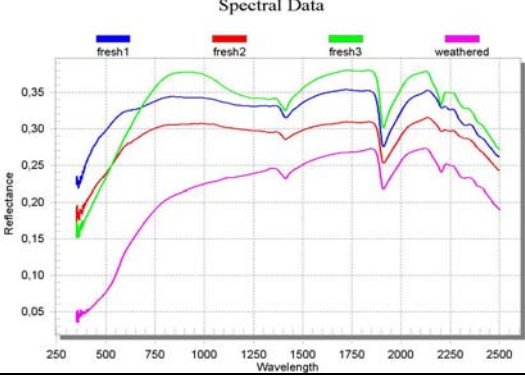
Location No	Coordinates		Samples	Spectra of samples
	X	Y		
13	407796	4432109	fresh	 <p>The graph for Location 13 shows four spectral curves: fresh1 (blue), fresh2 (red), fresh3 (green), and weathered (magenta). The x-axis represents Wavelength from 250 to 2500 nm, and the y-axis represents Reflectance from 0.05 to 0.35. The fresh samples show higher reflectance across most wavelengths compared to the weathered sample, which has a notably lower reflectance in the 400-1000 nm range.</p>
			weathered	
14	408372	4431946	fresh	 <p>The graph for Location 14 shows four spectral curves: fresh1 (blue), fresh2 (red), fresh3 (green), and weathered (magenta). The x-axis represents Wavelength from 250 to 2500 nm, and the y-axis represents Reflectance from 0.10 to 0.35. The fresh samples exhibit higher reflectance than the weathered sample, particularly in the 400-1500 nm range.</p>
			weathered	
15	409047	4432931	fresh	 <p>The graph for Location 15 shows four spectral curves: fresh1 (blue), fresh2 (red), fresh3 (green), and weathered (magenta). The x-axis represents Wavelength from 250 to 2500 nm, and the y-axis represents Reflectance from 0.10 to 0.35. The fresh samples show higher reflectance than the weathered sample, with a significant difference in the 400-1500 nm range.</p>
			weathered	
16	408035	4433132	fresh	 <p>The graph for Location 16 shows four spectral curves: fresh1 (blue), fresh2 (red), fresh3 (green), and weathered (magenta). The x-axis represents Wavelength from 250 to 2500 nm, and the y-axis represents Reflectance from 0.05 to 0.35. The fresh samples show higher reflectance than the weathered sample, especially in the 400-1500 nm range.</p>
			weathered	

Table A1 continued: Spectral Measurements of Rock Samples.

Location No	Coordinates		Samples	Spectra of samples
	X	Y		
17	413701	4434642	fresh	
			weathered	
18	407053	4437882	fresh	
			weathered	
19	408392	4437763	fresh	
			weathered	
20	410175	4438140	fresh	
			weathered	

Table A1 continued: Spectral Measurements of Rock Samples.

Location No	Coordinates		Samples	Spectra of samples
	X	Y		
21	411852	4438667	fresh	
			weathered	
22	412306	4437749	fresh	
			weathered	
23	412828	4437388	fresh	
			weathered	
24	413477	4436178	fresh	
			weathered	

Table A1 continued: Spectral Measurements of Rock Samples.

Location No	Coordinates		Samples	Spectra of samples
	X	Y		
25	411155	4436355	fresh	
			weathered	
26	410750	4435394	fresh	
			weathered	
27	410330	4434700	fresh	
			weathered	
28	409909	4434613	fresh	
			weathered	

Table A1 continued: Spectral Measurements of Rock Samples.

Location No	Coordinates		Samples	Spectra of samples
	X	Y		
29	412092	4433767	fresh	
			weathered	
30	408882	4433414	fresh	
			weathered	
31	410070	4433808	fresh	
			weathered	
32	408444	4433404	fresh	
			weathered	

APPENDIX B

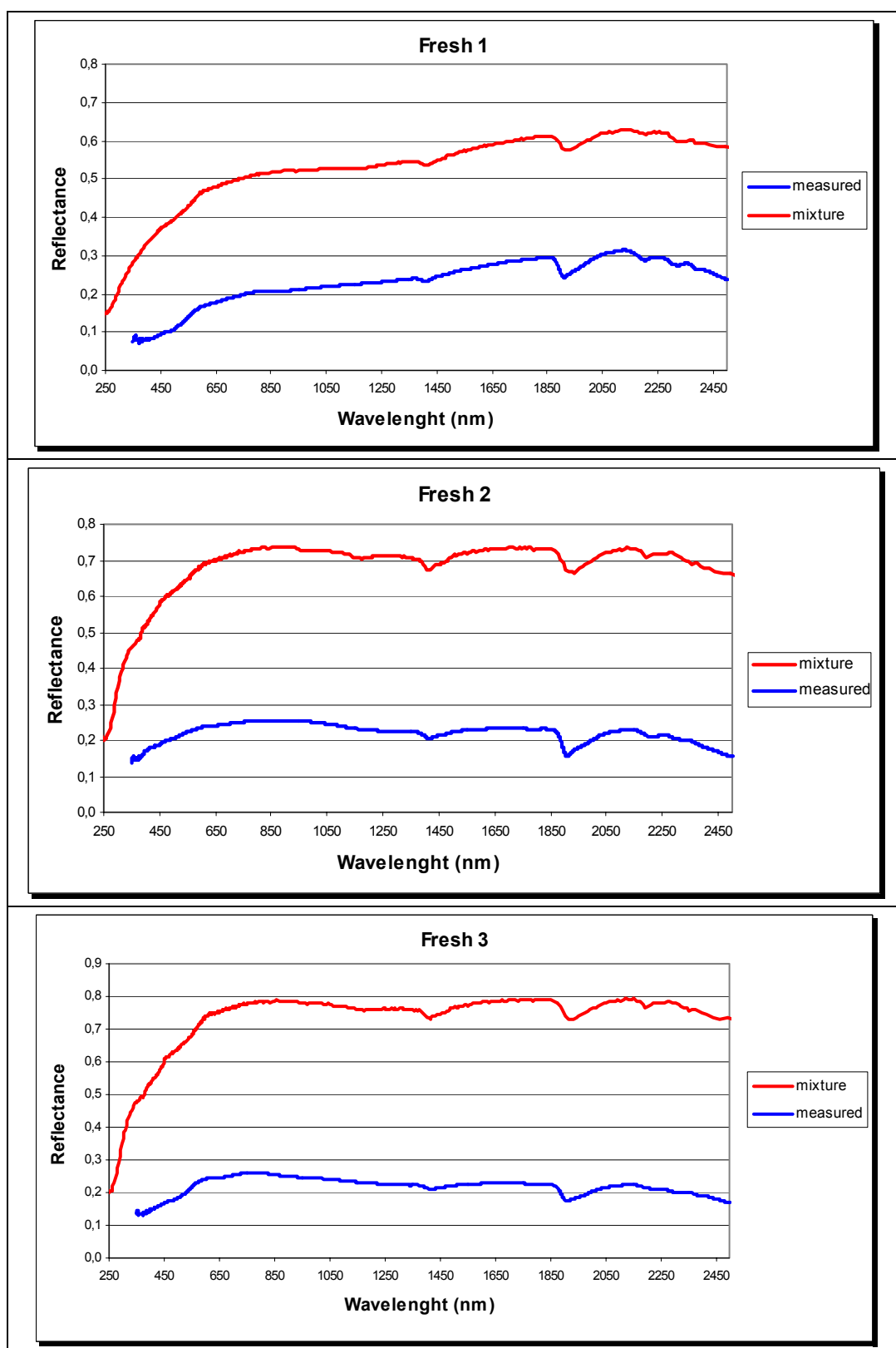


Figure B1: Measured and calculated spectra of fresh samples.

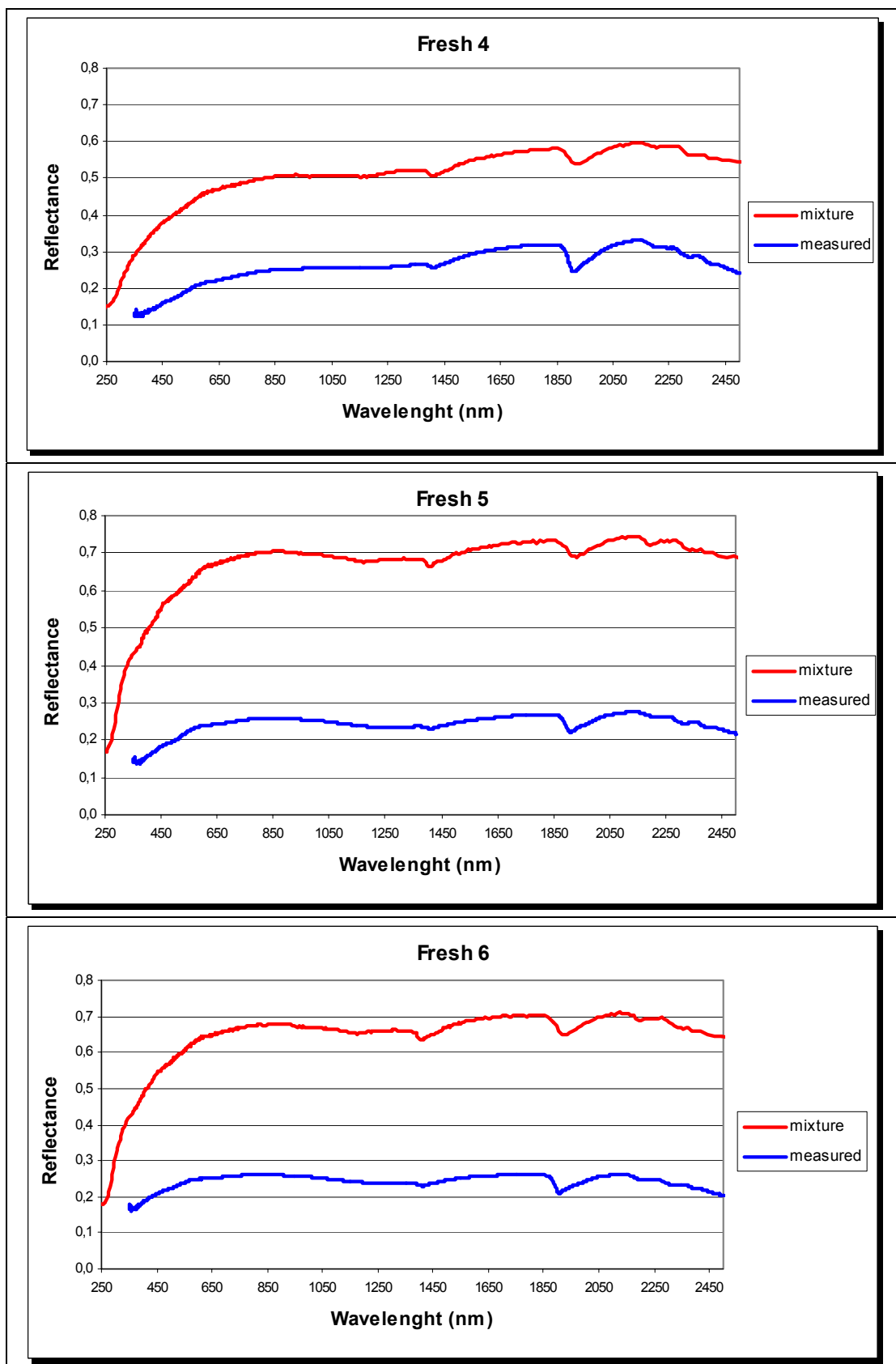


Figure B1 continued: Measured and calculated spectra of fresh samples.

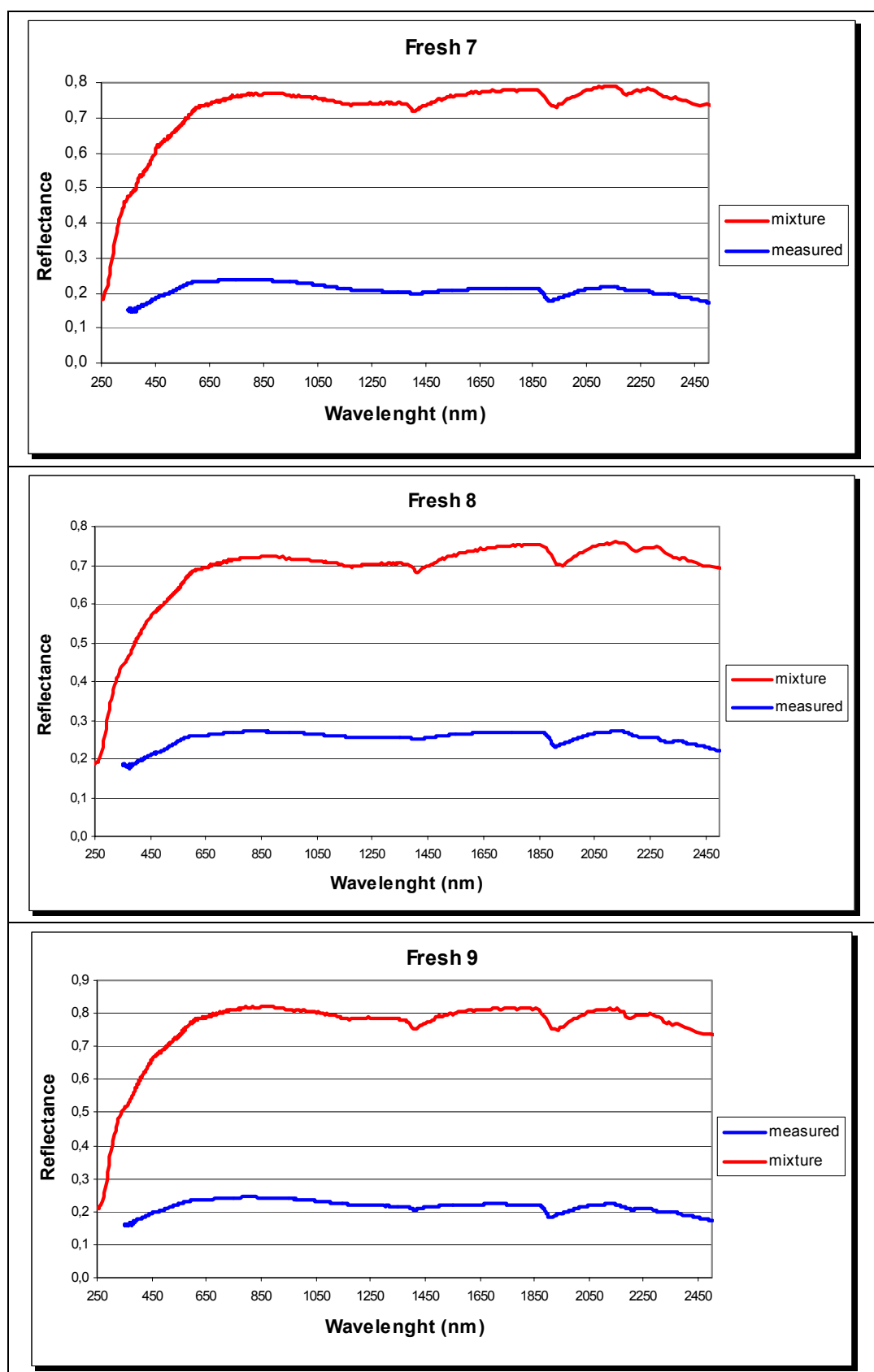


Figure B1 continued: Measured and calculated spectra of fresh samples.

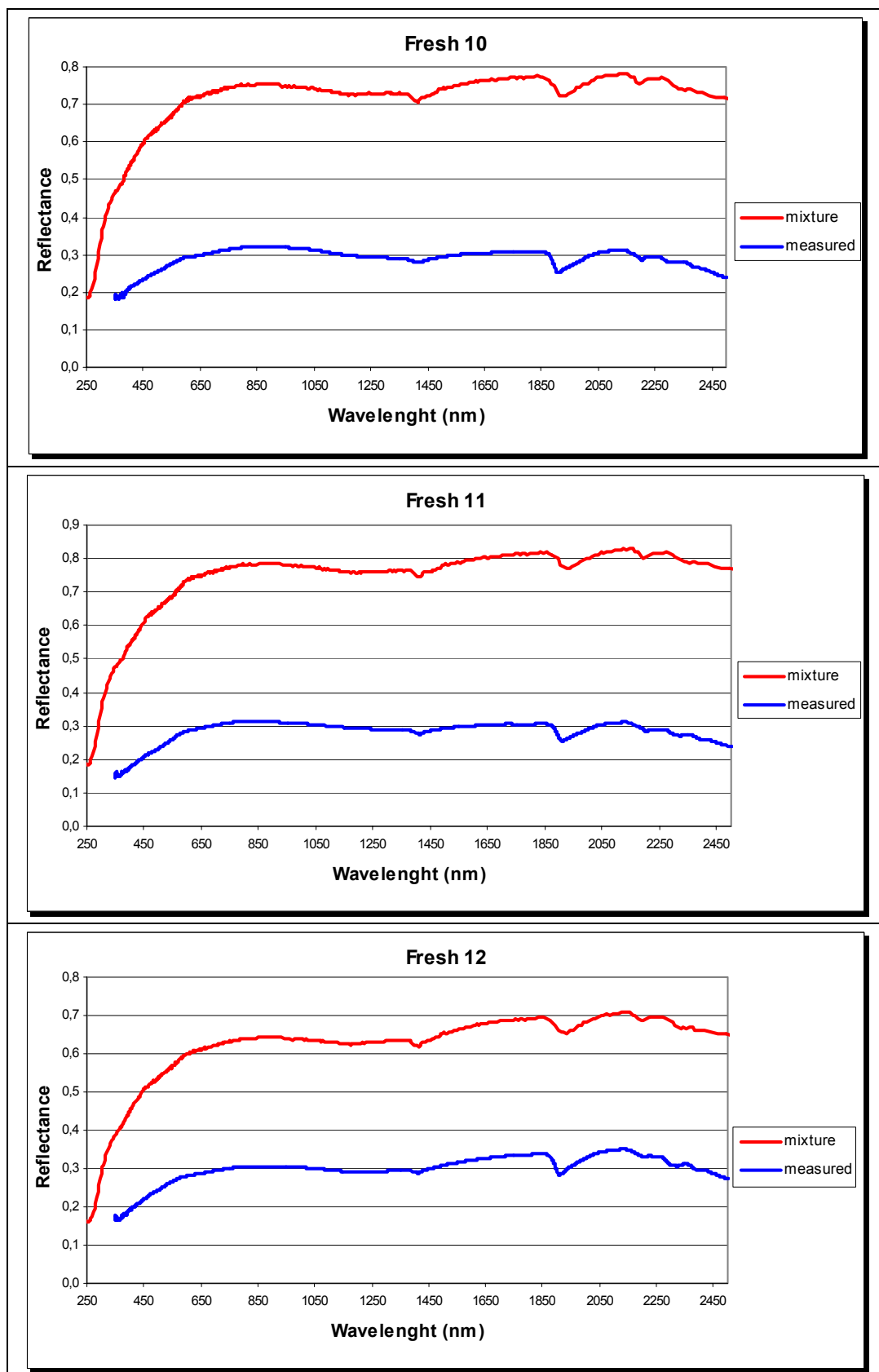


Figure B1 continued: Measured and calculated spectra of fresh samples.

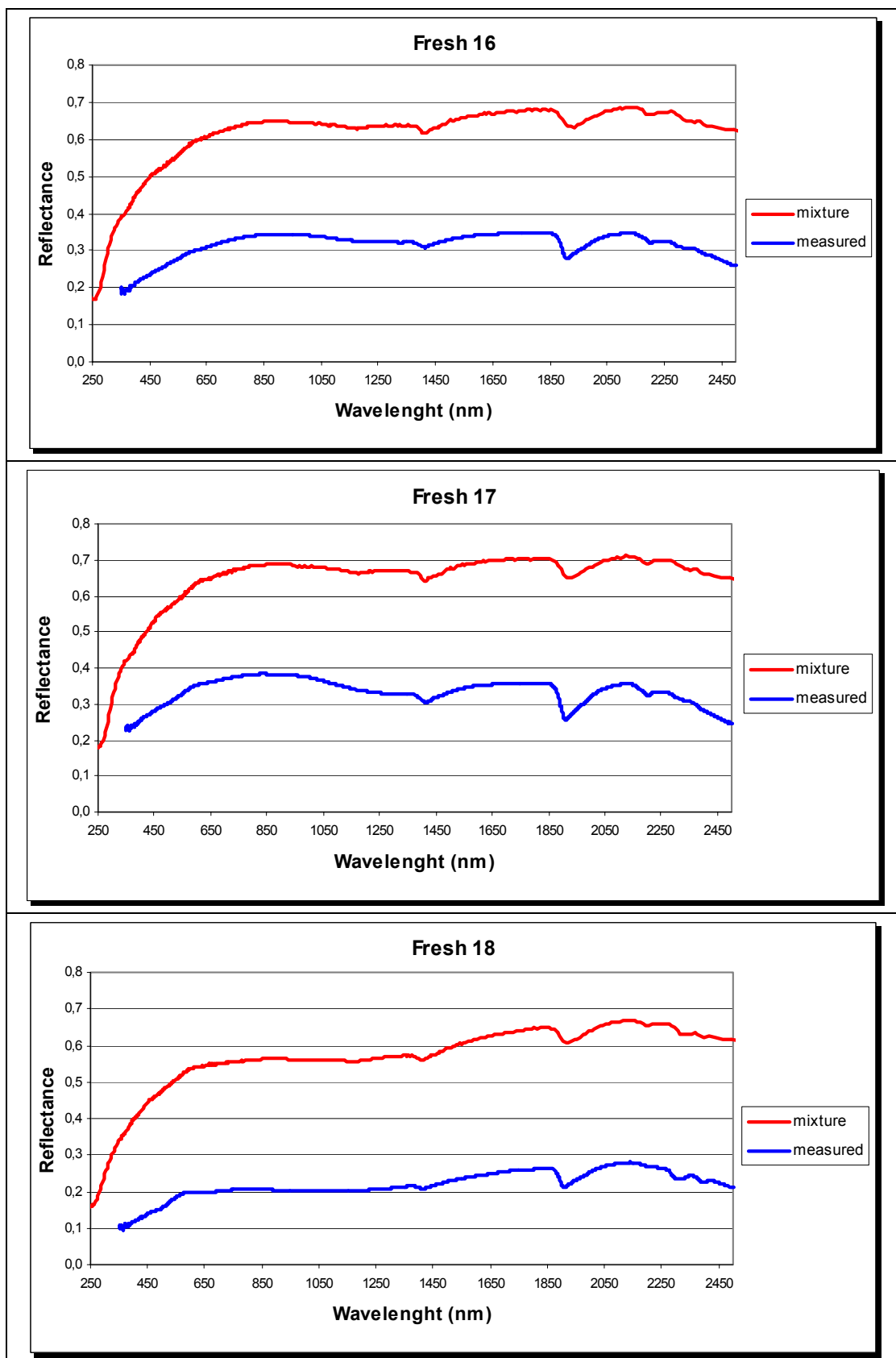


Figure B1 continued: Measured and calculated spectra of fresh samples.

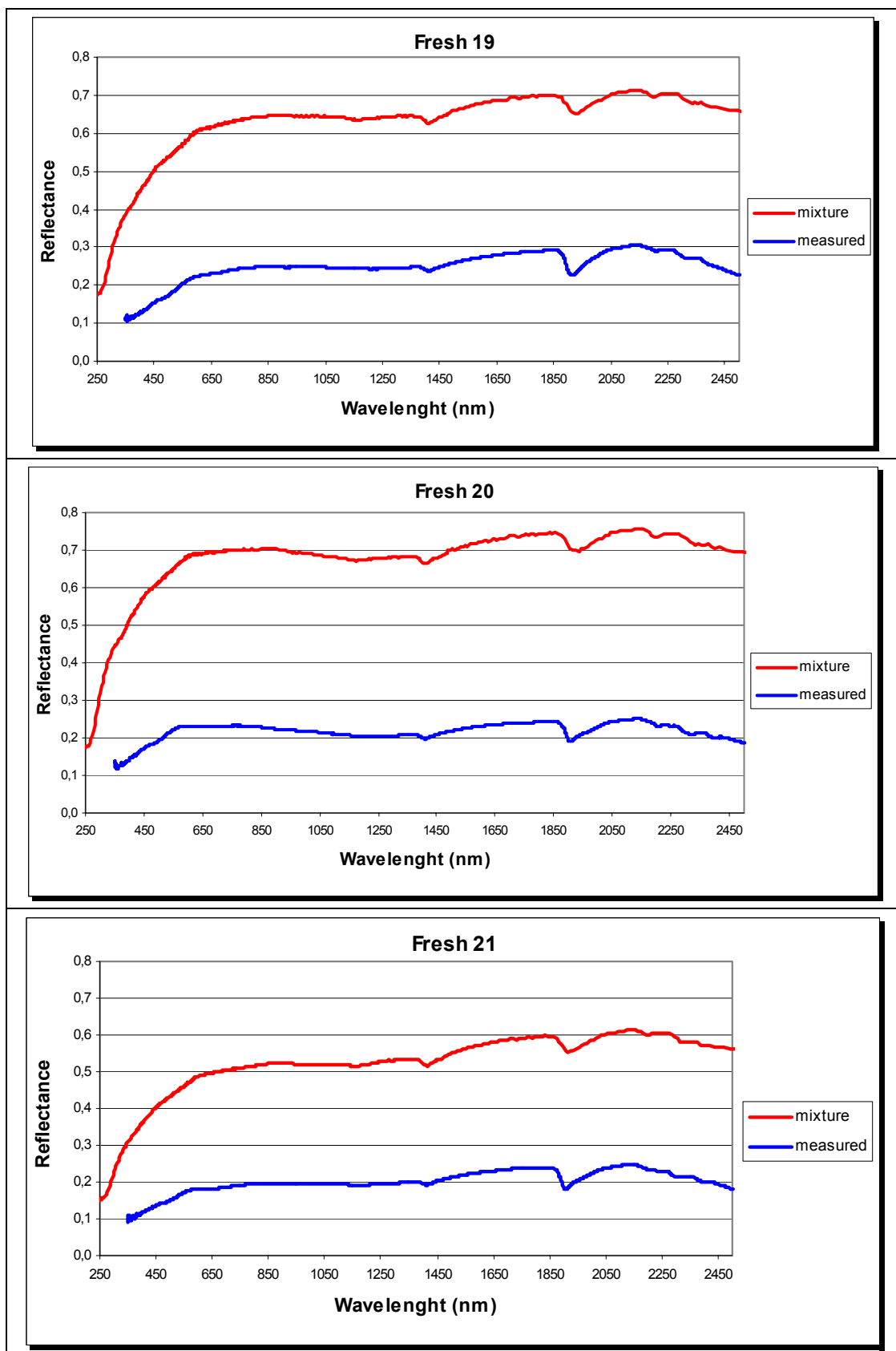


Figure B1 continued: Measured and calculated spectra of fresh samples.

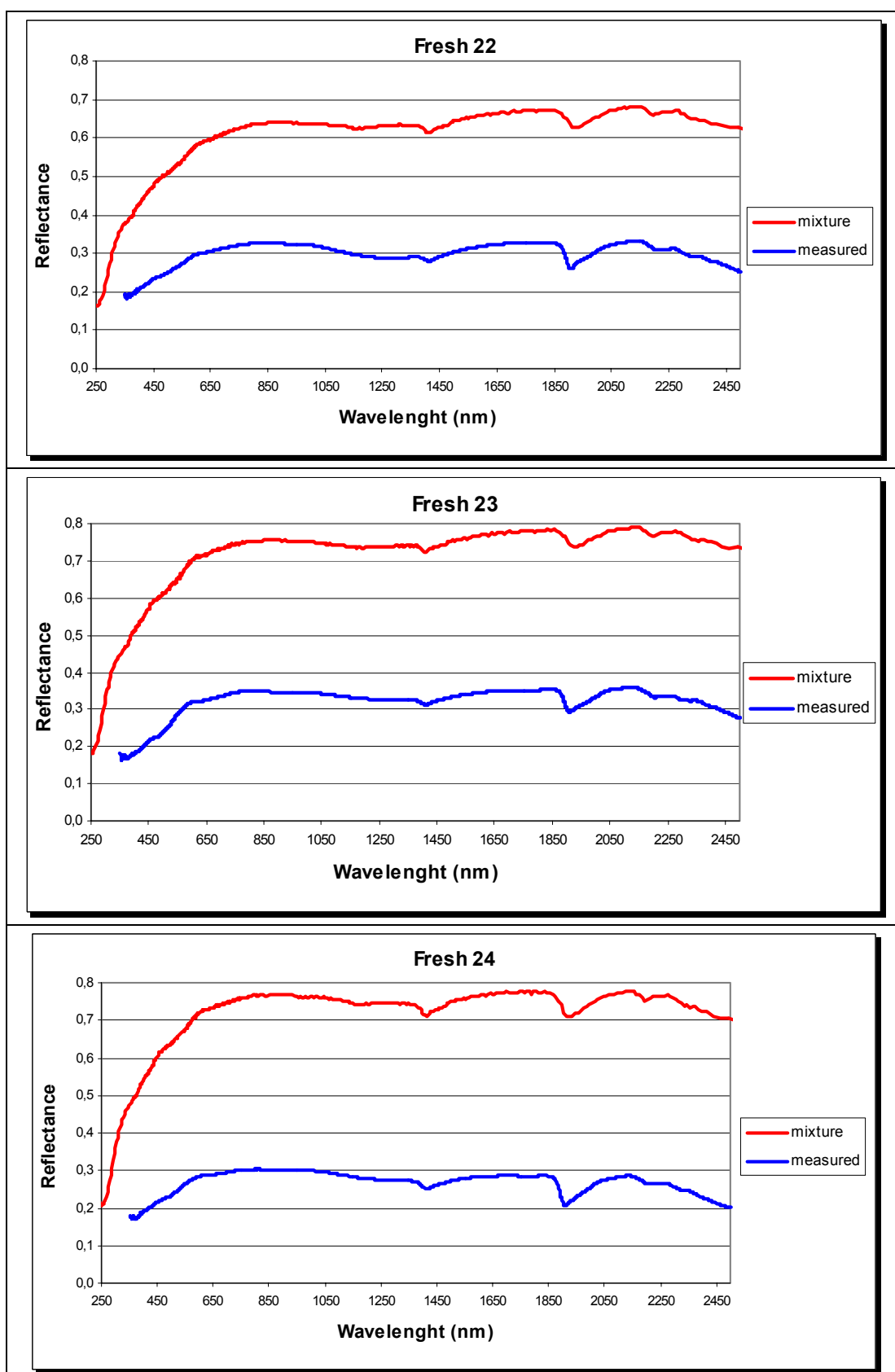


Figure B1 continued: Measured and calculated spectra of fresh samples.

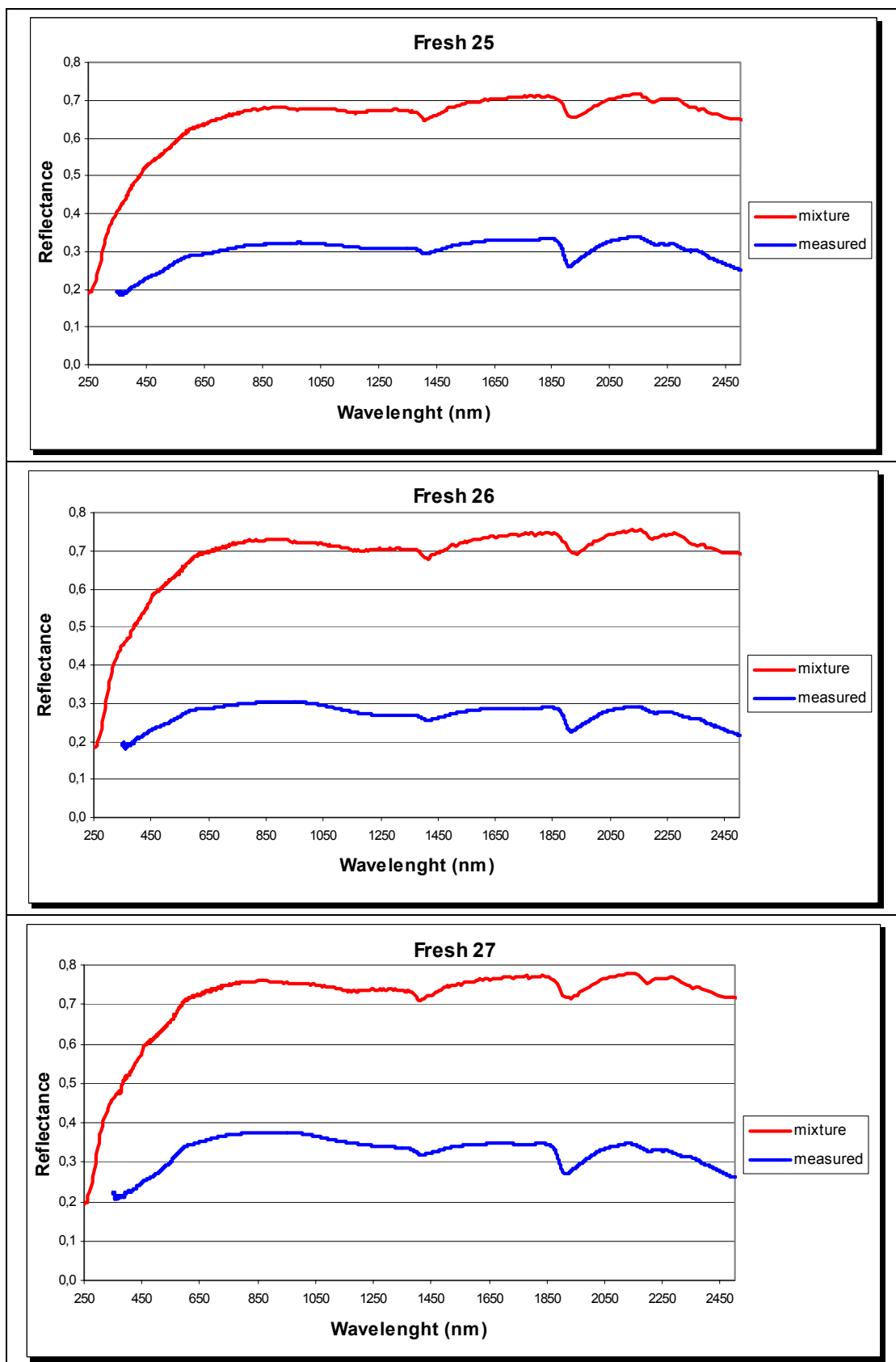


Figure B1 continued: Measured and calculated spectra of fresh samples.

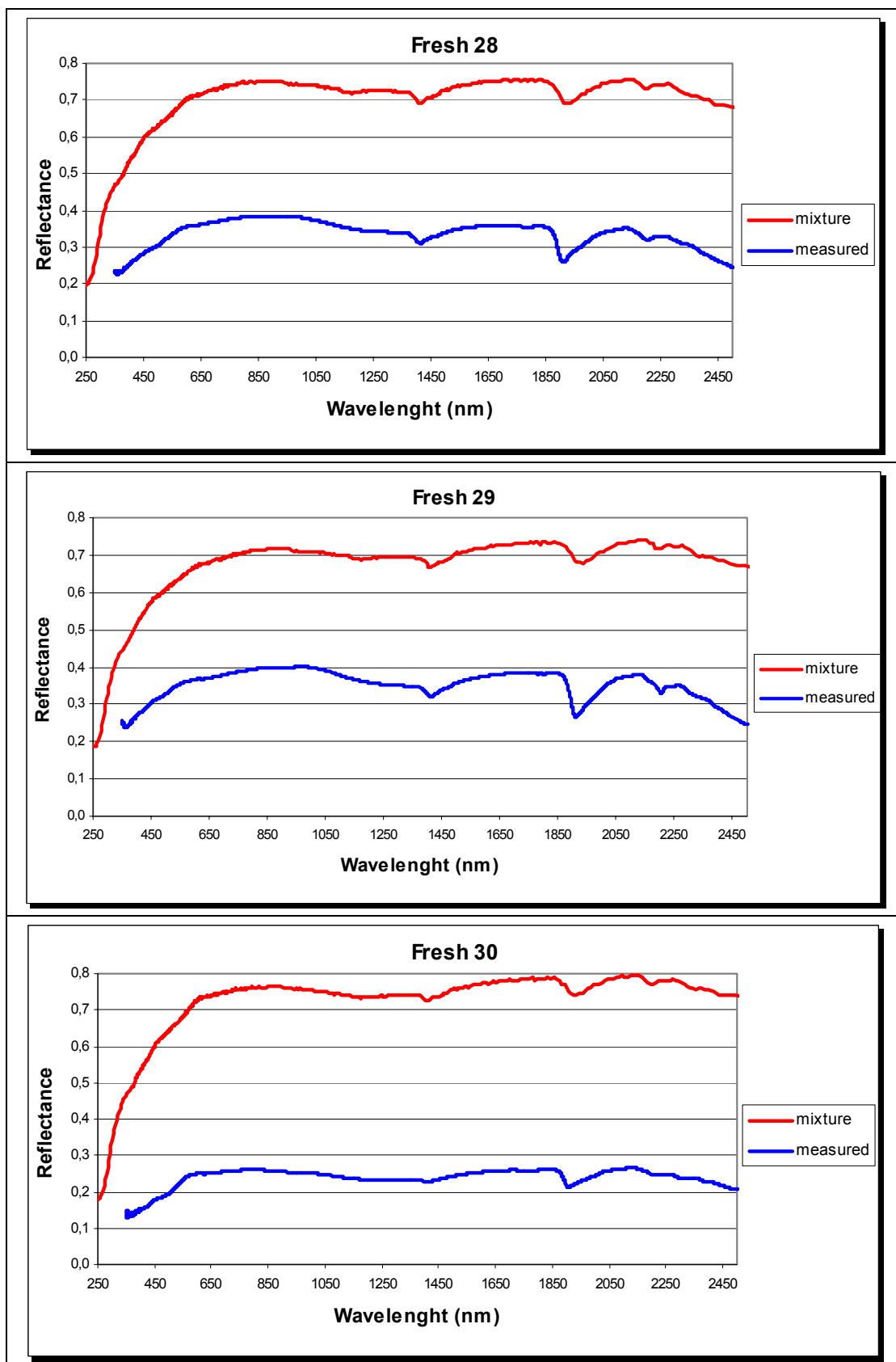


Figure B1 continued: Measured and calculated spectra of fresh samples.

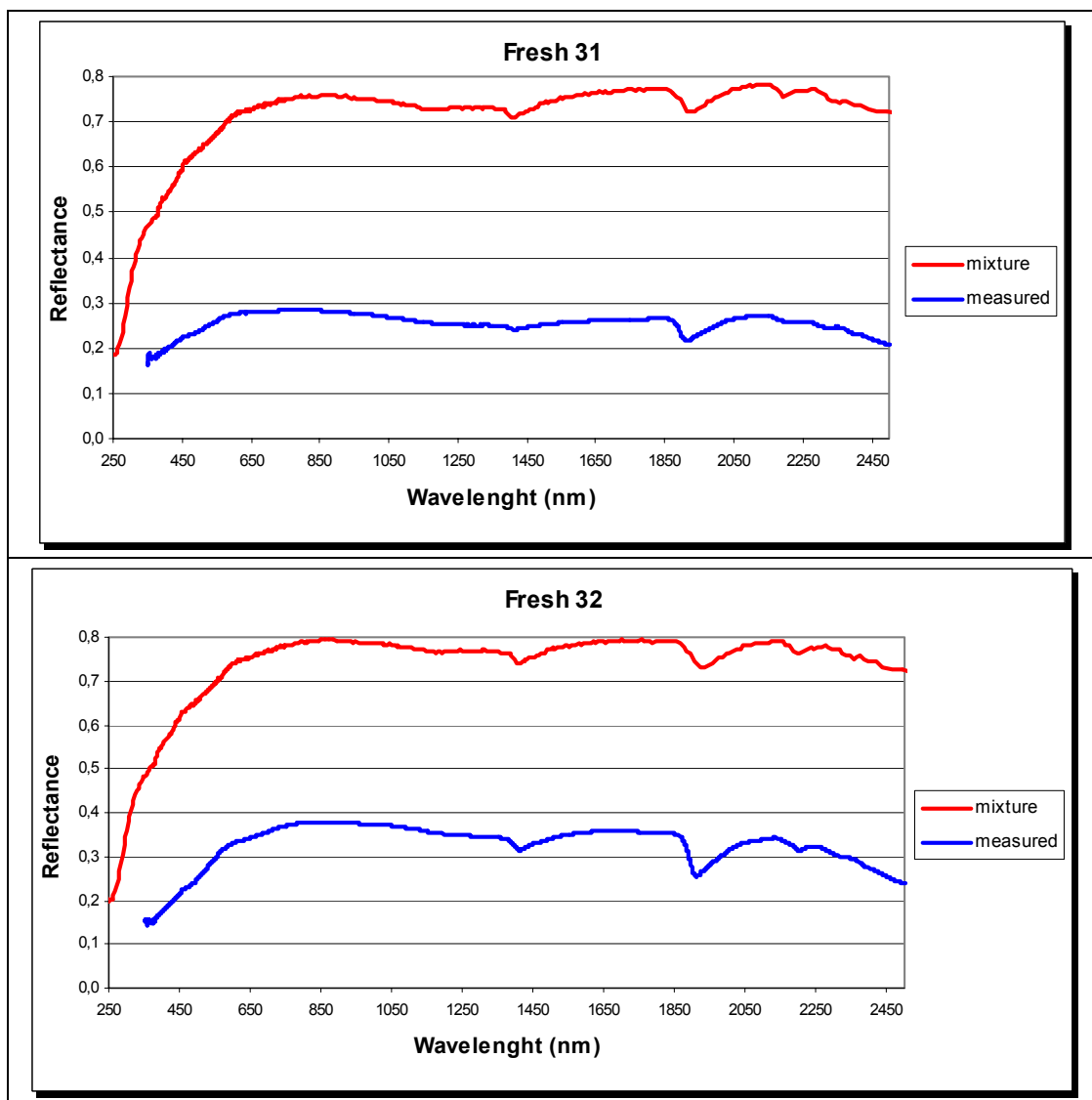


Figure B1 continued: Measured and calculated spectra of fresh samples.

APPENDIX C

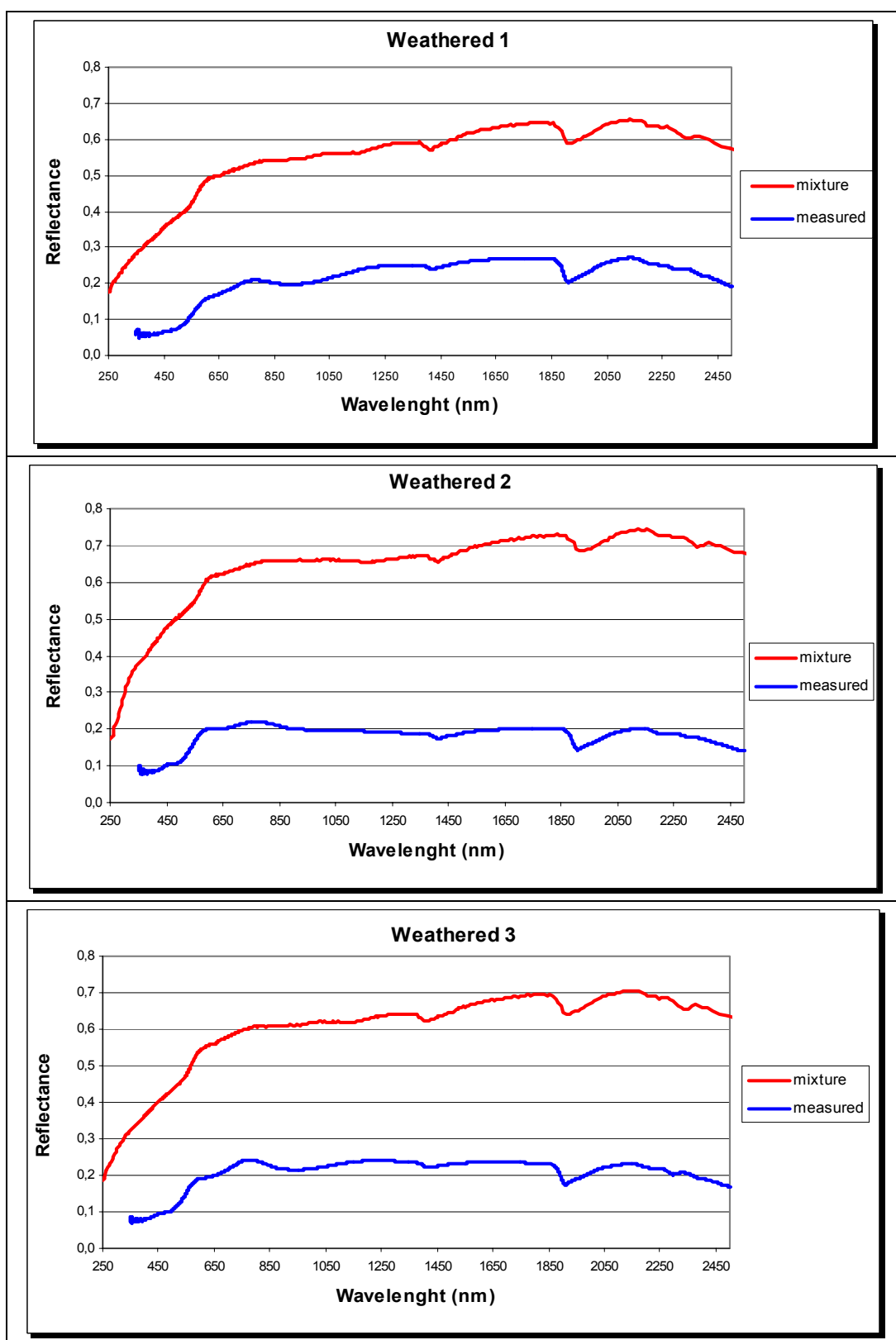


Figure C1: Measured and calculated spectra of weathered samples.

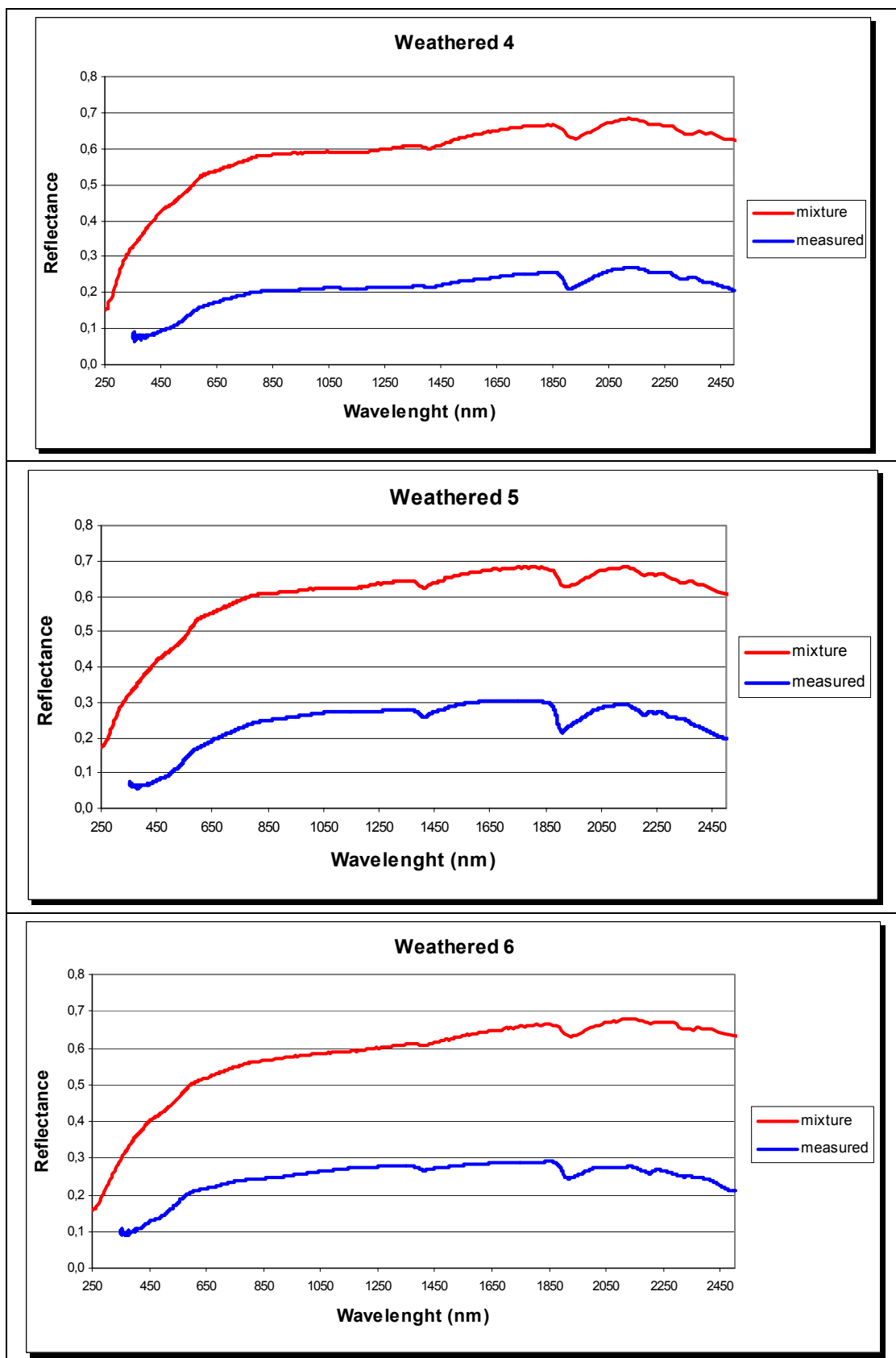


Figure C1 continued: Measured and calculated spectra of weathered samples.

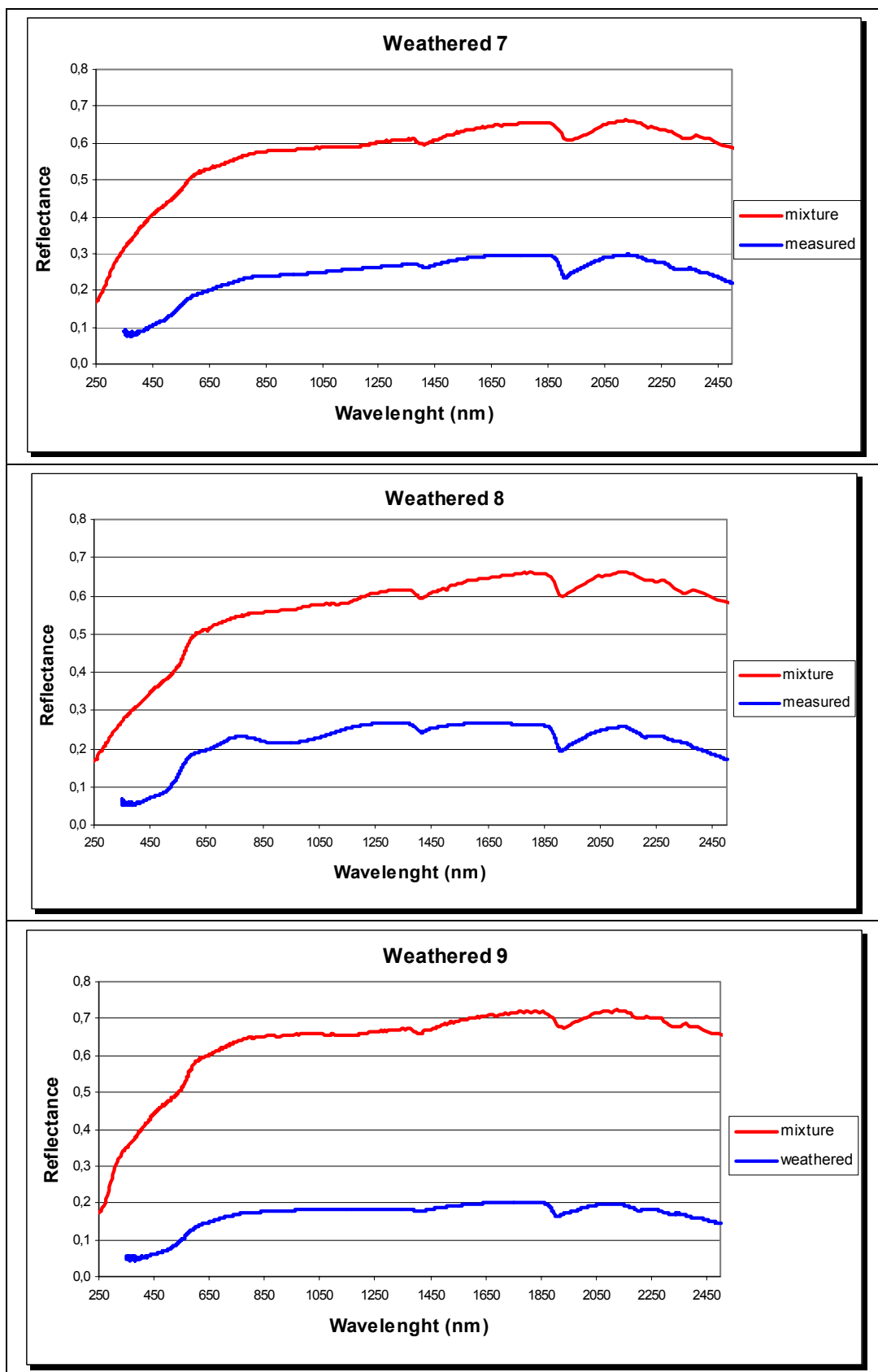


Figure C1 continued: Measured and calculated spectra of weathered samples.

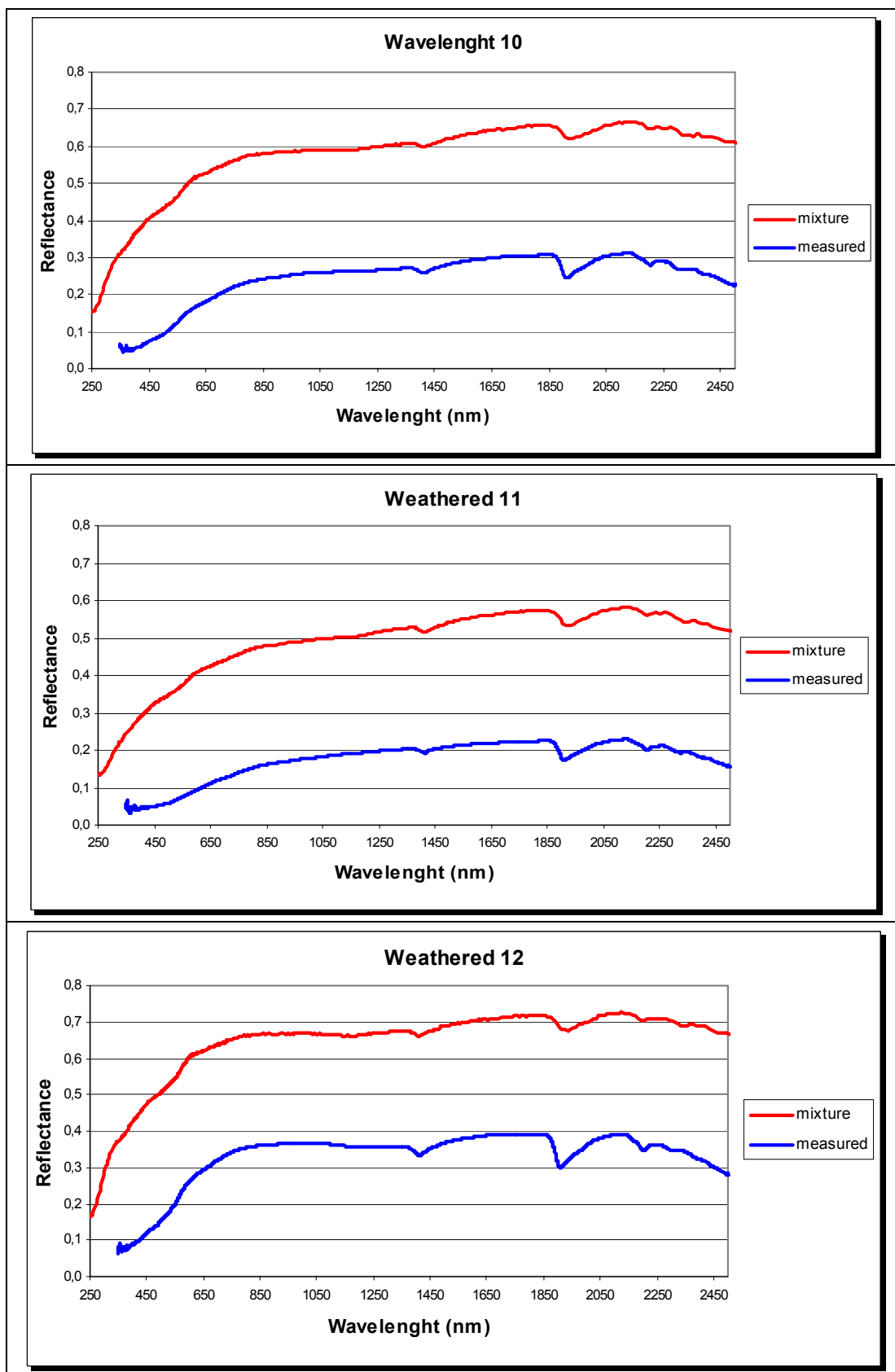


Figure C1 continued: Measured and calculated spectra of weathered samples.

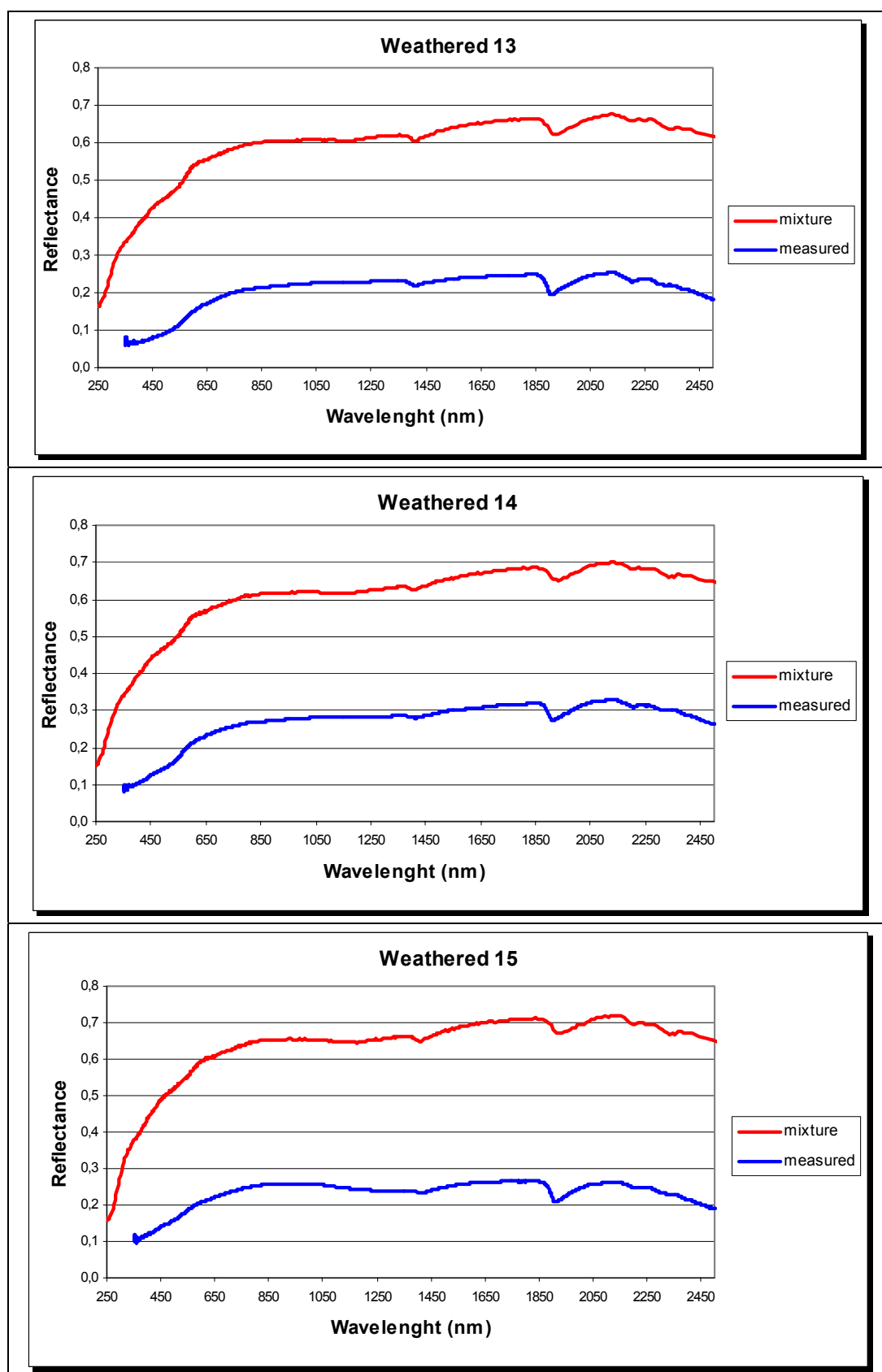


Figure C1 continued: Measured and calculated spectra of weathered samples.

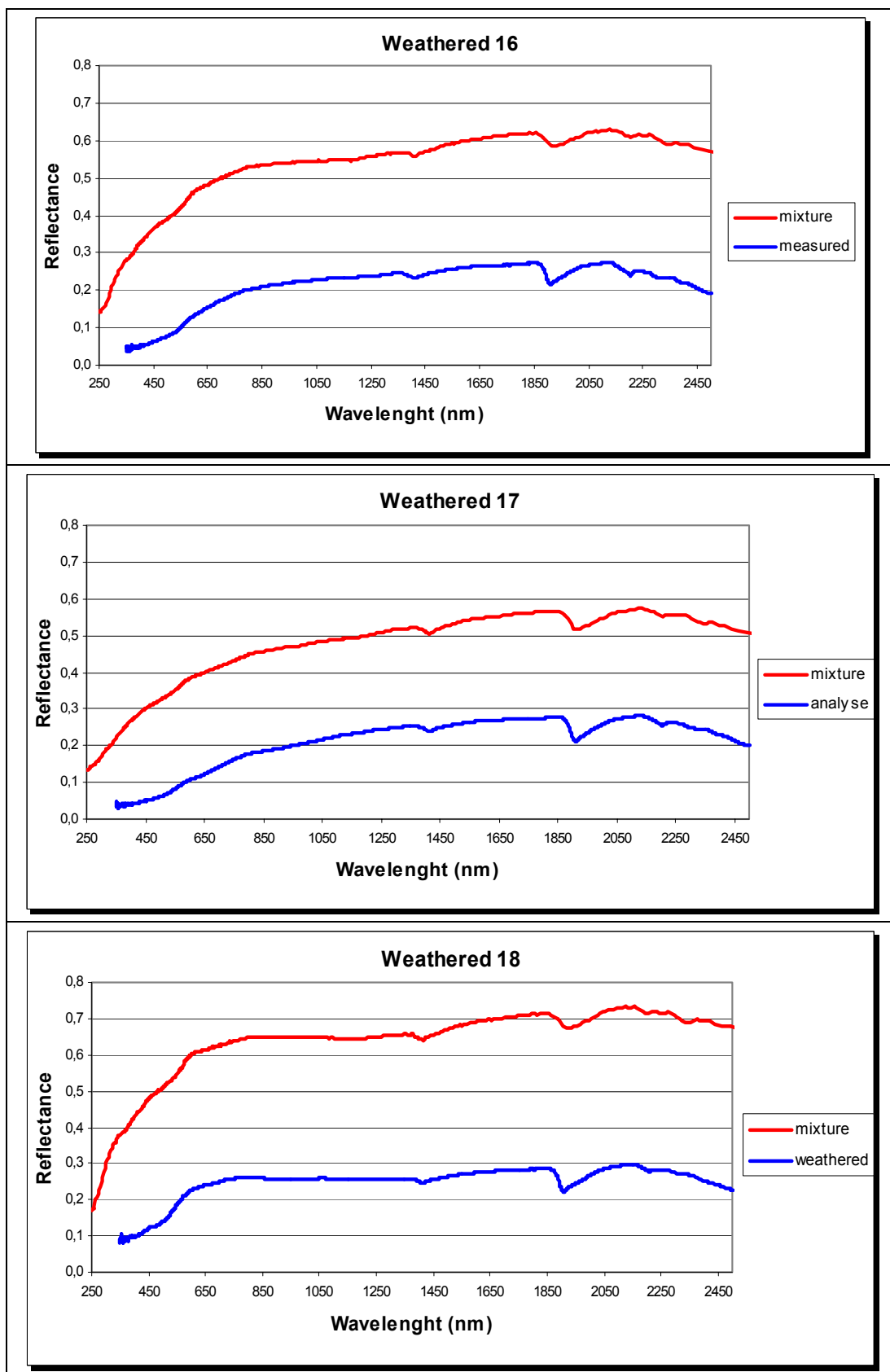


Figure C1 continued: Measured and calculated spectra of weathered samples.

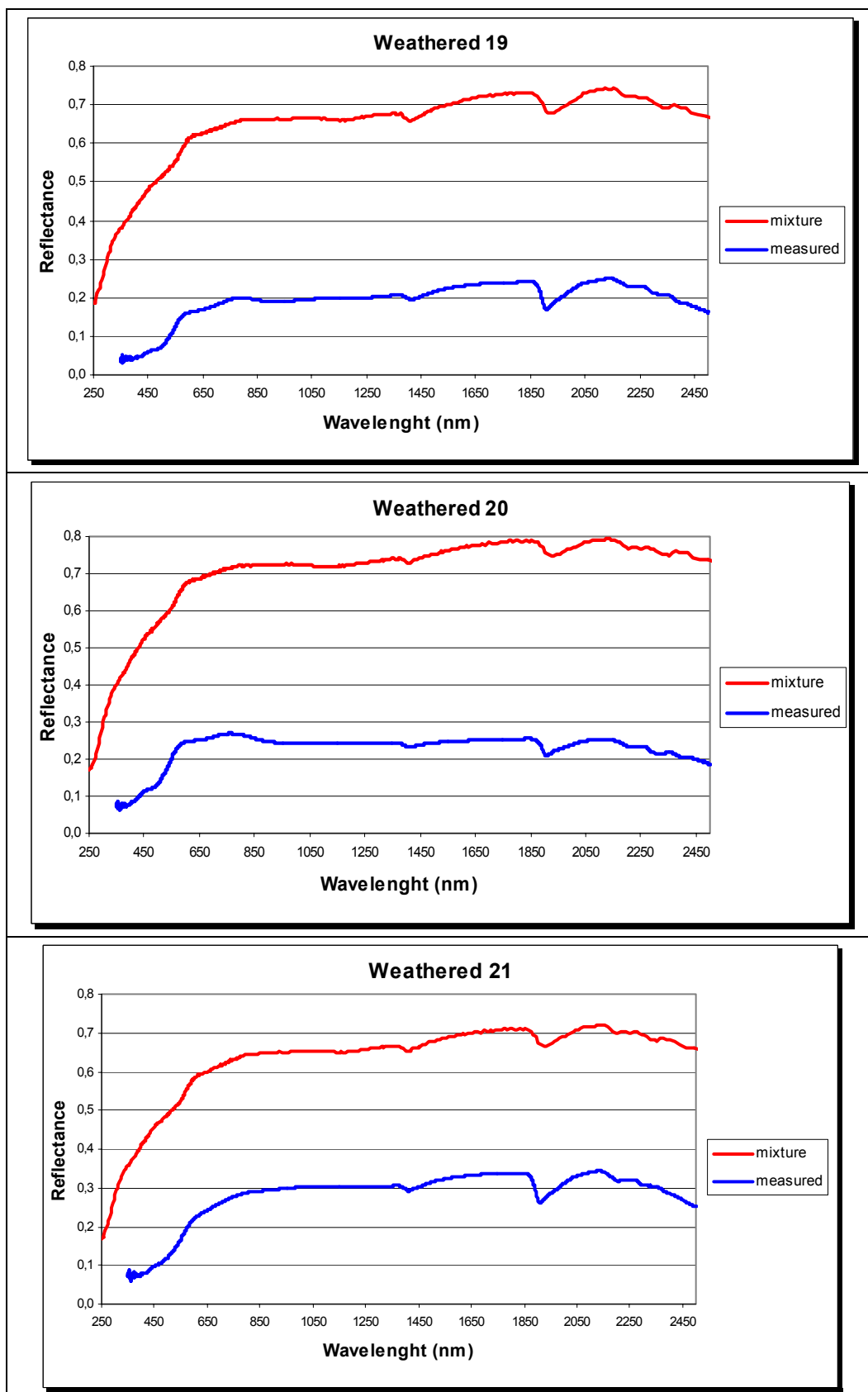


Figure C1 continued: Measured and calculated spectra of weathered samples.

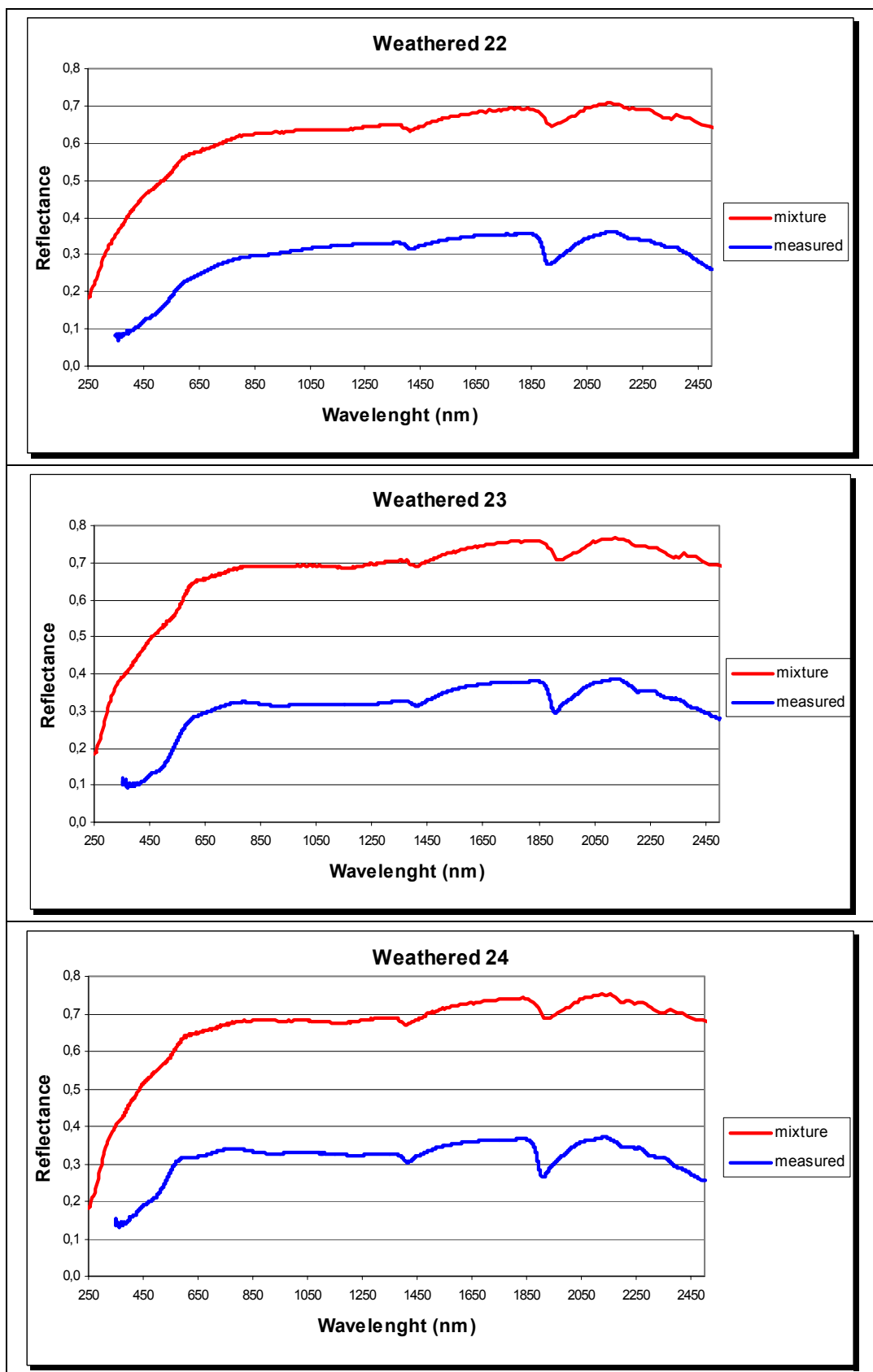


Figure C1 continued: Measured and calculated spectra of weathered samples.

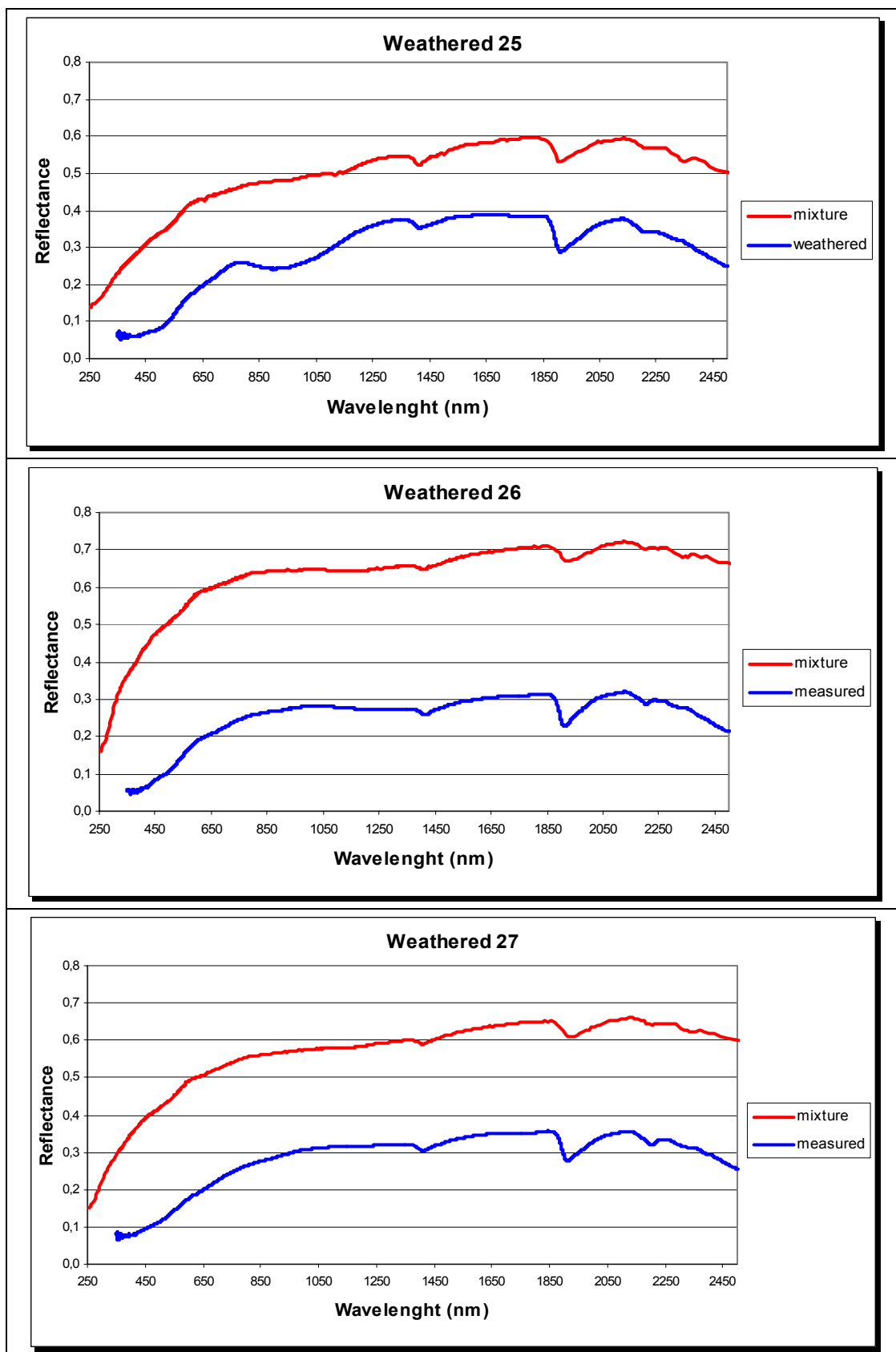


Figure C1 continued: Measured and calculated spectra of weathered.

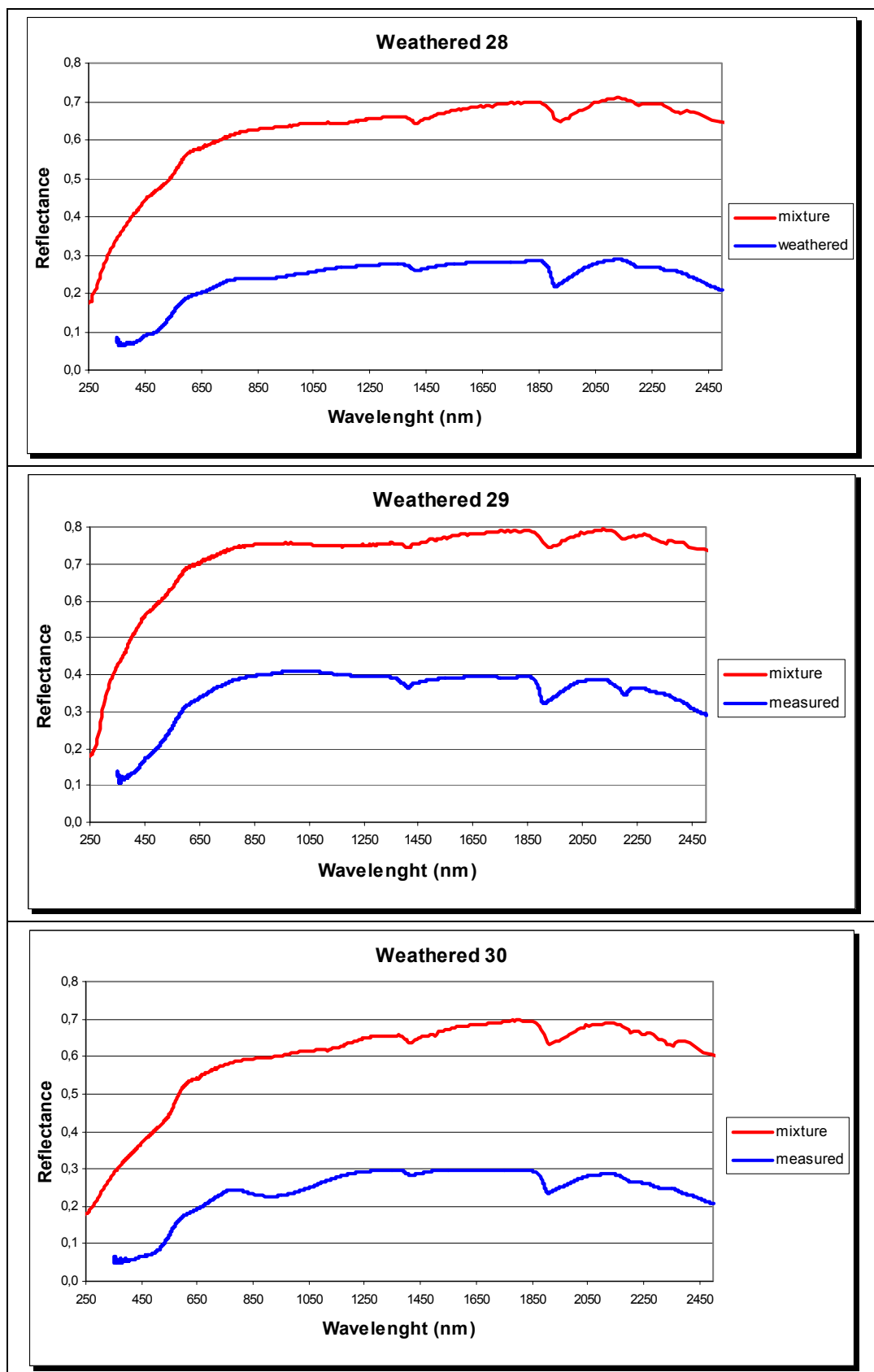


Figure C1 continued: Measured and calculated spectra of weathered samples.

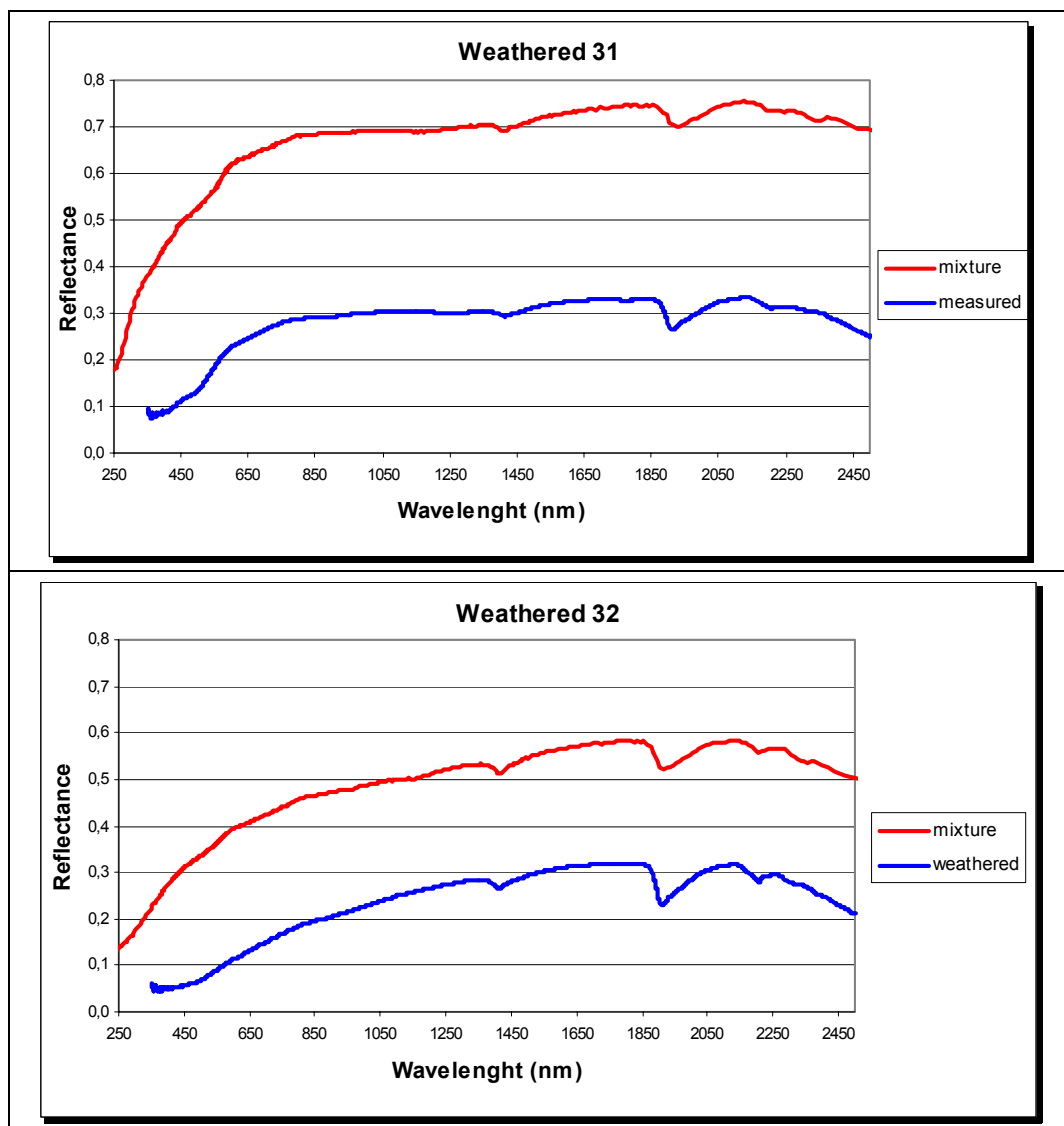


Figure C1 continued: Measured and calculated spectra of weathered samples.